5.14 Anomalous chemical bond formation in polycarbonate by cluster impact

K. Hirata*, Y. Saitoh**, K. Narumi***, Y. Kobayashi*, and K. Arakawa**

National Institute of Advanced Industrial Science and Technology (AIST), Tsukuba, Ibaraki 305-8565, Japan*

Advanced Radiation Technology Center, JAERI, Takasaki, Gumma 370-1292, Japan**

Advanced Science Research Center, JAERI, Takasaki, Gumma 370-1292, Japan***

1. Introduction

Incident ions passing through a matter are slowed down by electronic and nuclear interaction with target atoms. For ion irradiation of a polymer, its chemical structure is inevitably changed by the interaction. The effect of cluster ion irradiation is different from that of single ion irradiation in local energy deposition density because the constituent atoms originating from the same cluster simultaneously impact on a very small region. Therefore, cluster ion irradiation of a polymer is expected to provide unique chemical modification. In this paper, we present results of FTIR measurements for single-ion and cluster-ion irradiated polycarbonate (PC). The measurements were carried out to study chemical modification by the irradiations [1].

2. Experimental

Various single ions (B^+, C^+, Si^+, and Cu^+ ions at energies between 0.19 MeV and 2.255 MeV) and cluster ions (0.19MeV/atom-C_4^+, C_6^+ and C_8^+, 0.3MeV/atom-C_4^+ and C_6^+) were irradiated on amorphous polycarbonate (PC) films with a thickness of 100 μm and a density of 1.2 g/cm^3. Cluster ion irradiation was carried out at JAERI/Takasaki [2].

Attenuated total reflectance (ATR) Fourier transform infrared (FT-IR) spectroscopy was employed to sensitively detect chemical modification of the sample surface. All measurements were carried out on a Bio-Rad FTE-40 spectrometer at a resolution of 4 cm^{-1} employing a 45° cut ZnSe internal reflection element. 128 scans were collected and the signals were averaged to reduce spectral noise.

3. Results and discussion

ATR-FTIR spectra for unirradiated and 0.19 MeV/atom-C_n^+(n=1, 8)-irradiated PC are shown in Fig. 1. The spectra are normalized to the intensity of the 1504 cm^{-1} band (due to aromatic C-C), which is little affected by ion irradiation [3]. Characteristic changes in Fig. 1 are: (a) formation of the broad band between 2500 and 3650 cm^{-1}, with a peak around 3420 cm^{-1}, for the irradiated samples, (b) enhancement in the intensity at 2930 cm^{-1} for the C_8^+-irradiated sample. The broad band (a) mainly corresponds to hydroxyl OH species and the peak at 2930 cm^{-1} (b) is assigned to CH_2 stretching mode.

The spectra for irradiated PC around the wavenumber region, where the characteristic changes (a) and (b) were observed, consist of the several band contributions. We paid attention to three major peaks due to OH, CH_2 asymmetric stretching and CH_3 asymmetric stretching and evaluated these peak intensities, I_{OH}, I_{CH2}, I_{CH3}, by the following way; (I) the broad OH intensity I_{OH} was determined as the

peak intensity at 3420cm^{-1} and (II) the peak intensities of I_{CH2} and I_{CH3} were calculated based on least-squares analysis by approximating the band between 2900 – 3000 cm^{-1} with two Lorentzian functions (for CH_2 asymmetric stretching at 2930 cm^{-1} and CH_3 asymmetric stretching at 2968 cm^{-1}) after subtraction of the broad OH band contribution from the spectrum.

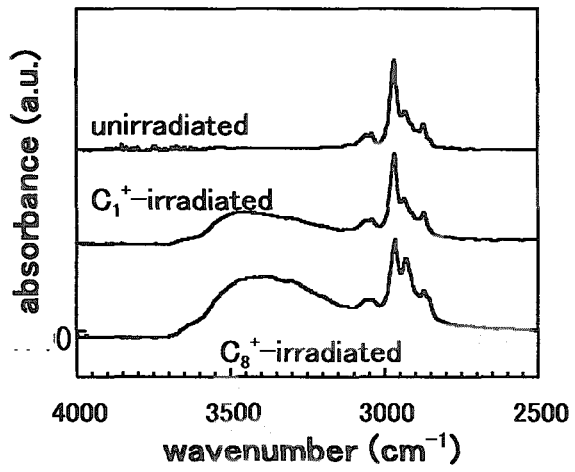

Fig. 1 ATR-FTIR spectra for unirradiated and 0.19 MeV/atom -C_n^+(n=1, 8)-irradiated PC.

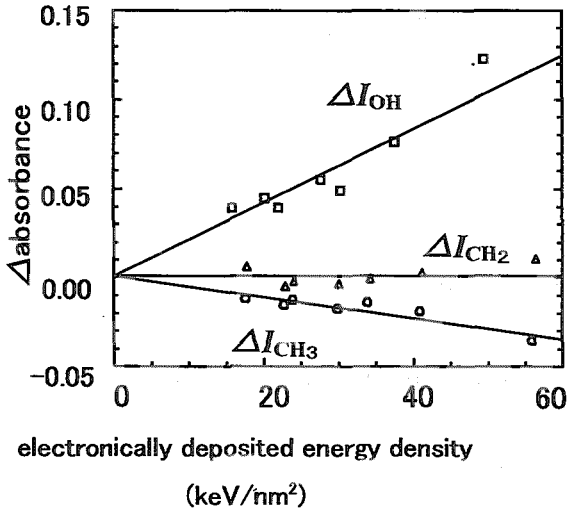

Fig.2 ΔI_{OH}, ΔI_{CH2} and ΔI_{CH3}, as a function of effective electronic energy deposition. The lines through the data points are a guide for the eye.

Chemical change by single-ion irradiation on PC is dominated by the electronically deposited energy density [4]. We plotted ΔI_{OH}, ΔI_{CH2} and ΔI_{CH3} (difference in I_{OH}, I_{CH2}, I_{CH3} between the irradiated and unirradiated samples) as a function of the electronically deposited energy density calculated by TRIM in Fig. 2. In this plot, depth and wavelength dependent amplitude of the evanescent wave was taken into consideration. The data for the cluster ion irradiated samples are not included in Fig. 2 because TRIM is not applicable to cluster ions. This figure shows that (1) the CH_2 bond is not formed in the deposition energy range studied and (2) the formation of the OH and decomposition of the CH_3 in PC structure progress with increasing the density of energy deposition on the sample.

As the enhancement of ΔI_{OH} is well correlated with the deposited energy density for single ion irradiation, we use ΔI_{OH} instead of the energy density for comparing the data for cluster and single ion irradiation with each other. Plots of ΔI_{CH2} and ΔI_{CH3} versus ΔI_{OH}, including the data of the cluster ion irradiated samples, are shown in Fig. 3. ΔI_{CH3} systematically decreases with ΔI_{OH}; and all the data fall on a single line. Thus there is no effect specific to cluster irradiation in the relation between the dissociation of CH_3 and the formation of OH. In contrast, no simple correlation is observed between ΔI_{CH2} and ΔI_{OH}; the data for 0.19MeV/atom-C_8^+ and 0.3MeV/atom-C_6^+ irradiated samples are anomalously deviated upward.

A radial size of the track for carbon cluster was reported to be comparable to that for single carbon in the region close to the surface [5]. The radial energy distribution for 0.19MeV-C_1^+ is calculated to be similar to that for 0.3MeV-C_1^+ using an equation proposed by Tombrello [6]. Taking the similar radial

track size and the additive rule of the individual cluster constituents to the electronic stopping [7] into consideration, there is the threshold value of anomalous CH_2 formation around 2.2-2.8 keV/nm for 0.19MeV/atom-$C_{n\ (n=1,4,6,8)}^{+}$ and 0.3MeV /atom-$C_{n\ (n=1,4,6)}^{+}$ irradiation to PC. High energy density of 0.19MeV/atom-C_8^+ and 0.3MeV/atom- C_6^+ irradiation is probably responsible for the anomalous chemical bond formation.

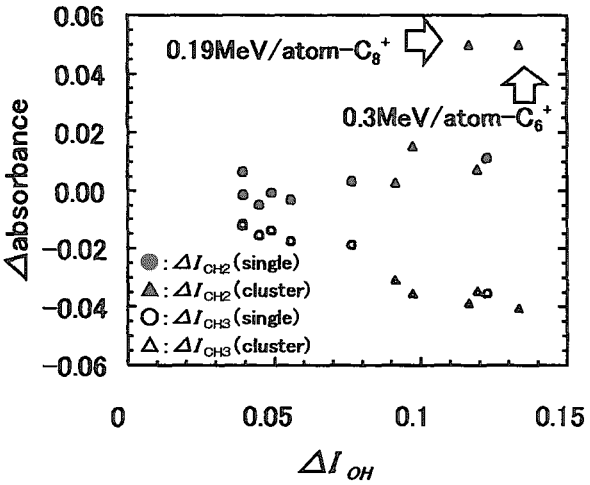

Fig. 3 ΔI_{CH2} and ΔI_{CH3} as a function of ΔI_{OH}. ΔI_{CH2} for 0.19MeV/atom-C_8^+ and 0.3MeV/atom- C_6^+ is anomalously enhanced and the formation of CH_2 is non-linear with respect to ΔI_{OH} and the cluster number.

References

1) K. Hirata, S. Saitoh, K. Narumi, Y. Nakajima, and Y. Kobayashi: Nucl. Instr. and Meth. in Phys. Res. B, in press.
2) Y. Saitoh, K. Mizuhashi and S. Tajima: JAERI-Review 97-015, 240 (1997).
3) D. Fink, R. Klett, W. H. Chung, R. Grunwald, M. Dobeli, F. Ames, L. T. Chadderton, J. Vacik, and V. Hnatowicz: Rad. Eff. Def. Solids 140, 3 (1996).
4) Y. Wang, Y. Jin, Z. Zhu, C. Liu, Y. Sun, Z. Wang, M. Hou, X. Chen, C. Zhang, J. Liu, and B. Li, Nucl. Instr. and Meth. in Phys. Res. B 164-165 (2000) 420.
5) A. Perez, M. Dobeli, and H. A. Synal, Nucl. Instr. and Meth. in Phys. Res. B 116 (1996) 13.
6) T. A. Tombrello, Nucl. Instr. and Meth. in Phys. Res. B 83 (1993) 508
7) K. Baudin, A. Brunelle, M. Chabot, S. Della-Negra, J. Depauw, D. Gardes, P. Hakansson, Y. Le Beyec, A. Billebaud, M. Fallavier, J. Remillieux, J. C. Poizat, and J. P. Thomas, Nucl. Instr. and Meth. in Phys. Res. B 94 (1994) 341.

5.15 Evaluation of Three Dimensional Microstructures on Silica Glass Fabricated by Ion Microbeam

H. Nishikawa*, T. Souno*, M. Hattori**, Y. Ohki**, T. Yamaguchi***,
E. Watanabe***, M. Oikawa****, T. Kamiya****, K. Arakawa****,
M. Fujimaki*****
Department of Electrical Engineering, Shibaura Institute of Technology*,
Department of Electrical, Electronics, and Computer Engineering, Waseda University**,
Department of Electrical Engineering, Tokyo Metropolitan University***,
Advanced Radiation Technology Center, JAERI****,
Japan Science and Technology Corporation*****

1. Introduction

Silica glass is a widely used optical material for telecommunications. Microbeam technique with MeV order ions is one of the promising approaches to modify the optical properties of micrometer-scale structures of silica glass for optical waveguides.

The objective of this research is the formation and evaluation of three-dimensional microstructures on silica glass formed by ion microbeam irradiation. Formation mechanisms and evaluation techniques of the micrometer-scale structures have been studied to understand the radiation effects induced by ion microbeam. We also discuss the possibilities of application for the fabrications of optical devices such as gratings on optical planer circuits.

2. Experimental Procedures

Samples are high-purity silica glasses with dimensions of $3 \times 3 \times 10$ mm^3 and $10 \times 10 \times 1$ mm^3. The H^+ and Si^{5+} ions, accelerated at energies of 1.7 MeV and 18 MeV respectively, were implanted into the silica samples using 3 MV single-ended and 3 MV tandem accelerators equipped with a microbeam line (TIARA, JAERI Takasaki, beam diameter: $\sim$ 1 μm). Radiation effects induced by ion microbeam were investigated by means of a micro-photoluminescence (PL) spectroscopy, an atomic force microscopy (AFM), and an optical microscopy. A micro-PL spectrometer system equipped with an Ar^+ ion laser (488 nm) was used for the mapping of the PL at 650 nm, which is due to nonbridging oxygen hole centers (NBOHCs : ≡ Si – O· , the symbol " · " denotes an unpaired spin). Topological changes of the silica surface and ion-implantation-induced refractive index changes were measured by an AFM

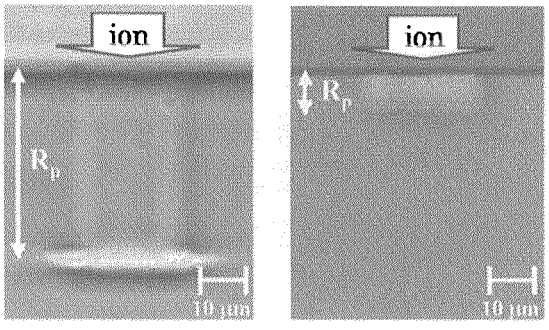

(a) 1.7 MeV H^+ (b) 18 MeV Si^{5+}

Fig. 1 Optical transmission images of the cross sections parallel to the incident planes of ion microbeam.

and an optical microscopy, respectively.

3. Results and discussion

3.1. Refractive index change induced by ion microbeam irradiation

In our previous experiments, 2.47 MeV H^+ ions were implanted into the core of optical fibers made of silica glass. The refractive index change at the projected range of ions, or at the core of fibers, was observed through cross-sectional observation by an optical microscope[1]. For a further possibility to apply this technique to planar optical waveguides, we have studied radiation effects on bulk silica glass. Figures 1 (a) and (b) respectively show optical transmission images of the cross sections, for the sample irradiated with 1.7 MeV H^+ ions (dose:1×10^{17} ions/cm^2) and the one with 18 MeV Si^{5+} ions (dose:1×10^{14} ions/cm^2). Irradiation width of ions microbeam was 20 μm.

As can be seen as bright regions in Fig. 1 (a), we observed a weak refractive index change at trajectories of H^+ ions, together with a strong refractive index change at the projected range. It is considered that the weak refractive index change is associated with electronic excitations, which have been regarded as a cause of defect generation in silica glass. Observation of such refractive index changes even at the trajectory can be attributed to the fact that the dose of ions was about one hundred times as large as that in our previous study [1].

As shown in the optical microscope image shown in Fig. 1 (b) for Si^{5+} ions, there is an area with higher refractive index, which is visible as a bright region from the surface to the projected range of the ions. Since the projected range becomes shorter with increased ion mass for a given acceleration energy, the deposited energy per unit length becomes larger for heavy-ion irradiation than light ions. It is therefore considered that a uniformly bright region with a higher refractive index was observed throughout the tracks of ions for the case of heavy ions such as Si^{5+} even for a relatively lower dose as large as 10^{14} cm^{-2}.

3.2 Evaluation of the local structures of ion implanted silica

In addition to the observed refractive-index changes, the densification of silica can induce structural changes at the surface of silica, which can be observed as a step with nanometer-scale height at the silica surface[2]. We irradiated ion macrobeam (2MeV, H^+) over the area at the half of a silica plate with dimension of 10×10 mm^2, with a thickness of 1 mm. Structural changes across the interface of irradiated and non-irradiated regions were studied by AFM.

The result of the AFM measurement is shown in Fig. 2. As shown in Fig. 2, there exists a step with a height about 18 nm across the interface of irradiated and non-irradiated regions, which is

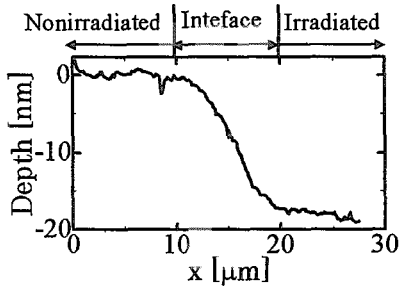

Fig.2 Profile measured by AFM of silica surface across the radiation interface.

accompanied by a transition region gradually decaying with a width ~20 μm.

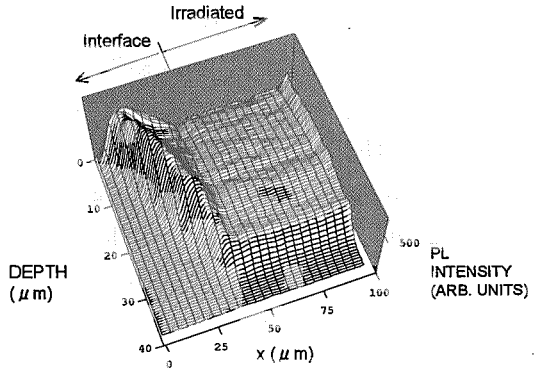

(a)

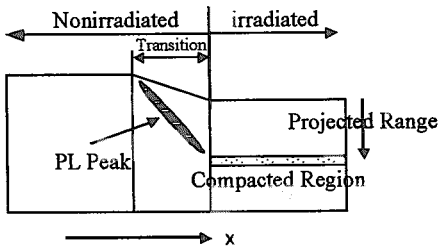

(b)

Fig.3 (a) Depth distribution of the PL intensity at 650 nm at the radiation interface, and (b) a schematic illustration of the radiation interface between irradiated and nonirrdiated regions.

The PL mapping measurement of this transition region was carried out, as shown in Fig. 3 (a).The maximum of the PL intensity can be observed at the interface region. From the existence of such an enhanced PL intensity at the interface, the buildup of stress is suggested at the interface plane. Such an interfacial stress is expected due to the significant compaction at the projected range. It is suggested here that the generation of NBOHC, which is an origin of the 650 nm PL, was promoted at the site of the radiation interface. Based on these observations, a schematic illustration of the radiation interface is shown Fig.3 (b).

3.3 Application of ion microbeam irradiation to the fabrication of optical elements

On the basis of the result of Fig. 1, we further discuss a possibility of the ion microbeam irradiation to the fabrication of optical elements. The MeV-order H^+ ion irradiation has been used for writing gratings at the core of optical fibers, since it can induce refractive index changes at the projected range, or at the depth of up to a hundred μm [3]. On the other hand, for the case of heavy-ion irradiation, refractive index increases can be made not only at the projected range, but at the trajectory of ions from the surface to several μm in depth.

It is implied here that together with a precise beam scanning technology of ion microbeam developed at TIARA, heavy-ion irradiation can be applied to the fabrication of functional optical elements on planar optical waveguide structures with a thickness below 10 μm. Aiming at the development of the heavy-ion microbeam technique for optical elements on planar optical waveguides, evaluation of the radiation effects with micrometer-scale dimensions, will be made on the basis of the AFM and micro-PL measurements techniques developed in this study.

References

1) H. Nishikawa et al., JAERI-Review 2001, TIARA Annual Report 2000, pp.235-237.

2) H. Nishikawa et al., Nucl. Instr. and Meth. B 191(2002) 342-345.

3) M. Fujimaki et al., Opt. Lett. 25 (2000) 88-89.

5.16 Uptake of Heavy Metals by Synthetic Mica and Apatite

Naofumi Kozai[*], Toshihiko Ohnuki[*], Sridhar Komarneni[**], Tomihiro Kamiya[***], Takuro Sakai[***], Shoichi Oikawa[***], Takahiro Sato[***]
Dept. of Environmental Science, JAERI[*]
Materials Research Institute, The Pennsylvania State University[**]
Advanced Radiation Technology Center, JAERI[***]

1. Introduction

Heavy metals are generally toxic to plants and animals including humans and heavy metal contamination of soils and water is a worldwide problem. Appropriate techniques for protection and remediation of environment are thus needed to be developed.

We have been investigating performances of various sorbents for removing and decontaminating heavy metals in soils and water. A synthetic mica named Na-4 mica and apatite are promising sorbents for heavy metals. Na-4 mica has high ability to sorb heavy metal cations such as Ra, Cd, and Pb[1, 2]. This clay has a layered structure and immobilizes heavy metal cations in the interlayer of the layered structure. Apatite ($Ca_5(PO_4)_3(OH, F)$) is a calcium phosphate mineral with very low solubility and the heavy metals sorbed on apatite form phosphate minerals with very low solubility[3, 4]. However, the performances of those sorbents in sorption and removal of heavy metals were investigated under limited conditions.

The objectives of this study are to get better understanding of 1) performance of those sorbents in removing and decontaminating heavy metals from water and 2) sorption behavior of heavy metals on solids. For these purposes, this study investigated uptake of heavy metals on Na-4 mica, apatite, and their mixture by a combination of batch type sorption experiments and micro-proton-induced X-ray emission (micro-PIXE) analysis. The spatial resolution of the micro-PIXE analyzing system developed in the TIARA facility, JAERI is less than 1 μm in diameter [5], which allows us to obtain highly sensitive two-dimensional element-mapping and is thus suited for investigating distribution of elements sorbed on a mixture of solids.

This study chose Ba and Cd as objective elements. Ba was used as a simulant of Ra. Ra is a radioactive nuclide contained in wastes generated through refinement of uranium and rare earth elements from their ores. Cd was used as a representative of non-radioactive toxic heavy metals.

2. Experimental

Na-4 mica was prepared as described elsewhere[7]. The synthetic apatite used was fine powder of calcium phosphate (Wako Pure Chemical Industries, Ltd.) having a hydroxyapatite ($Ca_5(PO_4)_3OH$) composition and structure.

Ba and Cd solutions were prepared by dissolving $BaCl_2$ or $CdCl_2$ in $1x10^{-2}$M $NaClO_4$ solution to have a Ba or Cd concentration of $1x10^{-4}$ M.

For the uptake experiments, the starting pH of 4 ml aliquots of the Ba solution in a centrifuge tube was adjusted at 5. Similarly, the starting pH of the Cd solution was adjusted at 3. At those pHs, Ba and Cd exist as cation. After the pH adjustment, a weighed amount (20mg) of the sorbent was added to the solution.

After a prescribed period of time of the contact at room temperature, the solid and liquid phases were separated by centrifugation. The Ba and Cd concentrations in solutions were measured by an inductively coupled plasma atomic emission spectrometer (ICP-AES). Uptake of Ba and Cd was determined as the distribution coefficient, K_d (ml/g), defined as the ratio of the amount of the Ba or Cd sorbed per gram of solid to the amount of the Ba or Cd remaining per ml of solution. The higher the K_d value, the higher the uptake of the element.

The solid separated from the solution was washed with purified water. Then, the spatial elemental distribution of a portion of the solid phases spread on a glassy carbon plate was measured by the micro-PIXE analyzing system in the TIARA facility, JAERI.

3. Results and Discussion

After 24 hours equilibration, the K_d of Ba for Na-4 mica (4.6×10^4 ml/g) was two orders of magnitude higher than that for apatite (4.4×10^2 ml/g). Figure 1 shows the distribution of Si, Ba, and Ca of the mixture of two sorbent contacted with a Ba solution, where Si is the component of Na-4 mica and Ca is that of apatite. The region where Ba was detected is in good agreement with the region where Si was detected, indicating that most of Ba was taken up by the Na-4 mica in the mixture. This result is consistent with what is expected from the K_d values of Ba for the two sorbents.

After 24 hours equilibration, the K_d of Cd for Na-4 mica (8.4×10^5 ml/g) was one order of magnitude higher than that of apatite (8.2×10^4 ml/g). Figure 2 shows the distribution of Si, Cd, and Ca of the mixture of Na-4 mica and apatite contacted with a Cd solution, where Si is the component of Na-4 mica and Ca is that of apatite. The region where Cd was detected is in good agreement with the region where Ca was detected, indicating that Cd was selectively taken up by the apatite. This result obtained by micro-PIXE analysis is inconsistent with what is expected from the above K_d values for Na-4 mica and apatite. As shown in Fig. 3, the uptake of Cd by apatite is more rapid than that by Na-4 mica. The sorption of Cd on apatite is irreversible[4]. It is thus believed that Cd was taken up by the apatite in the mixture immediately after the introducing the mixture into the solution and thereafter most of the taken up Cd remained on the apatite (little fraction of the Cd on the apatite was re-sorbed onto the Na-4 mica in the mixture).

The following conclusions may be drawn. Na-4 mica is excellent in removal of Ba (Ra) from solution and superior to apatite in K_d of Cd at sorption equilibrium. Apatite however may be a better sorbent for Cd than Na-4 mica because the uptake is more rapid than Na-4 mica. K_d of element for solid at sorption equilibrium is not the only factor to determine sorption and distribution of the element on between solid mixtures (e.g. soils). Kinetics and (ir)reversibility of the sorption are also important factors. Elemental mapping using micro-PIXE is convenient and powerful method for study on sorption of elements on solids.

Future Plan

Natural minerals such as clays and iron minerals are also candidates of sorbent for heavy metals. Chemical conditions of surrounding environment such as pH and coexisting anions determine chemical forms of heavy metals such as Cd. These are the subjects to be investigated in future studies.

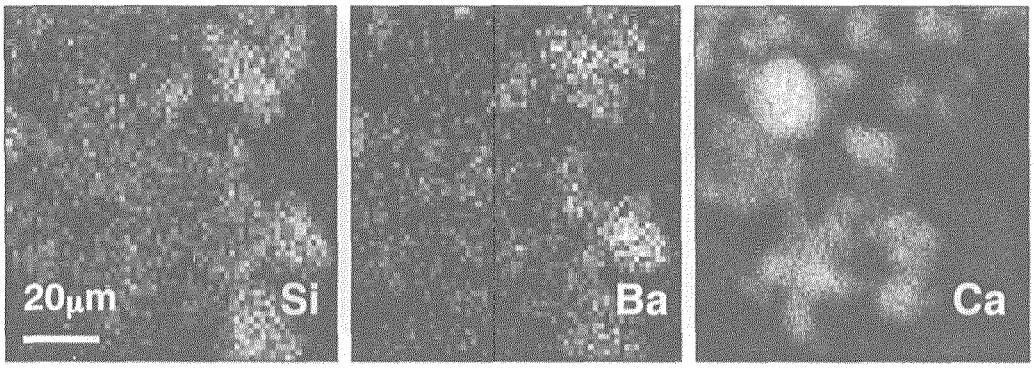

Fig. 1 Distributions of Si (Na-4 mica), Ba, and Ca (apatite) in the mixture of Na-4 mica and apatite obtained by micro-PIXE. The above pictures indicate the same region of the mixture spread on a carbon plate. A brighter region shows higher concentration of a given element.

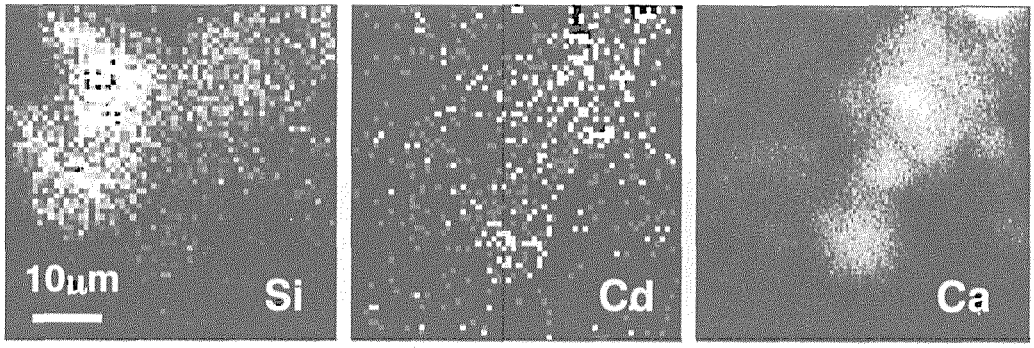

Fig. 2 Distributions of Si (Na-4 mica), Cd, and Ca (apatite) in the mixture of Na-4 mica and apatite obtained by micro-PIXE. The above pictures indicate the same region of the mixture spread on a carbon plate. A brighter region shows higher concentration of a given element.

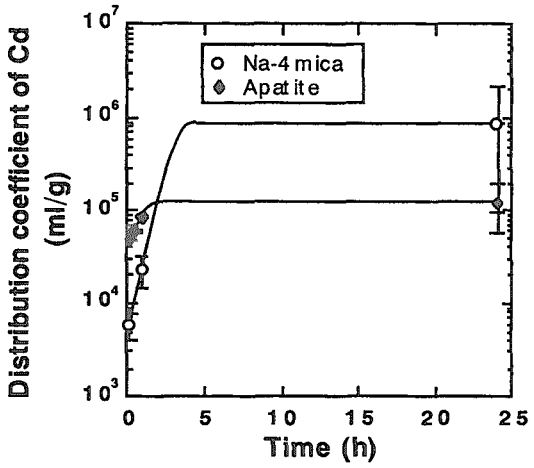

Fig. 3 Kinetics of Cd uptake by Na-4mica and apatite.

References

1) S. Komarneni, N. Kozai., W. J. Paulus, Nature, 410 (2001) 771

2) S. Komarneni, W. J. Paulus, R. Roy, Proc. Int. Conf. Ion Exchange, 51 (1991)

3) J. R. Brown, W. S. Fyfe, F. Murray, B. I. Kronberg, Canadian Mining J. Canada, 102 (1981) 71

4) Y. Xu, F. W. Schwartz, Environ. Sci. Technol., 28 (1994) 1472

5) T. Kamiya, T. Suda, R. Tanaka, Nucl. Instr. Meth. B, 118 (1996) 447

6) T. Ohnuki, N. Kozai, Radiochim. Acta, 68 (1995) 203

7) S. Komarneni, R. Pidugu, J. E. Amonette, J. Mat. Chem., 8 (1998) 205

This is a blank page.

6. Nuclear Science and RI Production

This is a blank page.

6.1 $^{13}NO_3^-$ yield in proton-irradiated water for different materials of a target chamber

N. S. Ishioka, S. Watanabe, T. Ito, C. Mizuniwa, S. Matsuhashi and T. Sekine
Department of Ion-Beam-Applied Biology, JAERI

1. Introduction

In the TIARA facility, compounds labeled with short-lived positron emitters such as ^{11}C, ^{13}N and ^{18}F, and the concomitant instrument, that is, the positron emitting tracer imaging system[1] (PETIS), are available to the biological researcher as tools for visualizing physiological functions of a living plant.

In plant physiology, it is particularly important to know behavior of various nitrogen compounds as nutrients needed for growth of a plant. The $^{13}N(t_{1/2}=10$ min)-labeled nitrate($^{13}NO_3^-$) as a radiotracer is valuable for this aim. Our earlier work illustrated that $^{13}NO_3^-$ can be produced using the $^{16}O(p,\alpha)^{13}N$ nuclear reaction on natural pure water.[2] In proton-irradiated water the major chemical species observed are $^{13}NO_3^-$, $^{13}NO_2^-$ and $^{13}NH_4^+$. To obtain $^{13}NO_3^-$ of high radiochemical purity, $^{13}NH_4^+$ can be separated from irradiated water using a cation exchange resin. However, it is difficult to separate $^{13}NO_2^-$ from irradiated water. Therefore, irradiated water is required to have high radiochemical purity of $^{13}NO_3^-$.

Dose effects of ^{13}N product distribution in irradiated water were observed in several studies.[3,4] In general, with increasing dose, the proportion of the higher oxidation state ($^{13}NO_3^-$) increases at the expense of the lower oxidation states ($^{13}NO_2^-$, $^{13}NH_4^+$). This dose effect is observed only in low dose region of about 0.3 μA·h. The highest $^{13}NO_3^-$ yield in pure water is 85 ±5% in high dose region of about 30 μA·h.

In this paper, we report the results of our studies of a method for direct in-target production of $^{13}NO_3^-$ in low dose region. The parameter investigated for its effect on the ^{13}N product distribution is materials of a target chamber.

2. Experimental

Irradiation

Using the AVF cyclotron, we can produce ^{13}N by bombarding the target of natural water with protons. Our system has been characterized by the method of transport of water target.[5] Instead of transporting through a long tube (45 m×2), our water target contained in a metallic vial is transferred semi-automatically by a small truck between the irradiation port and the hot cell. The target vial is loaded with 6 ml of the target water, through which a stream of oxygen is bubbled in advance, kept in a refrigerator to freeze the water, and housed in an Al holder. The target set at the irradiation port is preceded by a 100 μm Ti vacuum isolation window and helium cooling is done between the two windows (vacuum and target). The incident energy on target is estimated to be 16 MeV for primary proton energy of 20 MeV. All irradiations were carried out with integrated beam currents of 1 μA × 8 min, that is, approximately 0.1μA·h.

Target vial

Four different body material and window-foil combinations with the same dimensions were used for the present experiments. The inside of a target body is 15 mm in diameter and 46.5 mm deep, and the foil thickness was 0.1 mm. The water was sealed with a silicon cap. These combinations included: (1) an aluminum body with an aluminum foil; (2) a titanium body with a titanium foil; (3) a silver body with a silver foil; (4) a platinum-plated nickel body with a platinum-plated nickel foil.

Product identification

The ^{13}N species were analyzed by radio-HPLC. Conditions were: Shimadzu Shim-pack IC-A1 column, 4×250 mm, 3.5 mM Phosphate buffer, pH=6.7, 1.5 ml/min, Shimadzu SPD-6A uv spectrophotometric detector coupled to Packard Radiometric Flo-One/beta Model A-500 radioactivity detector, 210 nm. Retention times of the radiolabeled products were compared with the calibrated retention times of known standards.

3. Results and Discussion

From Fig. 1, one can note that $^{13}NO_3^-$ and $^{13}NO_2^-$ were main products, and the yield of $^{13}NH_4^+$ was negligible. This indicates that the $^{13}NH_4^+$ was effectively oxidized even in low dose irradiation, because in the reaction mechanism proposed by Tilbury and Dahl,[4] and Mahmoud *et al.*[6] $^{13}NH_4^+$ is initially produced, and then oxidized successively into $^{13}NO_2^-$ and $^{13}NO_3^-$. This distribution of ^{13}N-labeled compounds can be changed dramatically when a small amount of ethyl alcohol is added to a water target as a radical scavenger to produce mainly $^{13}NH_4^+$, as described elsewhere.[4]

For the production of $^{13}NO_3^-$, the silver target body has yielded the largest yield of 92%; this value is at the same level with that in high dose region.[4] Meanwhile, the Pt-plated Ni target body has yielded the lowest yield of 56%. These results suggest that some catalytic effects contribute to the oxidation of $^{13}NO_2^-$.

References

1) Kume T., Matsuhashi S., Shimazu M., Ito H., Fujimura T., Adachi K., Uchida H., Shigeta N., Matsuoka H., Osa A. and Sekine T., Appl. Radiat. Isot., 48, (1997), 1035-1043.
2) N.S. Ishioka, H. Matsuoka, S. Watanabe, A. Osa, M. Koizumi, T. Kume, S. Matsuhashi, T. Fujimura, A. Tsuji, H. Uchida and T. Sekine, J. Radioanal. Nucl. Chem. 239, (1999), 417-421.
3) Parks N. J. and Krohn K. A., Int. J. Appl. Radiat. Isot., 29, (1978), 754-756.
4) Roy S. Tilbury and J. Robert Dahl, RADIATION RESEARCH 79, (1979), 22-23.
5) N. S. Ishioka, H. Matsuoka, S. Watanabe, A. Osa, M. Koizumi and T. Sekine, Synthesis and Application of Isotopically Labelled Compounds 1997, Wiley, Chichester, (1998), 669-672.
6) Mahmoud L. Firuzbakht, David J. Schlyer, Alfred P. Wolf and Joanna S. Fowler, Nucl. Med. Biol. 26, (1999), 437-441.

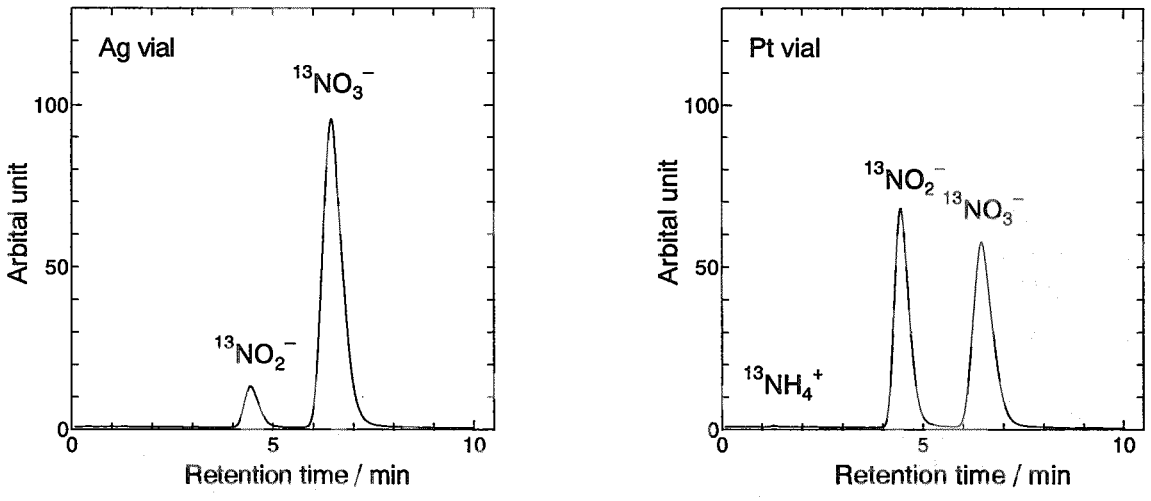

Fig.1 HPLC radiochromatogram of $^{13}NO_3^-$, $^{13}NO_2^-$ and $^{13}NH_4^+$

6.2 Dose Effects of the Production Yield of Endohedral ^{133}Xe-Fullerene by Ion Implantation

S. Watanabe*, N. S. Ishioka*, H. Shimomura**, H. Muramatsu**, T. Sekine*
Department of Ion-Beam-Applied Biology, JAERI*, Faculty of Education, Shinsyu University**

1. Introduction

The endohedral radioisotope-fullerene has been produced by using arc-discharge or nuclear-reaction-recoil processes. Products by these methods are mixtures of different species of fullerenes with different encapsulated radioisotopes. However, considering that the endohedral radioisotope-fullerene has a possibility of being new radiopharmaceuticals, a product containing one species of endohedral fullerene in high purity is desired. We have recently reported a production method to resolve this problem, confirming that by ion implantation endohedral ^{133}Xe-fullerene can be produced [1]. To achieve more efficient production of endohedral ^{133}Xe-fullerene, conditions of the ion implantation, especially ion dose, has to be studied. In the present paper, we describe dose dependence on the production yield of endohedral ^{133}Xe-fullerene from C_{60} and C_{70} targets in connection with amorphization of fullerene molecules.

2. Experimental [1]

Fullerene targets for ion implantation were made by vacuum evaporation of C_{60} or C_{70} on Ni foils. Implantation of ^{133}Xe ions into the targets was carried out with an isotope separator [2] at acceleration energies of 38 keV. Doses were in the rage of $1x10^{12}$ to $1x10^{14}$ cm^{-2}. After ion implantation, the fullerene part on the target was dissolved in *o*-dichlorobenzene. The solution was filtered through a millipore filter to remove insoluble materials. The filtrate was analyzed by high performance liquid chromatography (HPLC) with a Cosmosil Buckyprep column. Elution was done with *o*-dichlorobenzene at a flow rate of 1 ml/min. The concentration of fullerene in the effluent was continuously monitored by a UV detector. The effluent after UV measurement was collected in glass vials each for 1 min until 20 min and the ^{133}Xe radioactivity in each vial was measured by γ-ray spectrometry.

3. Results and Discussion

^{133}Xe dose was obtained from the ^{133}Xe radioactivity implanted into a target with correction for its decay during a period of measurement, storage and irradiation. Because in a ^{133}Xe beam spot area $^{132}XeH^+$ ions are considered to be implanted together with $^{133}Xe^+$ ions, the number of implanted $^{132}XeH^+$ ions was estimated from the observed beam current of $^{132}Xe^+$ ions and the $^{133}XeH^+/^{133}Xe^+$ radioactivity ratio. The resulting ^{132}XeH dose found to be one tenth of the ^{133}Xe dose is included into the ^{133}Xe dose in the following discussion.

Figure 1 shows elution curves of ^{133}Xe and C_{60} obtained from the C_{60} sample bombarded with ^{133}Xe ions at a dose of $2.0x10^{12}$ cm^{-2}. The strong correlation observed between the C_{60} and ^{133}Xe peaks corroborates the formation of ^{133}Xe@C_{60}.

HPLC data obtained from the other samples also corroborate the formation of $^{133}Xe@C_{60}/C_{70}$. In order to evaluate the efficiency of the formation of $^{133}Xe@C_{60}/C_{70}$, the yield of $^{133}Xe@C_{60}/C_{70}$ was defined as a percentage of the radioactivity of $^{133}Xe@C_{60}/C_{70}$ to that of ^{133}Xe implanted into the target. The radioactivity of $^{133}Xe@C_{60}/C_{70}$ was obtained from the sum of the ^{133}Xe radioactivities in the fractions from 3 to 10 min. The yields of $^{133}Xe@C_{60}/C_{70}$ were plotted as a function of ^{133}Xe dose in Fig. 2. The yields of $^{133}Xe@C_{60}/C_{70}$ were found to decrease with increasing dose. Because an increase of the dose leads to an increase of the number of damaged fullerene molecules as reported by Kastner *et al.* [3] from their Raman spectra measurements of fullerene targets bombarded with energetic-ions, those dose dependences of the production yields can be ascribed to amorphization of $^{133}Xe@C_{60}/C_{70}$. The slopes of the straight lines, which were fitted by the method of least-squares on log-log scales, are -0.72±0.01 and -0.69±0.06 on $^{133}Xe@C_{60}$ and $^{133}Xe@C_{70}$, respectively. The fact that both slopes obtained are almost the same suggests that the amorphization process does not differ very much between $^{133}Xe@C_{60}$ and $^{133}Xe@C_{70}$.

From comparison between both lines one can note that the yield of $^{133}Xe@C_{70}$ is about twice as large as that of $^{133}Xe@C_{60}$ for the same dose. Because solid C_{60} and C_{70} have almost the same density, the yield of $^{133}Xe@C_{70}$ per C_{70} molecule is twice more than that of $^{133}Xe@C_{60}$ per C_{60} molecule. Assuming that there is no difference between the amorphization of $^{133}Xe@C_{60}$ and that of $^{133}Xe@C_{70}$, a possible explanation for this difference is that C_{70} has a higher probability of encapsulating a ^{133}Xe ion into its cage than C_{60}. This is partly supported by the fact that a C_{70} molecule has 25 six-membered rings and a C_{60} molecule 20 six-membered rings.

References

[1] S. Watanabe *et al.*, J. Radioanal. Nucl. Chem. in press.

[2] T. Sekine *et al.*, J. Radioanal. Nucl. Chem. 239 (1999) 127.

[3] J. Kastner *et al.*, Appl. Phys. Lett. 65 (1994) 543.

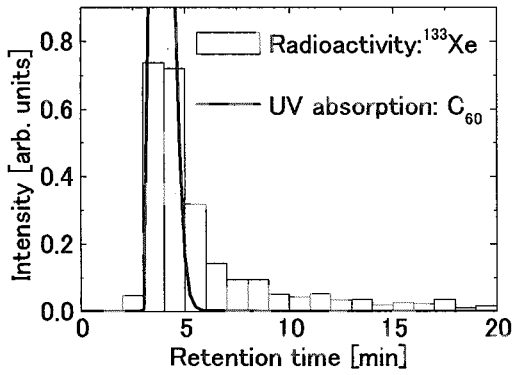

Fig.1. HPLC elution curves of ^{133}Xe and C_{60} obtained from the C_{60} sample bombarded with ^{133}Xe ions at a dose of 2.0×10^{12} cm^{-2}.

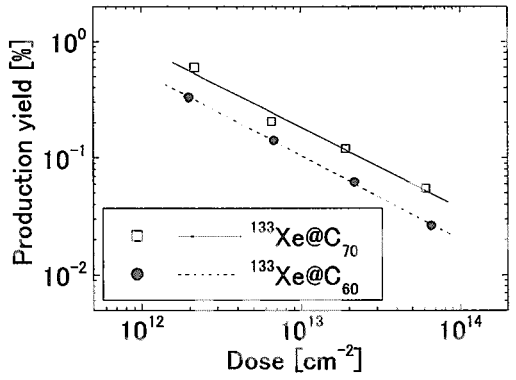

Fig.2. The yield of $^{133}Xe@C_{60}/C_{70}$ as a function of ^{133}Xe dose.

7. Microbeam Application

This is a blank page.

7.1 Development of High-Energy Heavy Ion Microbeam & Single Ion Hit System

T. Kamiya*, M. Oikawa*, W. Yokota*, Y. Kobayashi**, T. Funayama**
Advanced Radiation Technology Center, JAERI*
Department of Radiation Research for Environment and Resources, JAERI**

1. Introduction

In TIARA facilities of JAERI Takasaki, a focusing and scanning high-energy heavy ion microbeam system on the vertical beam line of AVF cyclotron was required for an application of biomedical science, such as radio microsurgery with a spatial resolution of 1 μm level. A collimate type microbeam and single ion hit system has been developed on another beam line (HZ course) of the cyclotron machine [1], and individual cell irradiation experiments have already been started using the system [2]. However, this existing system has limitation in the spatial resolution and irradiation speed of 10 μm and 2 sample positions per minute, respectively due to the collimate type microbeam forming and stage manipulate type sample positioning, although a fully automated single ion hit technique is applied to the system. The new system consisting of a two step slit system in object slits and divergence defining slits, a quadruplet quadrupole magnet system, and XY scanning coils was designed to irradiate sample positions in a spatial resolution of 1 μm with a irradiation speed of more than 1000 positions per minute. In consideration of chromatic aberration in lens focusing, it is necessary to minimize the energy spread $\Delta E/E$ of 10^{-4} or less for 10 MeV/u class heavy ion beams from the cyclotron machine. To make the high voltage in acceleration phase as constant as possible, a flat top acceleration technique was introduced into the cyclotron RF system [3]. Besides, in order to realize high-speed single ion irradiation of over 1000 positions per minute, a real-time single ion hit position detecting system was also designed.

This report describes an outline of the system and shows results of a preliminary experiment.

2. Detail of high-energy heavy ion microbeam system

The microbeam system is installed on HX course in heavy ion room 2. The conceptual scheme of the microbeam line is shown in Fig. 1. A beam from the cyclotron is bended down by a 90 degree vertical deflection magnet, and lead into the microbeam line. The microbeam line vertical and going-down is suitable to irradiate biological samples, which are set in the atmosphere just outside of a thin film. The slit systems are also shown in Fig. 1. The micro slits are composed of two wedged shape slits crossing perpendicularly to each other on the beam axe, while the divergence defining slits are composed of ordinary four slit chips. The motion control of each slit was made

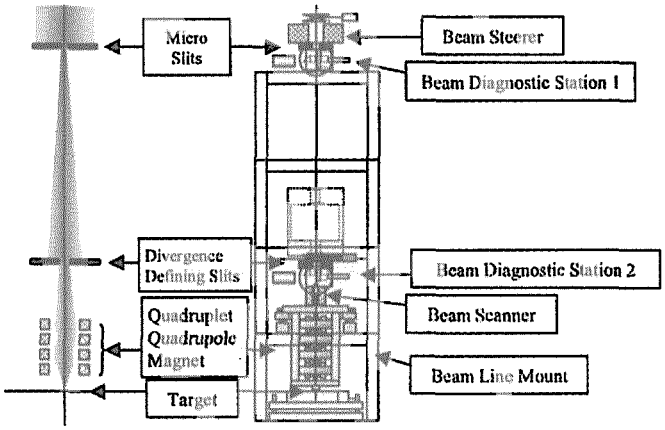

Fig. 1. Schematic of Microbeam System on the HX Course.

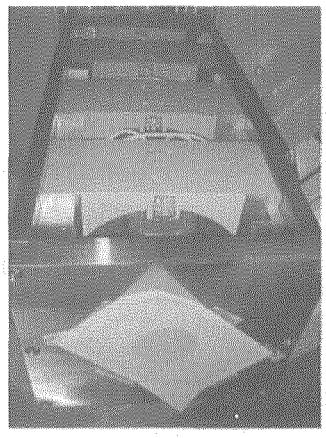

Fig. 2. Quadruplet Quadrupole Magnet.

by stepping motor drived precise stage. The beam diagnostic system consists of a beam viewer and a Faraday cup installed on the same rod manipulated by a two step pneumatic actuator. We chosen $CaF_2(Eu)$ scintillator as the beam viewer, which has a high luminous efficiency of 50, comparing with that of NaI(Tl) 100, so that lower current beam profiles can be observed by the high sensitivity camera. The focusing lens is quadruplet quadrupole magnet as shown in Fig. 2. The bore radius of the quadruplet quadrupole magnet is 15 mm, and the mechanical pole length is 150 mm. The working distance is 300 mm, and the demagnification factors in horizontal and vertical planes are 5. Air-core coils are used as the beam scanner, which has been designed to irradiate 1 mm×1 mm area of a sample in maximum for the highest rigidity of beams.

3. Outline of the real-time single ion hit detection system

In actual cell irradiation experiments, it is necessary that efficient detection of ion hit position for each cell be made for precise estimation of radiation effect. A real-time hit position detection is also required for high-speed single ion hits to a large number of target positions. Fig. 3 show an outline of the system, which we are developing. It consists of an optical microscope and super high sensitivity CCD camera to observe weak scintillation lights induced by single ion injections, as well as samples image. By super imposing single ion hit position to the sample image, irradiated positions of the sample can be obtained. Back ground noises can be filtered out with single ion detection signals by secondary electrons from the beam exit window, which single ion pass through.

4. Experiment and results

As a preliminary experiment of real-time single ion hit position detection, we examined a high sensitivity CCD camera combined with a scintillator plate to observe single ion hits at the collimate type system (HZ course). In this method, it is essential that a camera be higher sensitive and scintillator plate have higher luminous efficiency, colorless transparency and no deliquescency. A dual mode cooling CCD camera (C4884-30, Hamamatsu photonics) combined with an image intensifier unit (C8600-02, Hamamatsu photonics) and peace of sapphire plate with a thickness

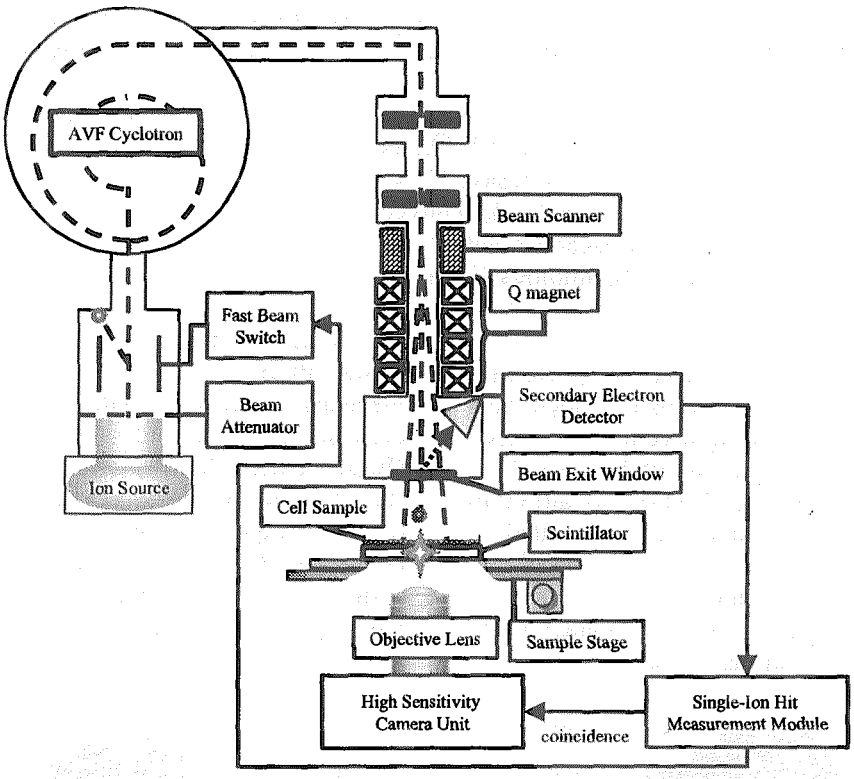

Fig. 3. Conceptual Scheme of The Real-Time Single Ion Hit Position Detection System.

of 1 mm were used in this experiment. Fig. 4 shows a 100 ms exposed photo image of scintillation by about 100 Ar ions with energy of 460 MeV. A black spot at the center indicates beam spot by the ions. The number of 100 for 460 MeV Ar ions seems to be a detection limit with this combination of the camera and the scintilator.

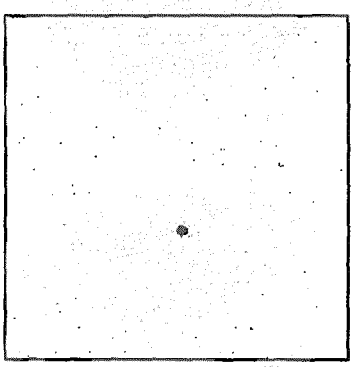

Fig. 4. Super High Sensitivity CCD Camera Image of Scintillation by about 100 Ar Ions with Energy of 460 MeV.

5. Summary

A focusing high-energy heavy ion microbeam system has been designed and under installation to the vertical beam line of TIARA AVF cyclotron accelerator. A real-time single ion hit position detection system has also been designed and preliminary experiments using super high sensitivity CCD camera system and a sapphire plate were performed at HZ course. From the result of this experiment, a perspective of real-time single ion detection could be obtained, if a scintillator with higher luminous efficiency, such as $CaF_2(Eu)$ and more sensitive CCD camera system will be used.

References

[1] T. Kamiya et al., Nucl. Instr. and Meth. B 181 (2001)27.

[2] Y. Kobayashi et al., TIARA Ann. Rep. 2000, JAERI-Review, 2001-039(2001)73.

[3] M. Fukuda, *Private Communications*.

7.2 Simultaneous Mapping of Fluoride Both in the Tooth and in the Dental Material Filled in a Cavity of the Tooth using PIGE

H. Yamamoto, Y. Iwami, S. Ebisu, M. Nomachi*, Y. Sugaya*, K. Yasuda**, T. Kamiya***, T. Sakai***, and M. Oikawa***
Graduate school of Dentistry, Osaka University
Graduate school of Science, Osaka University*
Wakasa-wan Energy Research Center**,
Advanced Radiation Technology Center, JAERI***

1. Introduction

In the dental field, the tactic of 'prevention before treatment' has been reconfirmed once again for the minimal intervention of tooth. Following the tactic, the role of fluoride (F) in the prevention of the tooth caries is attracting the more attention than before. Nevertheless, the characterization of the F in the tooth has been far from the quantitative one.

We have tried, as one of the F characterizing method, to establish a quantitative determination of F amount in a tooth with using PIGE. Today, a various kinds of F-releasing dental materials, such as a) conventional glass-ionomer cement (GIC) (Base Cement, Shofu), b) resin-modified GIC (GC Fuji II LC, GC), c) glassi-ionmer based resin composite (Reactmer, Shofu), d) compomer (Xeno CF, Sankin), e) F-releasing resin composite (Teethmate F-1, Clearseal F, Kuraray), are developed. These materials release F gradually after applying in a tooth.

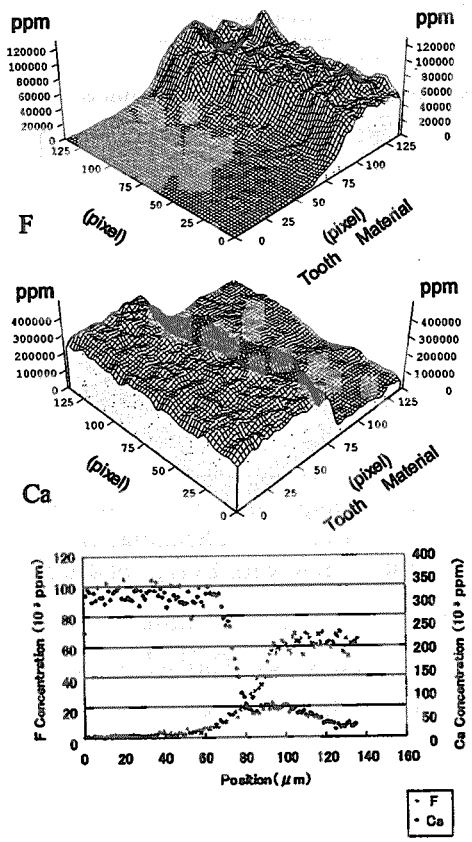

Fig.1 F and Ca distribution. Material ; the conventional GIC (Base Cement) The cement contains F necessarily included through the fabrication process, and releases the fluoride gradually after hardening in acid-base reaction. The hardening takes time.

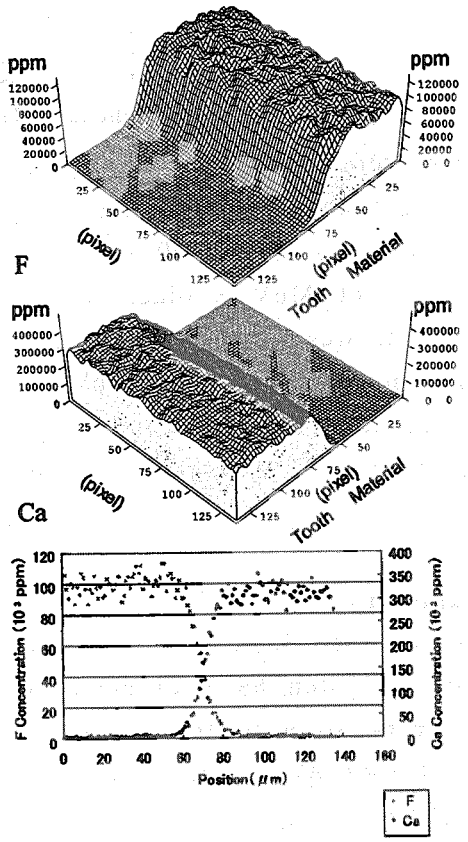

Fig.2 F and Ca distribution. Material : the resin-modified GIC (GC Fuji II LC). To reduce water sensitivity in the hardening of the conventional GIC and increase the hardness, resin composite which cures by the visible ray is mixed in the conventional GIC. The hardening of the surface layer is early.

The paper reports the quantitative simultaneous measurements of F and Ca amounts in a tooth and F-releasing material filled in the cavity in a tooth.

2.Experimenal procedure

2. 1 Experimental set-up

The experimental facility of the 1.7 MeV proton beam accelerated by the TIARA single-ended accelerator at JAERI-Takasaki, was used for this work. Precise conditions of the measurement conditions were already published in the previous report [1].

2.2 Specimens

Class V cavities were prepared at the cement-enamel junction in the buccal face of extracted human teeth and the cavities were filled with the F-releasing materials mentioned above (a-e).

The precise pre-treatment of the specimens were the same as previous experiments and precisely described in the previous reports [1,2].

3. Results and Discussion

In Fig.1-6 are shown the obtained results as the 2D mapping form.

Firstly the F penetration from the F-releasing materials to the teeth was observed in all cases.

Secondarily the aspects of both F localization in the F-releasing materials and F penetration to the tooth were somewhat different depending on the kind of releasing materials. As for the resin-modified GIC (GC Fuji II LC), large amount of F was

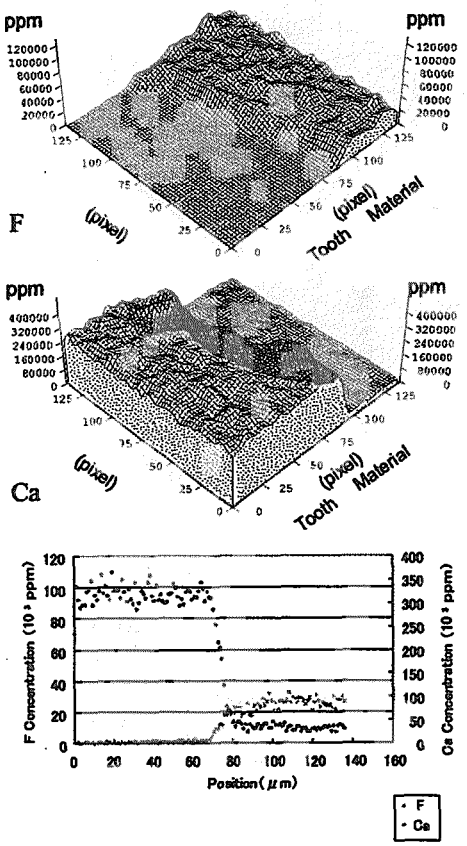

Fig.3 F and Ca distribution. Material : the glass-ionomer based resin composite (Reactmer). In order to force the characteristic of the conventional GIC and reinforce the disadvantage of GIC, the cement is the mixture of glass-ionomer phase and resin.

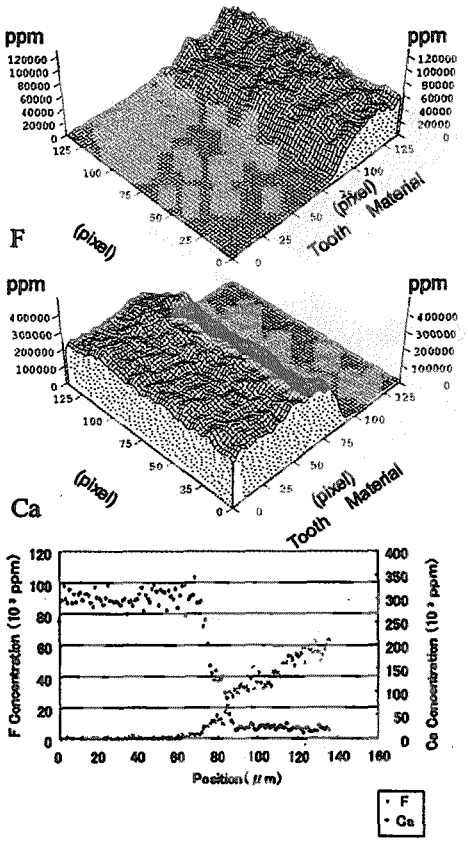

Fig.4 F and Ca distribution. Material : the compomer (Xeno CF). In order to add the characteristic of F-releasing in the conventional GIC, the part of conventional GIC is included for the resin composite.

located homogeneously in the material and high concentration F was observed at the surface of cavity dentin wall (Fig.2). The F concentration decreased rather steeply from the surface toward the inner part of the tooth. As for the Base Cement and Clearseal F, the F distribution was inhomogeneous and distributed like an island in the material (Fig.1, 6). The F distribution in the tooth showed the equal tendency to the above case. In the case of Teethmate F-1 (Fig.5), F distribution in the material was rather smooth, but in the tooth it showed rather unique or somewhat curious feature. That is to say the F concentration was the highest at the dentin surface. In the both sides of the surface, one side of which made of F-releasing material and the opposite side was the tooth, F concentrations were lower than that of at the dentin surface. Therefore it looks like a kind of mountain rage is running alongside the dentin surface. The phenomenon is different from the anticipation deprived from the simple Fuck's diffusion model in the solid and no satisfactory explanation was obtained yet.

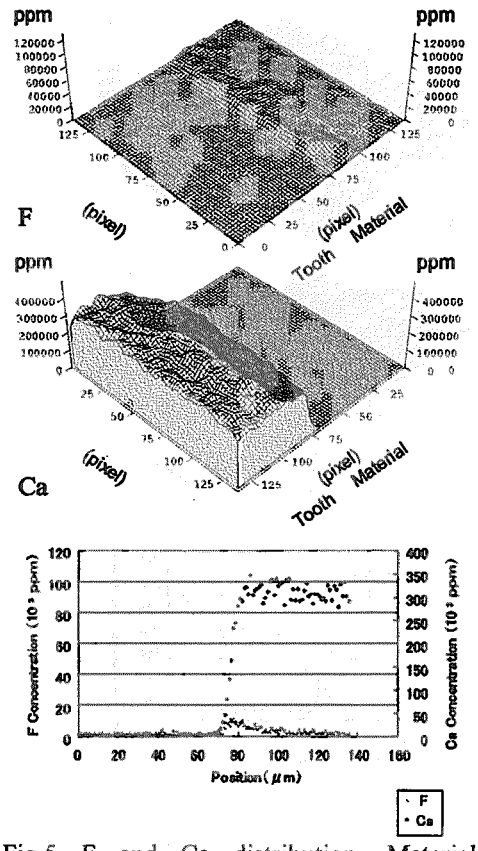

Fig.5 F and Ca distribution. Material : the F-releasing resin composite (Teethmate F-1). This resin composite contains methacryloyl F-methylmethacrylate copolymer and releases fluoride by hydrolysis.

4. Acknowledgements

We would like to thank members of TIARA, JAERI TAKASAKI for operating the accelerator facility.

References

1) M. Nomachi et al., TIARA Ann. Rep. 2000, JAERI-Review 2001-039 (2001) 244-246

2) H.Yamamoto et al., Oper. Dentistry 25 (2000) 104~112

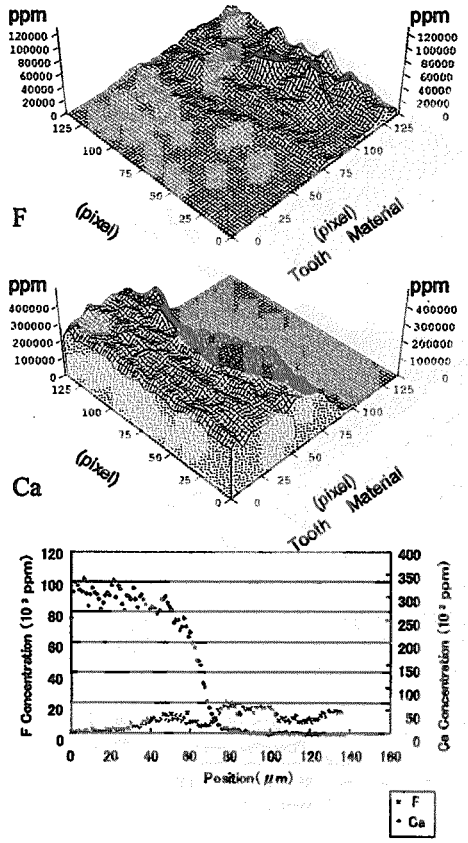

Fig.6 F and Ca distribution. Material : the F-releasing resin composite (Clearseal F). The resin contains the same co-polymer with that of Teetmate F-1 and NaF in a capsule type.

7.3 Development of In-Air Micro-PIXE Analysis System

A.Tanaka, K.Ishii, Y.Komori, S.Matsuyama, H.Yamazaki, K.Kubota*, H.Fukuda*,
T.Kamiya**, T.Satoh**, T.Sakai**, M.Oikawa**, K.Arakawa**, M.Saidoh**
Department of Quantum Science and Energy Engineering, Tohoku Univ.
Institute of Development, Aging and Cancer, Tohoku Univ.*
Advanced Radiation Technology Center, JAERI**

1. Introduction

Accelerating heavy-charged particles like protons or α particles by an accelerator at several MeV and irradiating a sample, we observe characteristic x-rays of elements contained in the sample. Since the cross sections of characteristic x-rays are very large (1000b~10000b), we can use these x-rays to analyze trace elements. This method is called PIXE (Particle Induced X-ray Emission) analysis method and all elements (except for the light elements hydrogen ~oxygen) can be simultaneously detected with high sensitivity. Therefore PIXE is widely applied to medicine, biology, engineering, environmental science, archeology and so on. Moreover, focusing the beam spot within 1μm, then scanning the surface of the sample and recording the beam position when the characteristic x-ray is detected we obtain the spatial distribution of elements in the sample. We are now developing a micro-PIXE system at the Division of Takasaki Ion Accelerators for Advanced Radiation Application (TIARA) in JAERI[1-3]. Since this system takes pictures of elemental distributions, we call it a Micro-PIXE Camera.

In a micro-PIXE analysis, Volatile elements can not detected because samples are usually irradiated in the vacuum and the volatile elements evaporate. This is serious in the case of biomedical samples that contain some important volatile elements. To analyze biomedical raw samples, we developed a micro-PIXE analysis system in which the target is set up in air and be cooled by helium gas. We call this system In-Air Micro-PIXE. The target cooling reduces the damage to target samples from beam heating. When the biological sample is irradiated in vacuum, it shrinks due to beam heating, its shape is deformed and the correct distribution of elements can not be obtained[4]. These problems are resolved by the In-Air micro-PIXE Camera[5].

The measurement of the spatial distribution of elements in a cell is one of the most useful applications. Target preparation techniques of cellular samples for the In-Air Micro-PIXE Camera are under development. Up to the present, we established the technique for single

cells which are incubated on a Mylar film of 4μm thickness. Here, we report on the target preparation techniques for tissue slices.

2. Experiment and results

We examined three techniques for target preparation of tissue slices:

1. cellular fixation with acetic acid ethanol
2. freeze-drying
3. drying in air

The tumor cells of AH109A were subcutaneously planted into the back of Donryu rats. A week after implantation, bromodeoxyuridin (BrdU) (0.5ml/rat) was administered the rats 3 times with the interval for 6 hours. The rats were sacrificed by an over dose of anesthesia and immediately their tumor tissue and liver were removed and frozen with liquid N_2. The frozen sections were cut into 10 μm thick slices with a microtome.

1) Target preparation based on the cellular fixation with acetic acid ethanol

The frozen slices were placed on a 4μm thick Mylar film, soaked in 5% acetic acid ethanol, then removed after one minute and dried in air. Figure 1 shows the PIXE spectrum of the tissue slice. Though the element S, P, and Ca are observed, electrolytic elements like K and Cl can not be detected and Br is also missing. The elemental maps of the tissue slice are shown in Fig.2. The positions where P is highly concentrated do not correspond to those of S.

2) Target preparation based on the freeze drying method

We placed the frozen slices on the 4μm thick Mylar film, placed the sample on the copper stage of a Peltier element cooled to −10℃, and dried in vacuum for two days gradually heating the copper stage to room temperature. The sample was removed after 12 hours and irradiated.

Figure 3 shows the PIXE spectrum of the sample in the case of the freeze drying method. We can recognize some elements contained in the tissue slices. Figure 4 shows the maps of P and S. In contrast to Fig.2, the high density positions of P coincide with those of S.

3) Target preparation based on drying in air

The frozen slices were placed on the 4μm thick Mylar film, put on the copper stage, thawed quickly, and dried in air. As shown in Fig. 5, the PIXE spectrum is equivalent to that of Fig.3. However, the structure of the distribution of P is different from that of S (see Fig.6).

3.Conclusion

Three methods of target preparation for tissue slices were examined. Our previous result[5] of single cells showed that the peak position of P corresponds to the nucleus and that S is distributed around the nucleus. This result just coincides with that of Fig.4. We conclude that, as far as target preparation for tissue slices is concerned, freeze-drying can be used.

The medical applications based on the present method are now being developed.

References

1) T. Kamiya, T. Suda, and R. Tanaka, Nucl. Instr. and Meth. B104 (1995)43.
2) S. Matsuyama, K. Ishii, A. Sugimoto, T. Satoh, K. Gotoh, H. Yamazaki, S.Iwasaki, K. Murozono, J. Inoue, T. Hamano, S. Yokota, T. Sakai, T. Kamiya, and R. Tanaka, Int. J. PIXE 8 (1998)203.
3) T. Sakai, et al., Nucl. Instr. and Meth. B136/138 (1998)390.

4) M.Maetz,W.J.Przybylowicz,J.Mesjasz-Przybylowicz, A. Schussler, Kurt Traxel, Nucl. Instr. and Meth. B158 (1999)292.
5) K. Ishii et al., Nucl. Instr. and Meth. B 181(2001)448.

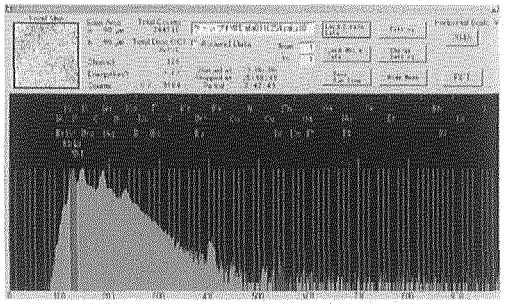

Fig. 1 PIXE spectrum of tissue slice by processing with acetic acid ethanol

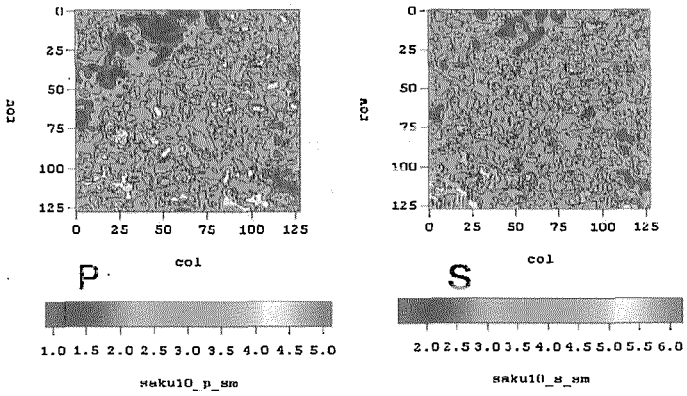

Fig. 2 Elemental maps of P and S in the tissue slice by processing with acetic acid ethanol

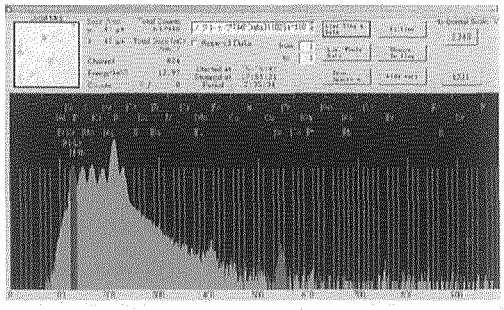

Fig. 3 Same as Fig.1 except for freeze-drying

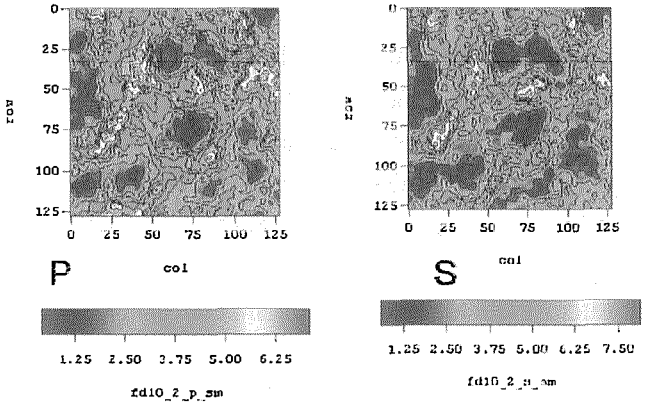

Fig.4 Same as Fig.2 except for freeze-drying

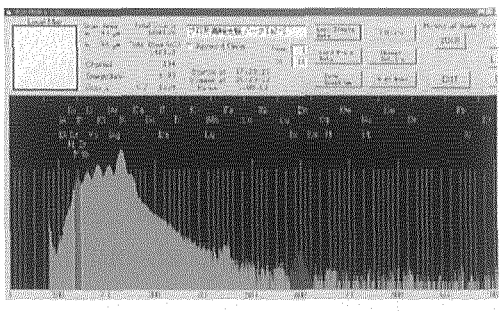

Fig.5 Same as Fig.1 except for drying in air.

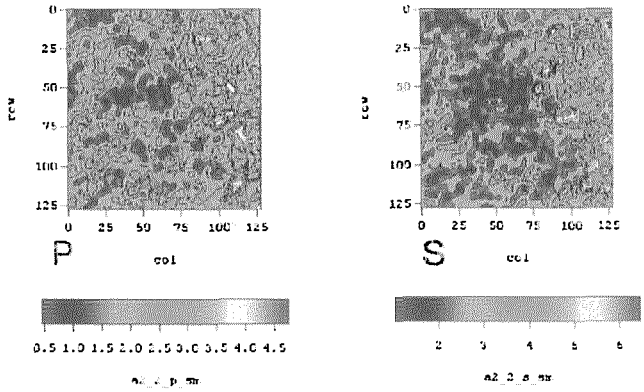

Fig.6 Same as Fig.2 except for drying in air.

7.4 Preliminary Study on Quantitative Elemental Analysis for Environmental Samples Using Micro-PIXE

M. Kasahara, C.- J. Ma, Y. Inoguchi,
T. Kamiya*, T. Sakai*, M. Oikawa* and T. Sato*
Graduate School of Energy Science, Kyoto University
Advanced Radiation Technology Center, JAERI*

1. Introduction

Investigation of the physicochemical properties of individual atmospheric pollutants like individual particles and individual raindrops is an essential prerequisite for understanding their sources, properties, and changes. Because the analysis of these samples as bulk phase leads to a loss of detailed information.

Micro-Particle Induced X-ray Emission (PIXE) is one of the most powerful micro-analytical techniques. Its greatest advantage is excellent sensitivity. Also it has the merit of being a multielement non-destructive technique with a wide range of elements for various samples. Till now, the experimental results about the individual environmental specimens using micro-PIXE have been reported[1),2)]. However, as the defective points of this micro-PIXE, quantitative elemental analysis is not generalized. One of the reasons is the difficulty of preparing of standard samples. Therefore, in this study, we made an attempt to prepare several standard samples for the subsequently quantitative analysis of individual environmental samples

2. Experimental procedure

To prepare the standard samples with uniform thickness, Si, KCl, CaF_2, and Fe reagents were deposited on polycarbonate substrate film by vacuum evaporation system (Sinkukiko Co. VPC-1100). Fig. 1 illustrates the diagram of vacuum evaporation system.

Micro-PIXE measurements were performed with a scanning 2.6MeV H^+ micro beam accelerated by 3MV single-end accelerator. To apply this quantitative elemental analysis method using micro-PIXE, individual small sized raindrops, namely, drizzle droplets were collected. For the purpose of sampling of individual drizzle droplets, collodion film method introduced by our laboratory was applied[2)]. Fallen drizzle droplets were allowed to settle on the surface of collodion film (130±10 μm) without bounce off.

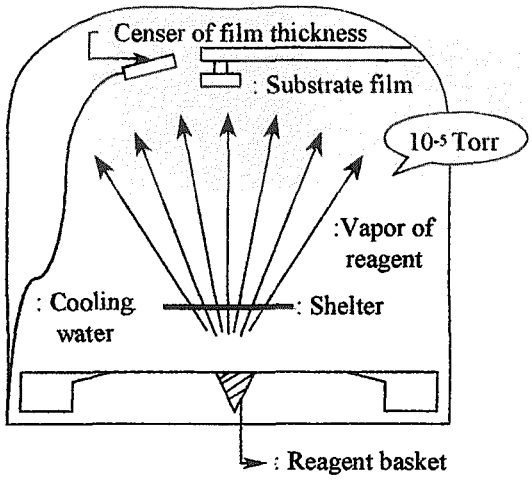

Fig. 1 Diagram of vacuum evaporation system.

3. Results and Discussion

From the analysis of standard samples, it was possible to resolve each elemental peak corresponding to channel number of micro-PIXE spectrum without concerns about filter rupture and blank concentration of contaminations. Fig. 2 shows an example of micro-PIXE spectrum of Ca standard sample.

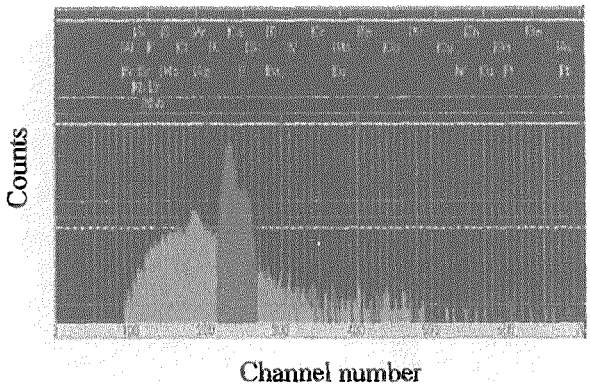

Fig. 2 An example of micro-PIXE spectrum of Ca standard sample.

After analysis of these standard samples, each element calibration curve was successfully plotted by mass thickness (μg cm^{-2}) and peak counts (counts nC^{-1}) obtained from 2.6 MeV H^+ micro beam[3]. Calibration curves for K and Cl were drawn by three points mass thickness. And those of Si, Ca, and Fe were plotted by two points mass thickness. Fig. 3 shows the calibration curve of each element plotted by mass thickness and peak count.

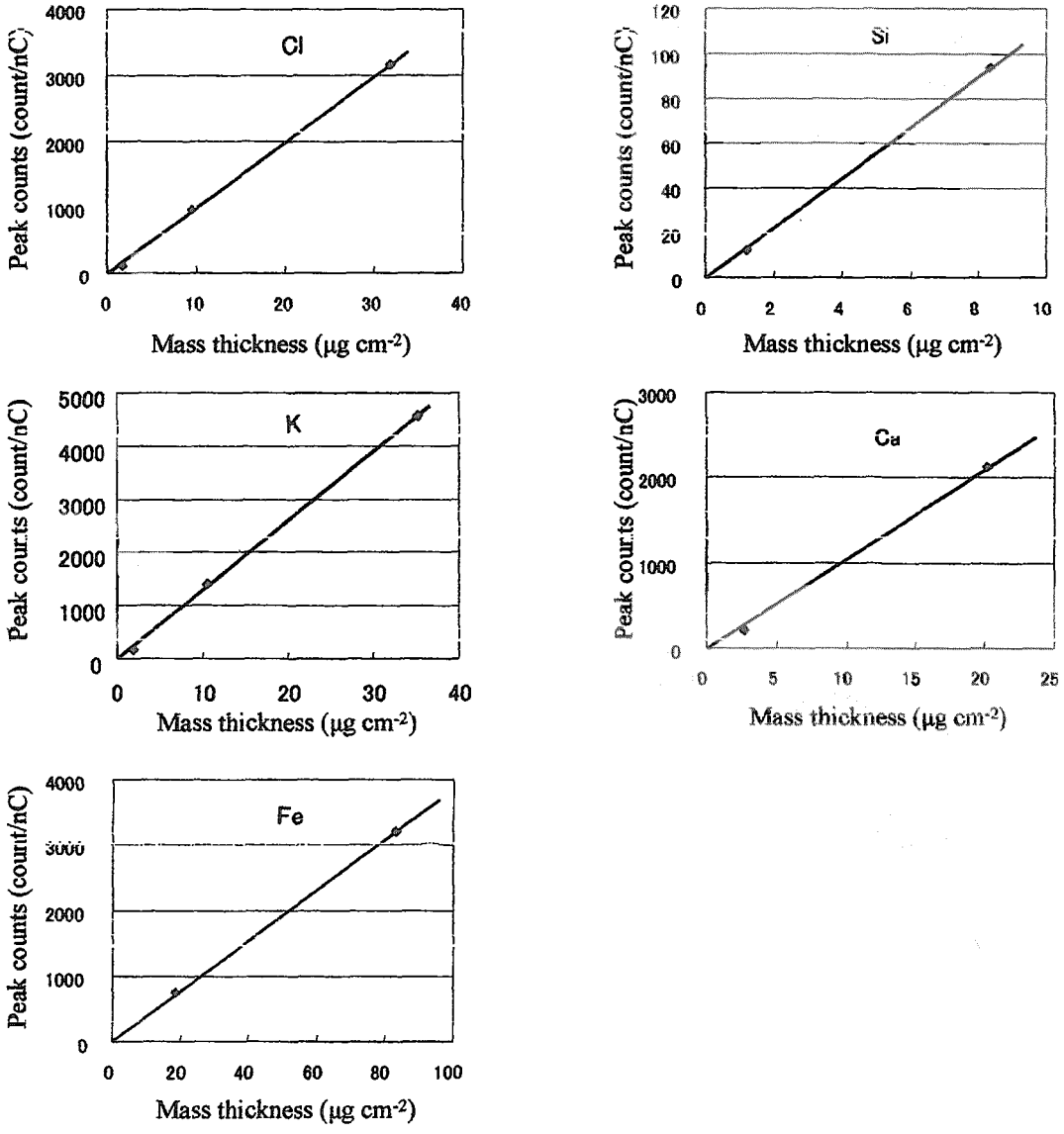

Fig. 3 Calibration curve of each element plotted by mass thickness and peak count.

In the Fig. 3, every plotted point is lying on the straight line showing good correlation coefficient between mass thickness and peak count. Furthermore we made certain of the high degree of analytical accuracy from the analysis of standard samples.

As shown in Photo 1, by collodion method, a drizzle droplet was successfully replicated on the collodion film.

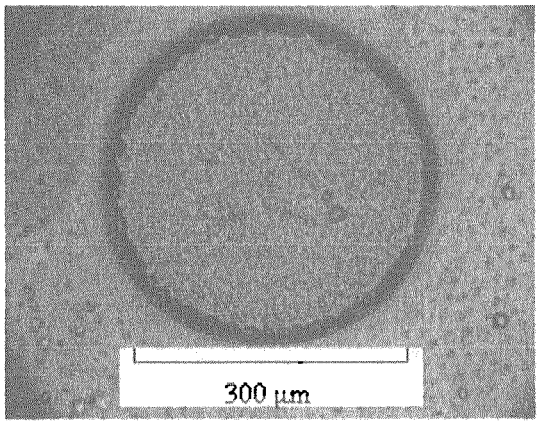

Photo 1 Digital microscopic image of a drizzle droplet replica formed on collodion film.

Ca distribution and micro-PIXE spectrum of a whole single drizzle droplet are shown in Figs 4 and 5, respectively. Ca was found to be quite distributed at rim portion of a droplet.

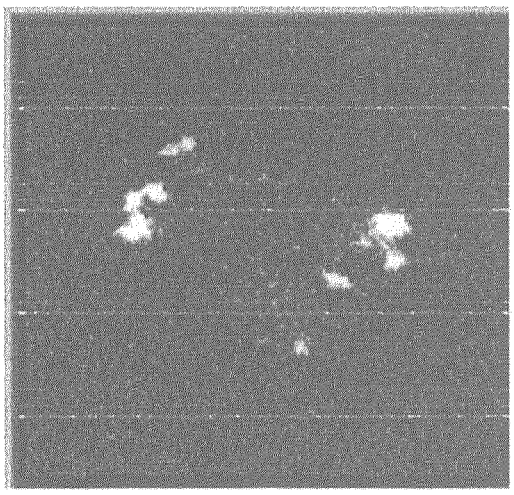

Fig. 4 Ca maps obtained by micro-PIXE analysis on a drizzle droplet. Scanning area is 580 μm × 580 μm.

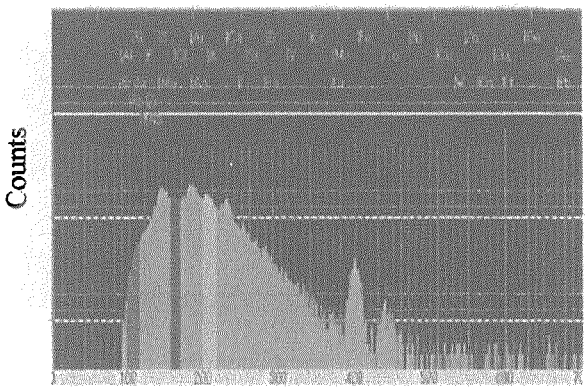

Fig. 5 Micro-PIXE spectrum of a whole single drizzle droplet collected on the collodion film.

Also other soil originated components like K and Fe formed significant peaks with that of S. Kuroiwa (1961)[4] observed the chemical composition of the residues from cloud droplet. His observations implied that particles derived from soil account for about 28 % of the residue left by evaporated cloud droplet. It is therefore, suggested that cloud condensation nucleation was mainly initiated from soil components in our sampling periods.

We attempt to calculate the mass thickness and mass of each element retained in individual drizzle droplets using each element calibration curve, sample's net counts, and micro beam scanning area. Each elemental mass in a single drizzle droplet (300 μm diameter) is ranged from 0.1 ng to 0.19 ng.

Further studies such as increasing the kind of standard samples and applying to this quantitative analysis to other elemental samples are in progress.

References

1) E. Koltay, I. Rajta, J.R. Morales, I.B. Kiss and A.Z. Kiss, Nucl. Instr. And Meth. B 150 (1999) 375-383.

2) C.-J. Ma, M. Kasahara and S. Tohno, Water, Air and Soil Pollution 130 (2001) 1601-1606.

3) Y. Inokuchi, Thesis of master degree in Graduate School of Energy Science, Kyoto University (2001).

4) D. Kuroiwa, Tellus 13 (1961) 252-259.

7.5 Application of In-Air Micro-PIXE Analysis System to the Study of Metabolic Function in the Cell

K. Kubota*, H.Fukuda*, K.Ishii, A.Tanaka, S.Matsuyama, H.Yamazaki,
T.Kamiya**, T.Satoh**, T.Sakai**, M.Oikawa**, K.Arakawa**, M.Saidoh**
Department of Quantum Science and Energy Engineering, Tohoku Univ.
Institute of Development, Aging and Cancer, Tohoku Univ.*
Advanced Radiation Technology Center, JAERI**

1. Introduction

Recently, we have developed in Air micro-PIXE Camera[1-3] in Takasaki Ion Accelerators for Advanced Radiation (TIARA), that enables analysis of tracer elements distribution with high spatial resolution of below 1 micron in samples placed in room air condition. Analysis of elemental distribution in a cell is difficult, and some technical developments for cultured cells have already been achieved by us[4,5]. Cells cultured on a thin membrane was processed for target sample together with the membrane, and PIXE was carried out in-air condition, resulted in successful measurement of elemental distribution with 10^{-13}g level of sensitivity and 0.2micron level of spatial resolution[4,5].

In addition to the analysis of cultured cells, there may be a need for analysis of tissue samples obtained from living subjects especially in the field of biology and medicine. A new target preparation method has also been developed for sliced section of animal tissue by us[6]. Here we reported the results of PIXE analysis of experimental tumor tissue transplanted in rats using our new methods.

2. Target preparation

In order to identify the location of nuclei in tissue samples, we have injected bromodeoxyuridine to rats intravenously. Bromodeoxyuridine is incorporated into DNA synthesis in the nuclei, and the nuclei labeled with bromine can be detected by PIXE. One week after transplantation of AH109A(rat hepatome cells) in the back of Donryu rats subcutaneously, rats were killed by overdose of anesthesia. Solid tumors of 1cm diameter were excised, frozen by liquid nitrogen, thin sectioned by crio-microtome. Ten and 30micron thick sections were mounted on 4micron thick Mylar film, fixed with 3% acetic acid ethyl-alcohol, and freeze-dried for the target of PIXE. Because 10 micron thick sections may destruct the cell structure by cutting the middle of cell, 30 micron samples were prepared to preserve the whole cell structure.

3. Results of PIXE analysis

The target samples prepared as above have been set at the target holder of in-air micro PIXE camera and bombarded with proton micro-beam of 2.6 MeV. The area of 45micron square was scanned. Figure 1 shows the photograph of 10

micron section after irradiation observed by phase-contrast microscope. We distinguished the cellular region from the empty region by this figure. In the characteristic X-ray spectrum, the elements P, S, Cl, Ca, K, and Br were identified. Figure 2 shows the elemental maps for these elements, where the cellular regions recognized by Fig.1 are surrounded with the blue line. Distribution of phosphorus was localized both in 10 and 30 μm sections. Other elements were distributed surrounding the high concentration area of phosphorus. The counts of both zinc and bromine were too low to form any specific localization within the tissue. There is a tendency that higher concentration of bromine was observed in the same area of high phosphorus concentration. The samples of 30 micron were cracked during the ion bombardment.

4. Discussion

In this experiment, clear images of the cell as seen in previous single cell experiments were not observed. We considered for this reason that the cell structure was destructed by cutting the middle of cell because of 10 μm thickness. In this experiment, therefore, 30 μm section samples were also prepared to preserve the whole cell structure. However, the results of 30 μm sections were the same as 10 μm sections. We observed 10 μm sections after beam irradiation by a phase-contrast microscope (see Fig.1). As the results, the areas of elements distribution were corresponded to the area of viable cancer cells. When we used the elements distribution image of single cells as the reference, the localized distribution of phosphorus was considered to delineate the shape of nuclei of individual cancer cells.

A little of bromine distribution was observed in the area of nuclei in this experiment. In cultured cell, bromine will be transferred to the cell directly from the medium through the cell membrane, while in the tumor tissue in vivo, the delivery of bromine to cancer cell depends on the blood flow to the tumor and on the micro circulation within the tumor tissue. In addition, the growth fraction of in vivo tumor tissue seems to be lower than that of cells in vitro. That will affects the incorporation rate of bromodeoxy-uridine into the tissue. As the results of these factors, the amount of bromine detected seems to become small. A little but definite counts of bromine were recorded, it suggested that if we can use a large field of view X-ray detector that has the sensitivity of 10 times higher than that of the current system, we can analyze the specific localization of various metal compounds within tissue samples. That may open a new possibility of PIXE analysis for biological samples, especially for tissue localization study of metal compound given in vivo.

References

1) T. Kamiya, T. Suda, and R. Tanaka, Nucl. Instr. and Meth. B104 (1995)43.
2) S. Matsuyama, K. Ishii, A. Sugimoto, T. Satoh, K. Gotoh, H. Yamazaki, S.Iwasaki, K. Murozono, J. Inoue, T. Hamano, S. Yokota, T. Sakai, T. Kamiya, and R. Tanaka, Int. J. PIXE 8 (1998)203.
3) T.Sakai, et al., Nucl. Instr. and Meth. B136/138 (1998)390.
4) A. Sugimoto, K. Ishii, S. Matsuyama, T. Satoh, et al. International Journal of PIXE,, 151 (1999).
5) K.Ishii, A.Sugimoto, A.Tanaka, T.Satoh,

S.Matsuyama, H.Yamazaki, C.Akama, T.Amartivan, H.Endoh, Y. Oishi, H.Yuki, S.Suegara, M.Satoh, T.Kamiya, T.Sakai, K.Arakawa, M. Saidoh, S.Oikawa, Nuclear Instrument and Methods in Physics Research B 181, 448-453 (2001).

6) A.Tanaka et al., JAERI-Review 2000-024, p230-p232.

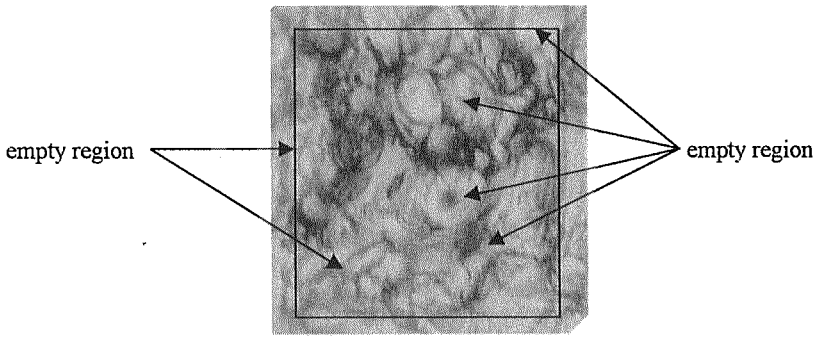

Fig.1 Photograph of the 10 μm tissue slice of AH109A tumor after beam irradiation

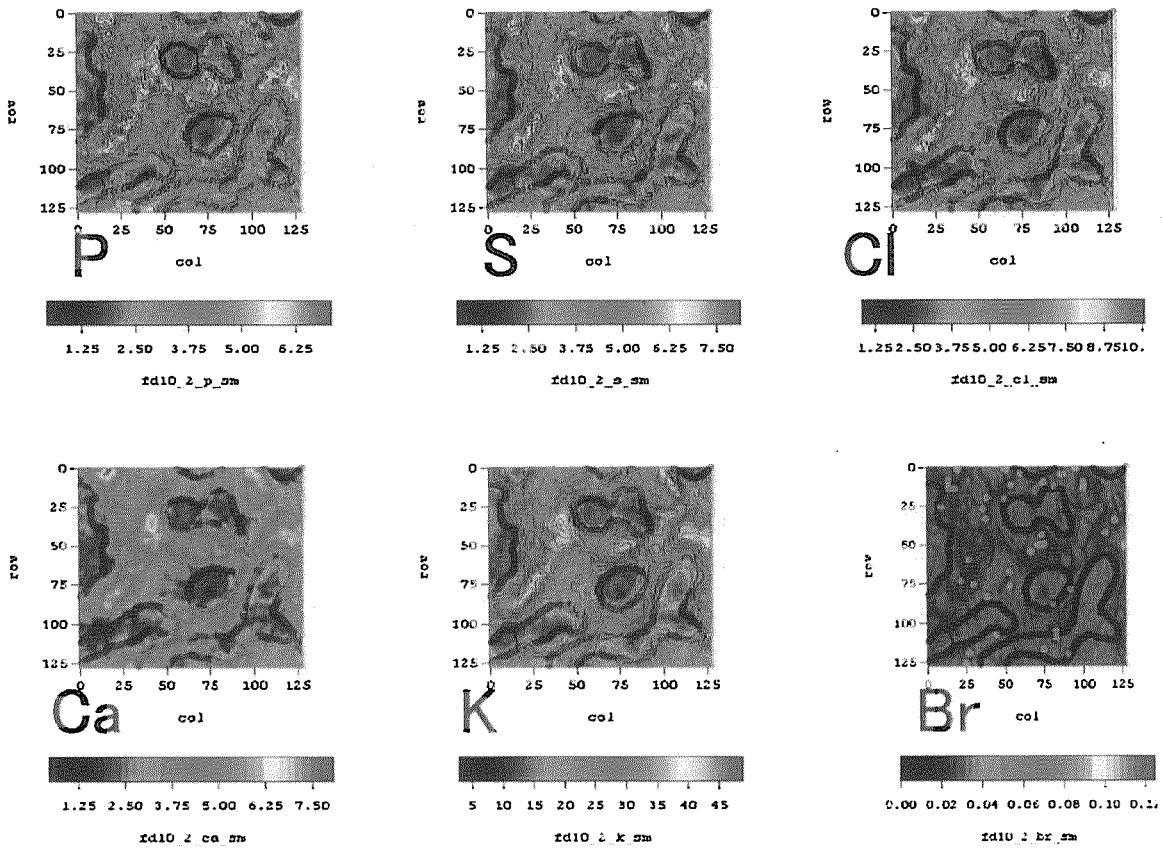

Fig.2 Elemental maps of P, S, Cl, Ca, K, and Br in the 10 μm tissue slice. The tissue was freeze-dried under vacuum.

7.6 Development of a Large-Solid-Angle Multi-Element Detection System for High-Sensitivity Micro-PIXE Analysis

T. Satoh*, T. Kamiya*, T. Sakai*, M. Oikawa*, K. Ishii**, S. Matsuyama** and H. Yamazaki**
Advanced Radiation Technology Center, JAERI*
Department of Quantum Science and Energy Engineering, Tohoku University**

1. Introduction

Since detection efficiency is strongly limited in the micro-PIXE analyzing system using a single X-ray detector, a few hours are required in order to measure the distribution of trace elements in a single cell. Moreover, biological samples such as cultivation cells require very low irradiation intensity. Therefore, reduction in measurement time is an important problem which should be solved for application to medicine, biology and so on.

The purpose of this development is enlarging solid angle of an X-ray detector and reducing measurement time by about 1/10. The easiest method of enlarging a solid angle is bringing a large sensitive area detector close to a sample as much as possible. Our large solid angle detector is realized by placing many minute detection devices in a same vessel. The counting rate of back-scattered protons per detection element is small despite lack of a passive absorber. It appears possible that X-rays from the very small quantity of elements contained in a cell could also be detected.

2. Experiment

A new detection apparatus consists of a multi-element detector (EPIX 60-26, EURISYS MEASURES Co., Ltd.), built-in preamplifiers with active reset system, main amplifiers (Model 572, EG&G ORTEC), multiplexers (MR476, Seiko Instruments Inc.), analog-to-digital converters (2201A, Laboratory Equipment Co., Ltd.) and a data acquisition controller (NT-2400, Laboratory Equipment Co., Ltd.). The details of the multi-element detector are shown in Fig. 1 and Fig. 2.

The detector elements are arranged in the shape of a pentagonal pyramid and fully cover the sample. On each one detection side, 9 detector elements are arranged. The entire detection system consists thus of 45 detector elements. The micro beam irradiates the sample through the center of the pentagonal pyramid and X-rays emitted from the sample are detected in close to π geometry.

Since the detector consists of many detection elements, it is difficult to prepare all circuit systems. In this system, outputs of the main amplifier from four elements are inputted into one ADC by using a multiplexer router. Since a signal to indicate a detection element is sent to a list-memory from a router, energy signals from four elements is simultaneously measured by one ADC. The irradiation position of micro-beam is simultaneously sent to the list-memory from a beam position controller.

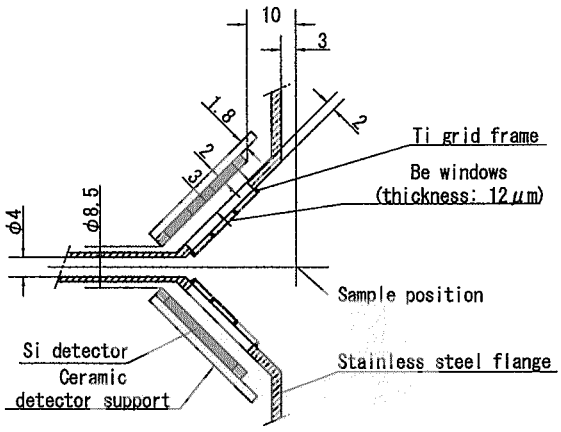

Fig. 1 Internal structure of the multi-element detector (side view). Micro-beam is irradiated through a φ4 central pipe to a sample. Titanium grids support beryllium windows.

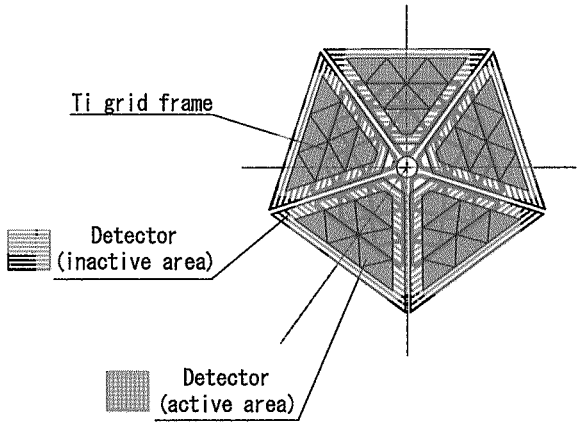

Fig. 2 Internal structure of the multi-element detector (front view).

Moreover, an output signal from a preamplifier of each detection element is branched to two. One is for X-ray measurement, and another is for RBS measurement (Fig. 3).

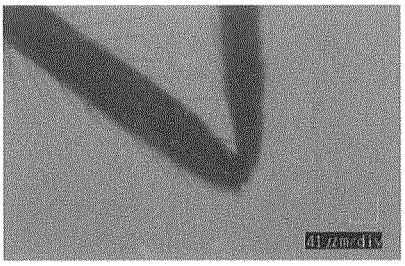

Fig. 4 Photograph of a mosquito's leg by a light microscope.

We performed micro-PIXE analysis of a leg joint of a mosquito by using this system. A proton micro beam with the energy of 2.0 MeV from the single-ended machine was used for that analysis. Figure 4 shows a photograph of a mosquito's leg by a light microscope. This sample was inserted into two sheets of PET film with a thickness of 4μm, and these are set on the atmosphere side of the acrylics holder. Micro beam was irradiated to the sample after it came to the atmosphere through the PET film.

3. Results and Discussion

Figure 5 shows micro-PIXE spectrum of the mosquito's legs. Since energy resolution

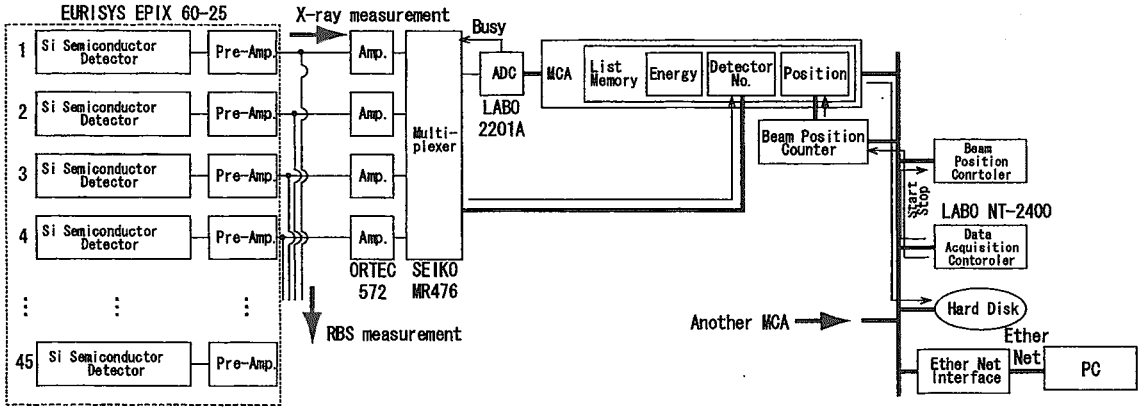

Fig. 3 Block diagram of measurement system.

of this system was not best (FWHM: 300eV), peaks of each characteristic X-rays cannot be divided easily.

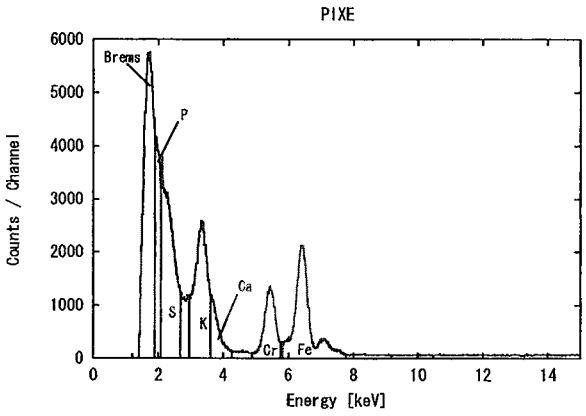

Fig. 5 Micro-PIXE spectrum of the mosquito's leg.

However, spatial distribution of potassium was obtained from counts corresponding to the energy of characteristic X-rays as in Fig. 6. The scanning area is 280 × 240 μm^2. It is visually confirmed that legs of mosquitoes are hollow.

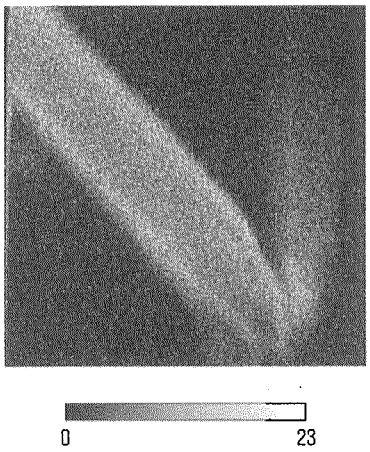

Fig. 6 Distribution of K in the mosquito's leg. The center of leg is a slightly darker than the outline because mosquito's legs are hollow.

Figure 7 is obtained from RBS spectrum. It means spatial distribution of some light elements, C, N, O and so on. It seems to be uniform everywhere because the sample wrapped in PET film. Most of RBS thought to be occurs in PET. So in order to take an image of RBS, a sample must be placed into a vacuum.

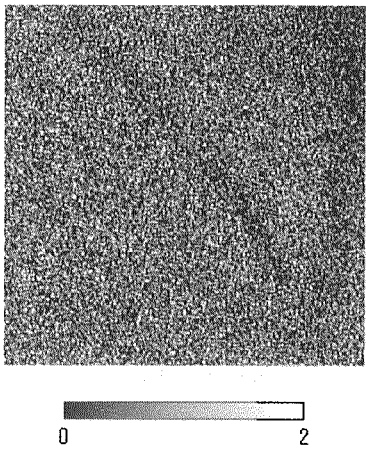

Fig. 7 RBS image of the same sample in case of Fig. 6. It is distributed uniformly because of PET covering the sample.

4. Conclusion

The large solid angle detector system was developed for reduction of the measuring time of micro-PIXE analysis. The spatial distributions of some elements which exist in the living body, such as sulfur and potassium, were measured although there was the problem on the energy resolution of the detector. For analysis of trace elements, improvement of the energy resolution is required.

It also turns out that measurement of RBS is possible with the system. But there must be a sample into a vacuum.

References

1) T. Satoh, et al., International Journal of PIXE 11 (2001) 49-59.
2) A. Sugimoto, et al., International Journal of PIXE 9 (1999) 151-160

7.7 Analysis of Arsenic Around an Arsenic Mine by μ-PIXE

T. Ohnuki*, F. Sakamoto**, N. Kozai***, M. Samadfam***,
T. Kamiya****, T. Sakai****, S. Oikawa**** and T. Sato****
Advanced Science Research Center, JAERI*, Department of Research Reactor, JAERI**, Department of Environmental Science, JAERI***, Advanced Radiation Technology Center, JAERI****

1. Introduction

The monitoring for chemically hazardous elements is important to protect the threat of the human health. Usually the concentrations of hazardous elements are measured in soils, rocks, plants, and groundwater and surface water[1]. Especially biomat and lower plants of lichens and mosses are used because of their ability to accumulate hazardous elements. So far the concentrations of hazardous elements in the lower plants have not been measured directly. One may dissolve the biomat and lower plants using appropriate methods to provide for the measurements using induced coupled plasma mass spectroscopy (ICP-MS) and induced coupled plasma atomic emission microscopy (ICP-AEM). However, the dissolving process is complicated and time consumable, and the information of the chemical forms is lost during the dissolving process.

Particle induced X-ray emission (PIXE) is one of the possible methods detecting elements in the level of ppm[2]. If we use probe beams of μm order or less in diameter, hazardous elements as well as other elements distribution in a lower plant sample can be determined with such spatial resolution. A light ion microbeam system[3] with the spatial resolution of less than 1 μm was constructed on a beam line of 3 MV single-ended accelerator in the TIARA facility at Japan Atomic Energy Research Institute (JAERI). And the in-air μ-PIXE analyzing system was developed on the TIARA facility for chemical analysis with a sub-micron level spatial resolution[4]. Thus, mapping of hazardous elements of ppm level is available by μ-PIXE.

Arsenic is a poison and one of the hazardous elements known to be carcinogenic to man[5]. We have applied the μ-PIXE technique to monitor As in biomat formed in As mine water, and in the lower plants of lichen and mosses around an abandoned As mine.

2. Site and samples

Abandoned As mine is located in Gunma-prefecture, Japan. The entrance of the mine was closed by concrete wall. Three foliose lichens were sampled from the rock at approximately 1.5 m from the closed entrance. Two mosses were collected from the different positions. One was collected from the rock where the lichen was collected from, and the other was from the concrete wall at approximately 3 m downstream from the mine water discharge position. The moss on the concrete wall was collected at the surface water level. The biomat was sampled in the surface water at 0.3 m downstream from the mine water discharge position.

As references, moss and lichen were sampled on rocks at distance of 5 to 10 m from the closed entrance. They are called the reference moss and lichen in the present paper. The concentration of As in the mine water

discharge was approximately 9.4×10^{-7} mole·L^{-1} measured by ICP-MS.

3. Experimental

The lichens, mosses and biomat samples were directly attached on the sample folders for μ-PIXE analysis. The samples were initially checked by optical microscope (OM). A Proton beam with the energy of 2.6 MeV from the single-ended machine was used for in-air μ-PIXE analysis developed at TIARA facility in Japan Atomic Energy Research Institute[3], so that the proton penetrates into the lower plants and biomat exiting elements both on the surface and internal region of the lower plants and biomat. The beam spot was approximately 1 μm in diameter. The maximum scanning area for the μ-PIXE analysis system was 740 x 760 μm^2.

4. Results and Discussion

The spatial distribution of As in the lichen on the rock at 0.3 m from the closed entrance obtained by μ-PIXE analysis is shown in Fig. 1(A). In μ-PIXE analysis the scanning area for the measurement is 740 x 760 μm^2. Bright regions in Fig. 1 show the existence of As. Figure 1(A) indicates that As is localized on and/or in the lichen. The spatial distribution of As in the area shown as white rectangular (160 x 180 μm^2) in Fig. 1(A) is shown in Fig. 1(B). The spatial distribution of As in Fig. 1(B) is more clearly recognized than in Fig. 1(A). This reveals that focus of the μ-PIXE analysis on the area where As is localized gives more precise spatial distribution. These show that the measurement in a wide area, for instance 740x760 μm^2 area, followed by the focus of the measurement on the restricted area where As is localized, is an advantage of the μ-PIXE analysis.

The μ-PIXE spectrum of the reference moss sampled from the concrete wall at approximately 5 m from the closed entrance is shown in Fig. 2(A). Arsenic is not detected in the reference moss. The μ-PIXE spectrum of the lichen sampled at approximately 5 m from the closed entrance also gives no As peak. These suggest that background level of As concentration in lower plants is below the detection limit of μ-PIXE analysis. Note that the Ti peak observed in the spectrum comes from glue of sample seal.

The μ-PIXE spectra of the lichen (Fig. 2 (B)) and moss (Fig. 2 (C)) collected at approximately 1.5 m from the closed entrance show that the peaks of As as well as Fe, S and Si are detected. This indicates that lichen and moss around the closed entrance accumulate not only As, but also Fe, Si and S containing compounds. Since no As is detected by the mosses and lichen collected at approximately 5 m from the closed entrance, As in the mosses and lichen near the closed entrance are probably originated from the mining area.

Spatial distributions of As, Fe, K, Ca, S and Si in the lichen sample collected from the rock at approximately 1.5 m from the closed entrance were obtained by the μ-PIXE analysis (figure not shown). The distribution of As does not correspond to Fe, K, Ca, S and Si. But, Fe, K, Ca, S and Si are detected in the region where As is detected. Similar results are obtained for the moss collected on the rock at approximately 1.5 m from the closed entrance. The Si distribution corresponds to the Ca distribution indicating that Si and Ca are originated from silicate minerals. The Fe distribution corresponds to the S distribution indicating that Fe containing compound is originated from iron-sulfur containing minerals. These indicate that in the lichen and moss As is accumulated with silicate minerals and

iron-sulfur compounds.

The μ-PIXE spectrum of the biomat (Fig. 2 (E)) indicates that the biomat contains As as well as Fe, Ca, S and Si. The μ-PIXE spectrum of the moss collected from the concrete wall (Fig. 2(D)) indicates that the moss contains As as well as Fe, Ca, S and Si. The spatial distributions of As, Fe, Ca and S in the biomat sample obtained by μ-PIXE shows that the distribution of As does not correspond to S and Ca, but to Fe. These show that As accompanies Fe containing compounds.

These results indicate that μ-PIXE is effective method to measure arsenic in lower plants. We have a plan to examine the migration behavior of arsenic around arsenic mine.

References

1) M.P. Elizalde-Gonzalez, J. Mattusch, R. Wennrich, J. Environ. Monit., 3, 22-26(2001): S. Yalcin, XC Le, J. Environ. Monit., 3, 81-85(2001).

2)Sueno S., Eur. J. Mineral., p1273-1297 (1995).

3) T. Sakai, et al., Biological Trace Element Research Vols. 71-72 (1999), p77-82.

4)T.Kamiya, T.Suda and R.Tanaka, Nuclear Inst. Method B 118 447-450(1996).

5) M. Goldman and J.C. Dacre, Environ. Geochemical Health, 13, 179-191(1991).

6) Fukushi, private communication (2001).

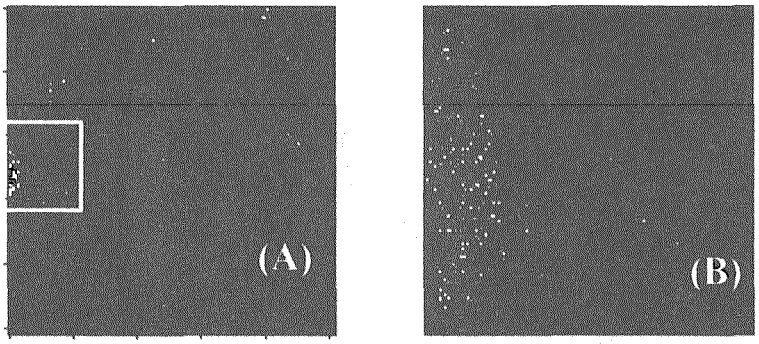

Fig. 1 Distributions of As in the same lichen on the rock collected at approximately 1.5 m from the closed entrance. The scanning areas in μ-PIXE analysis are 740x760 μm^2 for (A) and 160x180 μm^2 for (B) being the same area surrounded by white line in (A).

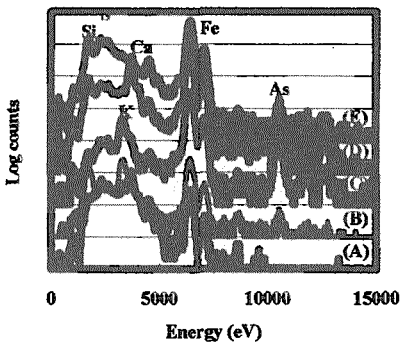

Fig. 2 Micro-PIXE spectra of reference moss (A), lichen (B) and moss (C) on the rock 1.5 m from the closed entrance, moss (D) on the concrete wall at the level of surface of the surface water and biomat (E) collected at 0.3 m from the mine water discharge position. For μ-PIXE measurements the proton beam is focused on the area where As is detected, and the scanning areas differ among the samples.

This is a blank page.

8. Radiation Shielding for Accelerator Facilities

This is a blank page.

8.1 Effects of Neutron Energy and Added Aerosol on Radioactive Aerosol Formation under High Energy Neutron Irradiation

K. Sato*, H. Noguchi*, A. Endo*, Su. Tanaka**, T. Iida*** S. Furuichi***, Y. Kanda**** and Y. Oki*****

Department of Health Physics*, Advanced Radiation Technology Center**, JAERI
Graduate School of Engineering, Nagoya University***,
Radiation Science Center, High Energy Accelerator Research Organization****,
Research Reactor Institute, Kyoto University*****

1.Introduction

In the air of accelerator and target rooms at proton accelerator facilities, airborne radionuclides such as radioactive aerosols or gases are produced[1-3]. The radiation protection against internal exposure due to the inhalation of induced airborne radionuclides is one of important problems for radiation safety at the accelerator facilities. For the assessment of internal doses due to the inhalation of airborne radionuclides, parameters such as a deposition rate in the respiratory tract and biokinetic models should be determined. The parameters are affected by the physicochemical properties such as particle size and chemical forms of airborne radionuclides. It is therefore important to clarify the mechanism of the radioactive aerosols formation which has a direct influence on the physicochemical properties.

We have already reported that the formation of ^{38}Cl and ^{39}Cl aerosols (^{38}Cl aerosols for short) due to an irradiation of high energy neutron (65MeV) to argon (Ar) gas can be explained by attachment of the radionuclides onto added di-octyl phthalate (DOP) aerosols[4]. It is however important to confirm whether the radioactive aerosol formation is affected by neutron energy and the physicochemical properties of aerosols or not, since the kinds of the aerosols and radiation energy are not uniform at the proton accelerator facilities. In the present study, the effects of neutron energy and added aerosols on the formation mechanism of radioactive aerosols formed by neutron irradiation have been examined.

2.Experimental methods

The experiment was carried out using LC0 course in light-ion room 3 of TIARA. The neutrons are generated by quasi-monoenergetic neutrons source facilities. Fig.1 shows the diagram of the experimental setup. It consists of an atomizer, an irradiation chamber, and two

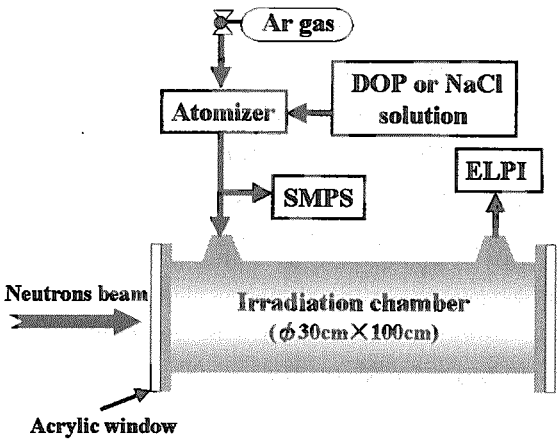

Fig. 1 Diagram of the experimental setup.

particle analyzers: a scanning mobility particle sizer (SMPS) (TSI SMPS 3936) and electrical low pressure impactor (ELPI) (DEKATI ELPI-2000).

Firstly, the irradiation chamber (diameter 30cm and length 100cm) that was placed in the beam axis was filled with high-purity (>99.995%) Ar gas. DOP or NaCl aerosols were then introduced to the irradiation chamber. The DOP aerosols were generated by introducing a 2-propanol solution containing DOP to the atomizer (TSI 3075). In the case of NaCl aerosols, a NaCl solution instead of the 2-propanol solution was used.

The Ar gas containing the aerosols was irradiated with the 45MeV quasi-monoenergetic neutron beam for 100 min. A neutron fluence rate in the monoenergetic peak at the acrylic window of the irradiation chamber was 1.9×10^{4} $cm^{-2}\cdot s^{-1}$. After the irradiation, the aerosol particles were collected from the irradiation chamber. The size distribution of aerosol particles was measured with ELPI. Then, the number size and activity size distributions of collected aerosol particles were analyzed. The number size distribution of collected aerosol particles on the each collection plates was measured using the electrometer of ELPI. To obtain the activity size distribution, the collection plates were removed from the impactor stages of ELPI after sampling, and the radioactivities of the collection plates were measured by a gas-flow counter. The γ-spectrum of the collection plates was also measured using a germanium semi-conductor detector.

3. Results

Fig.2 shows the γ -ray spectrum of the collection plates of ELPI. The ^{38}Cl and ^{39}Cl respectively formed from the (n, 2np) and (n, np) reactions of ^{40}Ar were observed.

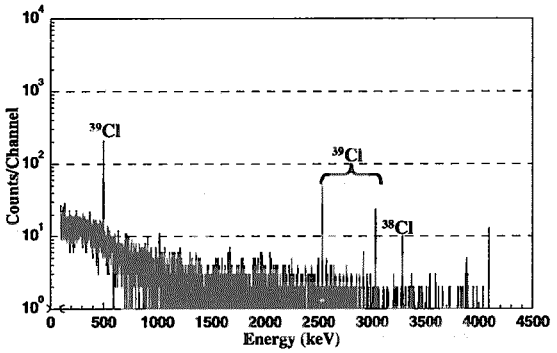

Fig. 2 Gamma-ray spectrum of the collection plates of ELPI after the irradiation of 45 MeV neutrons.

To study the effects of neutron energy on the formation mechanism, the number size and activity size distributions of ^{38}Cl aerosols were analyzed after the irradiation of 45MeV quasi-monoenergetic neutrons to Ar gas containing DOP aerosols (Fig. 3). In addition, an activity size distribution was calculated by using the

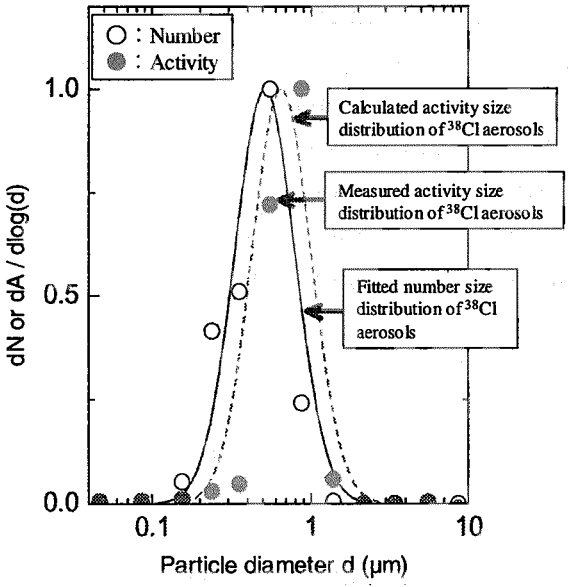

Fig. 3 Particles size distribution of ^{38}Cl attached DOP aerosols produced under the irradiation of 45MeV neutrons.

simple attachment model[5] and the number size distribution. Similarly to the results[4] of 65MeV quasi-monoenergetic neutron irradiation performed in 2000, the activity size distribution of ^{38}Cl aerosols measured by ELPI was in good agreement with the calculated distribution assuming the attachment of ^{38}Cl and ^{39}Cl to DOP aerosols. The result indicates that the formation mechanism of ^{38}Cl aerosols is not affected by a neutron energy (45 and 65 MeV).

Whether physicochemical properties of added aerosols influence the attachment model or not, was examined by using NaCl aerosols instead of DOP aerosols (Fig. 4). As a result of irradiation of 45 MeV neutrons to Ar gas containing the NaCl aerosols, the formation of the ^{38}Cl aerosols was also found. Assuming ^{38}Cl aerosols formation due to the attachment of ^{38}Cl and ^{39}Cl formed by neutron irradiation to the NaCl aerosols, the activity size distribution of ^{38}Cl aerosols was estimated by using an attachment coefficient and the number size distribution of NaCl aerosols. The formation of ^{38}Cl aerosols could be explained by the attachment model as well as the case of DOP aerosols.

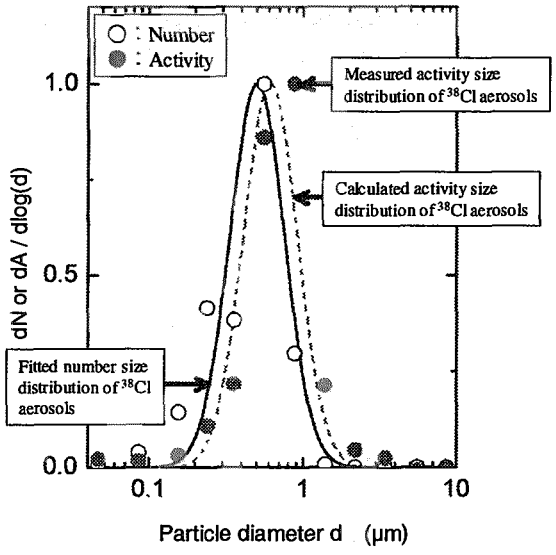

Fig. 4 Particles size distribution of ^{38}Cl attached NaCl aerosols produced under the irradiation of 45MeV neutrons.

The present results showed that the formation mechanism of radioactive aerosols in high energy neutron fields was not affected by the irradiation energy of neutron and the physicochemical properties of added aerosols.

Summary

The effects of a neutron irradiation energy and physicochemical properties of added aerosols on the formation mechanism of ^{38}Cl aerosols were examined by using the quasi-monoenergetic neutron source of TIARA. Similarly to the result[4] of 65MeV quasi-monoenergetic neutron irradiation, it was found that ^{38}Cl aerosols were formed under 45MeV neutron irradiation by the attachment of ^{38}Cl and ^{39}Cl to DOP aerosols. When the NaCl aerosols were added instead of the DOP aerosols, the formation of ^{38}Cl aerosols could be explained by the same attachment model as that used for the DOP aerosols.

References

1) Oki, Y., et al., *J. Radioanal. Nucl. Chem.*, **239**, 501-505. (1999).
2) Endo, A. et al., *Radiat. Prot. Dosim.*, **93**, 223-230. (2001).
3) Kanda, Y., et al., *J. Radioanal. Nucl. Chem.*, **247**, 25-31. (2001).
4) Endo, A. et al., *Appl. Radiat. Isotopes.*, **56**, 615-620. (2002).
5) Porstendörfer, J., *J. Aerosol Sci.*, **25**, 219-263. (1994).

8.2 Development of a Bragg Curve Spectrometer (BCS) for Fragment Spectroscopy in Neutron and Proton Induced Reactions

M. Hagiwara*, M. Hosokawa*, M. Baba*, T. Sanami**, M. Takada***, and S. Tanaka****

Cyclotron and Radioisotope Center, Tohoku University*, Radiation Science Center, High Energy Accelerator Research Organization**, National Institute of Radiological Sciences***, Advanced Radiation Technology Center, JAERI****

1. Introduction

Charged-particle production reactions for energetic neutrons and protons play a fundamental role in radiation effects by energetic hadrons. We have measured cross sections for light charged-particle (p, d, t, α) production reactions of accelerator materials for 40-75 MeV neutrons at TIARA[1,2].

For charged-particles heavier than lithium isotopes, i.e., fragments, data are very sparse despite of their importance in radiation damage and single event upset (SEU) due to a large local ionization density.

Direct fragment detection is rather difficult due to a lower yield, large energy loss in samples and large energy variation with emission angle. Furthermore, theoretical calculation treating fragment production is rather ambiguous yet. Therefore, it is important to establish efficient experimental methods for fragment detection.

A Bragg curve spectrometer (BCS) is a gas ionization chamber which enables particle identification and energy measurement of fragments with a single counter[3]. It has been utilized widely in heavy ion induced reactions but there has been no application to neutron-induced reactions. We have developed BCS and applied successfully to neutron induced-reactions.

2. Bragg Curve Spectrometer (BCS)

Figure 1 shows a schematic diagram of BCS. It is a cylindrical gridded ionization chamber (GIC). The cathode-grid distance is 27 cm, the grid-anode distance is 0.5 cm. Wire radius and spacing of the grid are 0.1mm and 1mm, respectively. Guard ring electrodes are arranged in 3 cm steps to obtain a uniform electric field between the anode and grid. The chamber is filled with a Ar + 10%CH_4 gas at a pressure of 2.7×10^4 Pa (200 Torr).

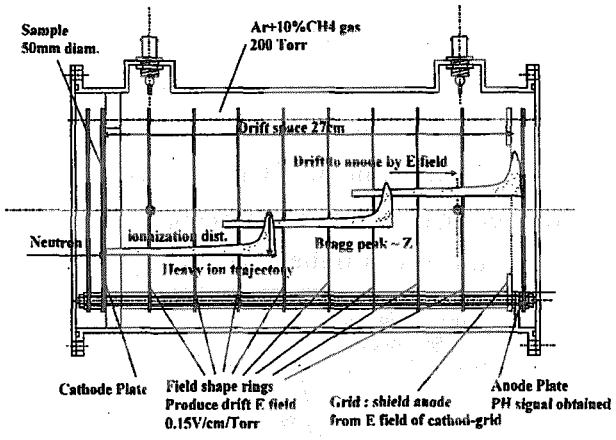

Fig.1 Schematic diagram of BCS

Ionized electrons drift to the anode by the electric field keeping a distribution of a Bragg curve. From the anode, a signal with a time-reversed form of the Bragg curve is obtained. Therefore the fast part of the anode signal is proportional to the Bragg peak that is proportional to the square of the atomic number of the fragment, and the integration of whole the anode signal represents the total charge proportional to the fragment energy[3]. Therefore,

the BCS method provides the data of energy and the atomic number of the fragments using only the anode signal.

To apply BCS to neutron- induced reactions, we set a sample inside the chamber to decrease the energy loss and make larger the solid angle. In this case, however, there arise problems of 1) backgrounds due to neutron irradiation of the chamber and the counting gas[4], and 2) distortion of anode signal due to angler spread. To solve 1), we adopted tight neutron collimation, thin high-Z electrodes and an additional shield electrode in front of the chamber with the same potential as the cathode[4,5]. For 2), the signal of large emission angle could be eliminated by use of the cathode signal having angle-dependence[4].

To prove the proper operation of BCS, the following tests were performed: 1) the saturation property by using ^{241}Am α source[4], and 2) particle identification and the Z resolution for fragments by 86 MeV α particle-induced reactions on carbon at NIRS (National Institute of Radiological Sciences) cyclotron. In the 2-nd experiment, fragments from lithium to carbon could be separated clearly each other.

The energy and Bragg peak signals are obtained by shaping the anode signal, respectively, with a long time constant (6 μsec) and a short time constant (0.25 or 0.5 μsec). To reduce background events and dead time of ADC, only coincidental data between anode and cathode were accumulated. Signals are collected as a two-dimensioned data by the KODAQ system[6] for CAMAC handling.

3.Application to Neutron-induced Reactions

The experiment for neutron-induced reaction was performed at the mono-energetic LC0 course of TIARA (Fig.2). Neutrons produced by the ^{7}Li(p,n) reaction were collimated by a ~3 m long neutron collimator, and ~60 cm long additional collimator to prevent neutron hitting of the BCS structures. The peak neutron energy was ~65 MeV [7] and a proton beam current was ~1 μA.

Fragments from carbon were measured using samples, 100 μm and 200 μm thick. Foils of nickel 100 μm. and aluminum 6 μm were employed too for study of backgrounds. Each sample was set on the cathode plate inside BCS.

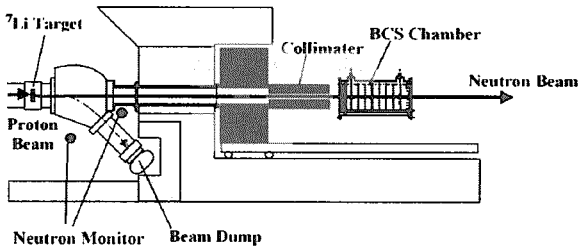

Fig. 2 Experimental arrange at TIARA[1]

Figure 3 shows the two-dimensional spectrum for energy *vs* Bragg peak in neutron-induced reaction in a 200 μm carbon sample. Figure 4 shows energy spectra for each particle. The spectrum was obtained by only ~4 hour's irradiation owing to large solid angle of BCS. The two-dimensional spectrum shows that fragments heavier than α particle are separated

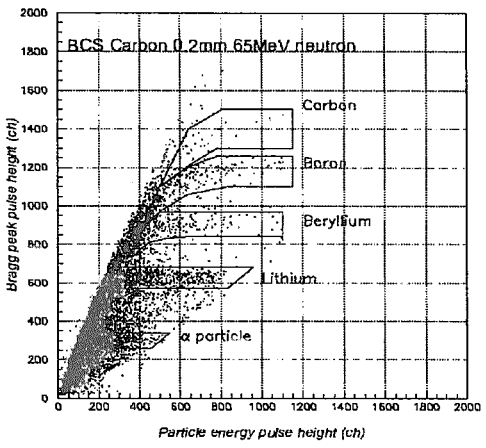

Fig. 3 The two-dimensional spectra for energy *vs* Bragg peak in the carbon 200 μm sample

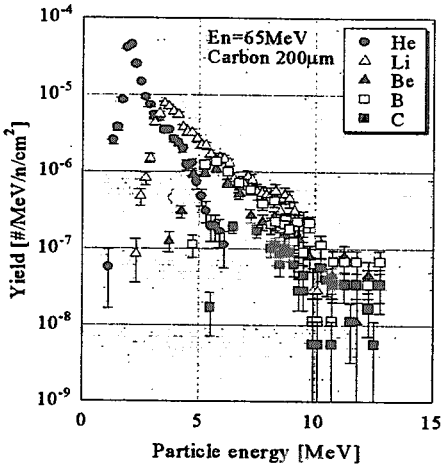

Fig. 4 The energy spectra of each observed particle for Carbon 200 μm

distinctly, although the data contain backgrounds in lower pulse-height region. The energy spectra of lithium and boron for each sample are shown in Figs. 5 and 6.

The results for two carbon samples show almost same values probably due to much shorter range of fragments than carbon thickness. The yields for nickel and aluminum samples are similar in magnitude and much smaller than those for carbon, and will represents approximately the backgrounds from materials other than samples.

Therefore, if backgrounds can be reduced further, this technique will be applied usefully for fragment detection in neutron and proton induced reactions in ten's of MeV region. We are planning to extend the dynamic range of the pulse-height spectrum both to higher and lower energy region by using data correction method.

References:

1)M.Baba et al. Nucl. Instrum. Meth. **A428** (1999) 454

2) T.Sanami et al: Proc. Int. conf. Nucl. Data (2001, Tsukuba), to be published

3) C.R.Gruhn, et al. Nucl. Instrum. Methods, **196** (1982) 33.

4) N.Ito, M.Baba, et al., Nucl.Instrum.Meth. **A337** (1994) 474

5) T.Sanami, et al. Nucl. Instrum. Meth. **A440** (2000) 403.

6)K.Omata et al., INS-Rep-884, Institute for Nuclear Study, University of Tokyo, 1991

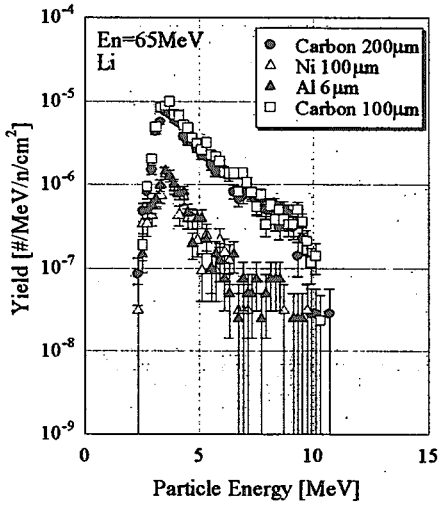

Fig. 5 The spectra of lithium

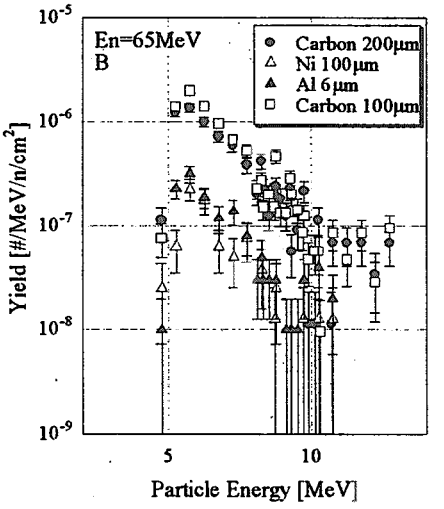

Fig. 6 The spectra of boron from various samples.

8.3 Response of Personal Dosimeters to High-Energy Neutrons

K. Oda*, T. Sawamura**, J. H. Kaneko**, Y. Nakane***,
S. Tsuda**** and Y. Yamaguchi****
Department of Nuclear Engineering, Kobe University of Mercantile Marine*,
Department of Quantum Energy Engineering, Hokkaido University**,
Center for Neutron Science, JAERI***, Department of Health Physics, JAERI****

1. Introduction

In recent years, accelerated proton beam and neutron beam have been widely utilized for a variety of up-to-date applications to material science, environment science, life science, medical cancer therapy, *etc.* A great number of accelerator facilities for high-energy, intense proton beam have already been in steady operation, and are in construction or planning in many countries; in Japan a collaborative project of JAERI and KEK is now in progress. Such a proton beam eventually generates high-energy neutrons in slowing down or stopping in a material. These high-energy neutrons are hard to be detected, because the efficiency of existing monitors and dosimeters becomes lower. Hence, it is very important to monitor them correctly, in other words, to establish a countermeasure, for a radiation protection purpose.

The detectors in actual radiation protection dosimetry use are divided into two groups; the area monitors and survey-meters belong to one group of active detectors, and the other is personal dosimeters, which are sub-divided into real-time type and accumulation type according to the length of measurement time period. For X- or γ-rays, for instance, a pocket-type semiconductor detector and a glass dosimeter (Radio-photo-luminescence) are commonly used as two sets of personal dosimeter, respectively. For neutrons with an energy lower than 14MeV, bubble detector (BD) and plastic nuclear track detector (PNTD) replace them, respectively.

The existing monitors and dosimeters used in neutron facilities have, in general, less sensitivity to high-energy neutrons than that to neutrons lower than 14MeV because of a rapid decrease in the cross sections for neutron interactions. The use of them without any corrections would lead a serious underestimate of the radiation dose and dose rate. Thus, our research members started to develop advanced techniques for enhancement of absolute detector sensitivity, and for an appropriate correction. These studies require a well-defined and clean neutron source, such as TIARA facility.

In this report, we state a few typical experimental results with BD and PNTD performed as a special project research between Japanese universities and JAERI.

2. Response of plastic track detectors

In an early study in 1990's for development of dose-equivalent response track detector for thermal to D-T neutrons, we finally proposed a combination of mildly boron-doped CR-39 plastic detector with a two-layer radiator consisting of polyethylene and deuterized hydro-carbon (CD2)[1]. In order to extend the neutron energy to be applied, it is indispensable both to enhance the intrinsic sensitivity of PNTD and to select radiator material suitable for higher energy neutrons.

An experiment has been carried out to investigate the relative sensitivity of three candidate PNTDs[2,3]. One is a pure CR-39, of which trade name is "BARYOTRAK". Second is called "TD-1", which is a CR-39 containing a

small amount of antioxidant to be improved in the sensitivity to low LET particles. The new detector called "TNF-1", copolymer of CR-39 and N-isopropylacrylamide developed by a group of Nihon University and JAERI (Ogura et al.), can register 27-MeV protons of normal incidence, corresponding to about 10 keV/μm in LET_{200} and also to about 4 in terms of z^*/β[4].

After neutron irradiation, each PNTD sample was chemically etched in a stirred NaOH solution at 70 °C. The concentration was 7.25 N for both BARYOTRAK and TD-1, and 5 N for TNF-1. The amount of etched bulk was estimated from the etch-pit radius of fission fragments from a ^{252}Cf source, and controlled to be 15±0.2 μm. Figure 1 shows the measured etch-pit density as a function of the radiator thickness for three PNTDs. Heavy recoils and α-particles are relatively easy to be registered in PNTDs because the etch rate ratio is much larger than the unity. On the contrary, the possibility of recording the proton recoils should depend largely upon the type of PNTDs. It is clearly seen in Fig.1 that the radiator has little contribution for BARYOTRAK, because of relatively low sensitivity to the protons. About twice and three times radiator effects were confirmed for TD-1 and TNF-1, respectively.

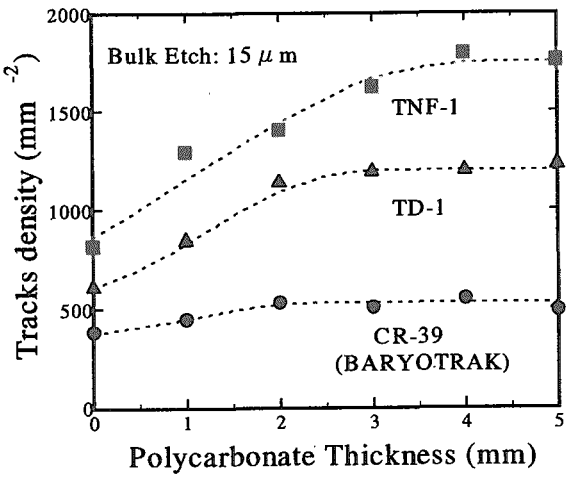

Fig. 1. Etch-pit density for three PNTDs exposed to 65MeV neutrons as a function of radiator thickness.

Furthermore, the species of particles recorded were identified by the technique already developed by the authors[5]. The ion tracks were then classified into three groups, *i.e.* proton relatives, α-particles and heavier ions. The fraction of proton tracks were evaluated to be about 30% and 70% for BARYOTRAK and TNF-1 exposed in a 65-MeV neutron field, respectively. This result could be explained by a great difference in the sensitivity to high-energy protons between two types of PNTD.

Table 1. Comparison between a pure CR-39 and TNF-1 in the fraction of registered particle classified into three groups of protons, α-particles and heavier ions.

Type	Neutron energy	Fraction of particles [%] p,d,t	α	heavy ions
CR-39	65MeV	29 ± 5	22 ± 5	49 ± 6
TNF-1	65MeV	68 ± 12	15 ± 6	17 ± 6
TNF-1	40MeV	69 ± 7	8 ± 3	23 ± 4

The TNF-1 detector, however, has a problem of a roughness on the post-etched surface. Since the size of the etch-pits induced by the neutrons should distribute so widely, the surface roughness is a decisive problem for practical application. We expect a drastic improvement to be performed as soon as possible.

3. Response of bubble detector

The response of bubble detectors, BD100R (BTI,Canada) with nominal sensitivities of 3.3 and 0.33 bubbles/μSv were measured for quasi-monoenergetic neutron beams in the 40-75 MeV range and the effects of a lead-converter enclosing the detector introduced to extend the response to the high energy region were discussed[6,7]. The sensitivities to 40, 60 and 75 MeV quasi-monoenergetic neutrons were found

to be 35-50 % of the nominal sensitivity measured for Am-Be neutrons. The lead-converter effect on the sensitivity was measured for 48 and 75 MeV neutrons. The sensitivities, which are normalized by the sensitivity without the lead converter, are shown in Fig.2. The sensitivity increased with the lead thickness and became similar to the nominal value with the 2-3 cm thick lead converter.

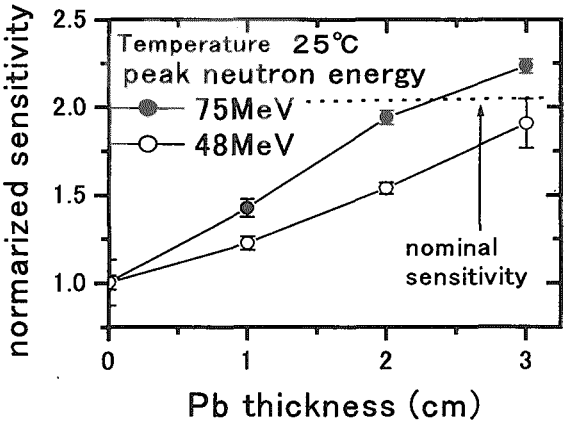

Fig.2. Sensitivity normalized by the sensitivity without the lead-converter as a fuction of converter thickness.

Monte Carlo calculations using MCNPX code were carried out to estimate the lead-converter effect on the neutron spectra in the detector exposed to quasi-monoenergetic source neutrons.. It is indicated that evaporation neutrons are produced in the 0.1-10 MeV energy region. These neutrons are expected to increase the bubble number, as the BD is sensitive to the neutrons in this energy region.

4. Conclusion

The characteristic response of PNTDs and BD to 40-75 neutrons have been investigated.

It was confirmed that the sensitivity of BD was lowered to about half the nominal one, and use of the lead-converter was effective to compensate.

As to PNTD, an establishment of a theoretical calculation technique is also very important for designing a special radiator for high-energy neutrons in the next step, and now in progress.

We are planning to carry out another experiment of 40 to 80-MeV neutron irradiation at TIARA, JAERI. An attention to a possible contamination of lower energy neutrons and secondary charged particles must be paid carefully to determine the absolute sensitivity.

Reference

1) K. Oda. M. Ito, H. Yoneda, H. Miyake, J. Yamamoto and T. Tsuruta: *Nucl. Instrum. Methods*, **B61** (1991) 302-308

2) K. Oda, H. Ichijo, N. Miyawaki, T. Yamauchi and Y. Nakane: *Radiat. Meas.*, **34** (2001) 171-175.

3) K. Oda, Y. Saito, N. Miyawaki, T. Yamauchi, Y. Nakane and Y. Yamaguchi: *Radiat. Prot. Dosimetry*, (2002), in press.

4) K. Ogura, M. Asano, N. Yasuda and M. Yoshida: *Nucl. Instrum. Methods*, **B185** (2001) 222-227.

5) K. Oda. M. Ito, H. Miyake, M. Michijima and J. Yamamoto: *Nucl. Instrum. Methods*, **B35** (1988) 50-56.

6) S. Agosteo, M. Silani and L. Ulrich: *Radiat. Prot. Dosimetry*, **88** (2000) 149-155.

7) T. Sawamura, J. H. Kaneko, M. Abe, M. Tamura, I. Murai, A. Homma, F. Fujita and S. Tsuda: *Proc.10th Symp on Rad. Meas. and Application*, 2002, to be published.

This is a blank page.

9. Accelerator Technology／TIARA General

This is a blank page.

9.1 Measurement of Secondary Charged Particles with MeV Energy Cluster Ion Irradiation

Y. Saitoh, Y. Nakajima

Advanced Radiation Technology Center, JAERI Takasaki

1. Introduction

Interaction of high energy molecular or cluster ions to materials has attracted attention in points of fundamental research such as non-linear effects at the surface of a target. Recently, a small enhancement in energy loss was obtained for carbon and boron cluster ions comparing to their single ions at the same velocity [1, 2]. Large enhancement for metal sputtering yield by irradiation of gold cluster ions was also reported[3]. It is expected that the massive energy deposition introduced by cluster ion irradiation in a very small volume will lead to non-linear phenomena[4]. We have developed various kinds of MeV energy cluster and molecular ions with mass-separated beam current of nano ampere order by the TIARA 3 MV tandem accelerator[5]. We can propel not only study of fundamental interactions mentioned above but also that of materials modification with the cluster ion beam.

Appling the cluster ion beam to materials modification, we must control the implanted ion dose into a target with measuring the accurate beam current. However, we observed that the value of measured beam current depended on materials of the target and irradiation time[6]. This phenomenon was not observed for single ion irradiation. It suggests that the amount of secondary charged particles from a target irradiated by a cluster ion beam be different from that irradiated by a single ion beam because of the non-linier phenomena. Therefore, it is important to investigate the non-linier phenomena on secondary particles from a target such as electrons and ions with cluster irradiation in MeV energy region. In a preliminary study, we simultaneously measured a target beam current and a secondary charged particle current with a biased suppressor electrode that covered the target. We also measured a mass spectrum of secondary ions emitted from a target.

2. Experimental setup

2.1 beam current measurement

The schematic drawing of a beam current monitor is shown in Fig. 1. The ion beams of C and C_8 were irradiated to an aluminum target. The target current I_t and the suppresser current I_s are measured with digital pico-ampere meters (Advantest 8800). The voltage of the suppressor electrode was changed from –200 V to 200 V .

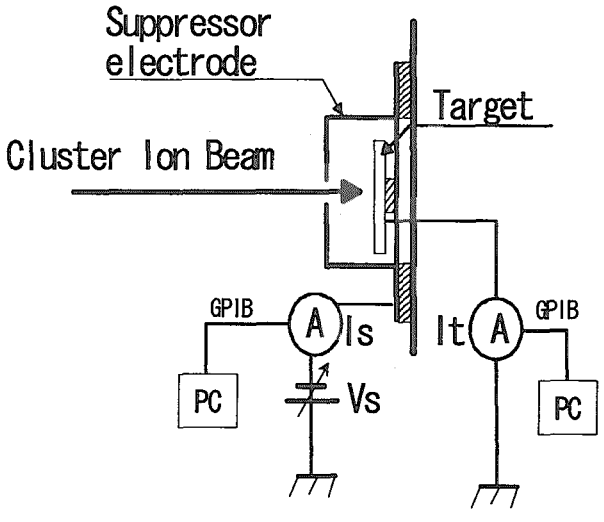

Fig.1 Schematic drawing of beam current monitor.

2.2 TOF measurement of secondary ion

A secondary ion mass spectrum was measured by means of TOF (Time of Flight) measurement. The incident ions are C, C_4, C_8 (0.5 Mev/atom), and the target is aluminum. A pulsed ion beam with a time range of 100 nS and a frequency of 10 kHz ~ 100kHz was generated by a chopping electrode equipped with the low energy beam line of the tandem accelerator. The flight time of secondary ions is measured by a TAC (Time to Analog Converter) with the TTL signal (start) from the pulse generator that controls the high voltage of the chopping electrode and MCP (Micro Channel Plate) signal (stop) that detects the secondary ions[7].

3. Results

The beam current of the I_t and the I_s versus the voltage of suppresser electrode from –200 V to 0 V are plotted in Fig. 2 and Fig. 3 for C and C_8 beam irradiation, respectively. In the case of C irradiation, the I_s current is negligible comparing to that of the I_t. It means that the most of secondary charged particles emitted from a target are electrons, and the negatively biased suppresser electrode repels them to the target. In the case of C_8 irradiation, the negative value of the I_t was observed in the voltage of –50 V to –200 V. And, the I_s showed a positive value. It implies that the amount of secondary positive ions from a target is larger than that of incident beam in the C_8 irradiation. Therefore, the measured beam current by a usual Faraday cup should indicate a smaller value than that of true beam current in large cluster ion irradiation.

Figure 4 shows the preliminary result of a secondary ion mass spectrum measurement. The ratio of H_2 and H_3 to H that may be caused of water on the target surface is remarkably increases in C_4 and C_8 irradiation comparing with C irradiation. It should be an evidence of high-density energy transfer in a small area of a target surface. In the next step,

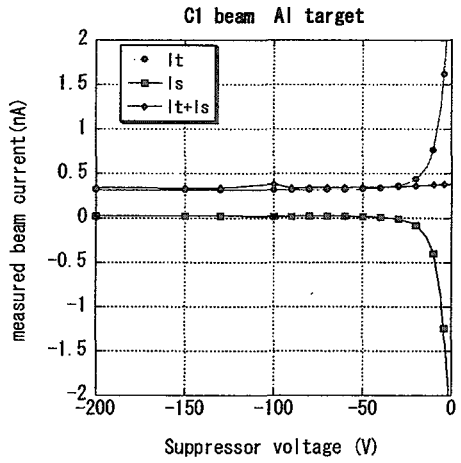

Fig. 2 Measured beam current of C_1.

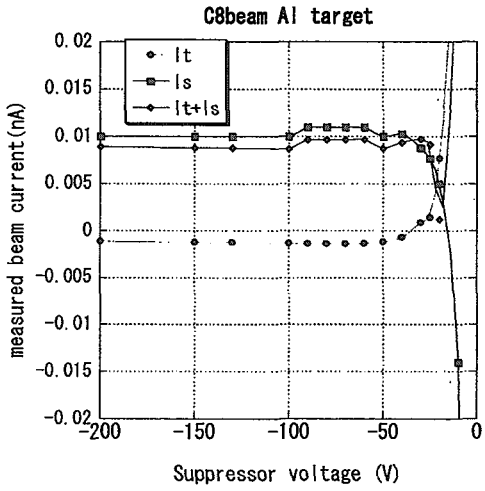

Fig. 3 Measured beam current of C_8

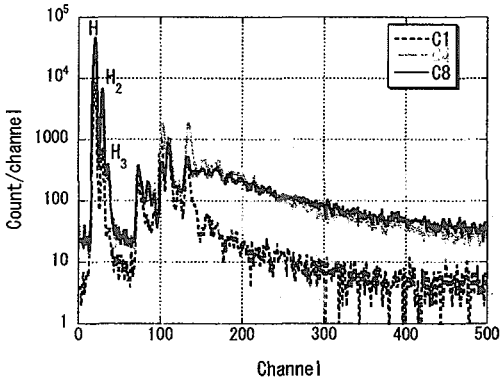

Fig.4 TOF spectrum of secondary charged particle with C_n irradiation.

we plane to quantify the amount of secondary ions with each cluster using a treated clean surface target.

References

1) K.Baudin, A.Brunelle, M.Chabot, S.Della-Negra, J.Depauw, D.Gardès, P. Håkanoss, y. Le Beyec, A. Billebaud, M. Fallavier, J. Remillieux, J.C. Poizat, J. P. Thomas, Nucl. Instrum. and Methods. B 94 (1994) 341-344.

2) K. Narumi, K. Nakajima, K. Kimura, M. Mannami, Y. Saitoh, S. Yamamoto, Y. Aoki, H. Naramoto, Nucl. Instrum. and Methods. B 135 (1998) pp. 77-81.

3) H. H. Andersen, A. Brunelle, S. Della-Negra, J.Depauw, D. Jacquet, and Y. Le Beyec, Phys. Rev. Lett. Vol. 80 No. 24 (1998) pp. 5433-5436.

4) Ch.Tomaschko, D. Brandl, R. Kügler, Schurr, H. Voit, Nucl. Instrum. and Methods. B 103 (1995)407-411.

5) Y. Saitoh, K. Mizuhashi, S. Tajima, Nucl. Instrum. Methods A 245 (2000) pp. 61-66.

6) Y. Saitoh, Y. Nakajima. JAERI-Review 2001-039, p. 238.

7) H. Shibata et. al. in this report.

9.2 Study of Secondary Ion Emission Processes from Solid Targets Bombarded by MeV Energy Cluster Ions

H. Shibata*, A. Itoh**, T. Majima**, Y. Saitoh***, Y. Nakajima***,
K. Narumi****
Research Center for Nuclear Science and Technology, The University of Tokyo*,
Graduate School of Engineering, Kyoto University**,
Advanced Radiation Technology Center, JAERI Takasaki***,
Advanced Science Research Center, JAERI****.

1. Introduction

The interaction of cluster ions with matter has been paid much attention in these years[1-3]. Because cluster ions can bombard a very small area of a solid surface by many atoms simultaneously and release large energy in a very short time (from femto- to pico-second region)[4]. These phenomena cause non-linear effects or synergetic effects, which are not normally caused by a single atom collision with solid targets.

As we are interested in processes of secondary charged particle emission from solid surfaces bombarded by high energy cluster ions, cluster ion beams accelerated by the TIARA tandem accelerator are used for this study. A time of flight (TOF) mass spectrometer for secondary ion measurement has been constructed last year, and in parallel a chopper has been installed in an injector beam line to generate a pulsed cluster ion beam. In this report we will present a preliminary results of secondary ion emission from aluminum target bombarded by C_1^+ and C_8^+ cluster ions.

2. Experimental

Figure 1 shows the experimental system of TOF mass spectrometry. A chopper and two sets of slits installed in an injector beam line generated pulsed ion beams by chopping continuous cluster ion beams from an ion source. A square wave from a master pulse generator controlled a high voltage applied to a parallel plate for chopping the beam. In this study 0.5 MeV/atom (~ 42keV/amu) C_1^+ ~ C_8^+ pulsed cluster ion beams were used.

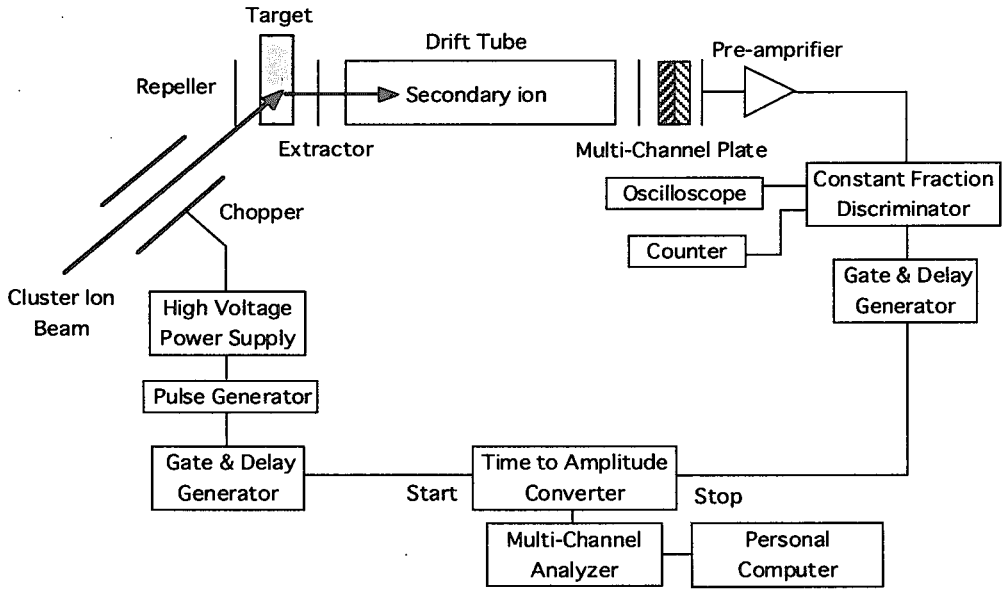

Fig.1. The schematic drawing of the experimental setup of the TOF mass spectrometry.

The duration and width of the pulse used in this experiment were 100 μs and 100 ns. C_4^+ and C_8^+ ions were produced in the ion source and C_1^+, C_2^+ and C_6^+ ions were fragments of C_8^+ ions after passing through charge stripper gas. As averaged beam currents of pulsed beams could not be measured, continuous beam currents were measured to be around pA for C_8^+ ions. The vacuum in a beam line and a chamber was kept at ~ 10^{-7} Pa to prevent cluster ions from breaking.

A linear type TOF mass spectrometer and a TAC (Time to Amplitude Converter) system for time measurement were adopted as secondary ion mass spectrometric system. The TOF mass spectrometer composed of a repeller, a extractor, a drift tube, a acceleration electrode and a multi-channel plate (MCP) detector. A TTL output from the pulse generator was used as a start pulse and a secondary ion signal from the MCP was used as a stop pulse of the TAC measurement system. Typical mass spectra were accumulated for 30 minutes in each run.

3. Results and discussion

Preliminary result of secondary ion mass spectra emitted from a 5mm$^\phi$ aluminum rod target bombarded by C_1^+ and C_8^+ cluster ions is shown Fig.2. The ordinate is the intensity of secondary ions in arbitrary unit, and the abscissa is the channel number of multi-channel analyzer. Several dominant peaks are seen in the spectra. These are H^+, H_2^+, H_3^+, C^+, Na^+, Al^+, K^+, etc. Many lines observed over 50 m/e are not identified. As the beam current was not measured in this experiment, these spectra could not be normalized and the yields could not be compared. This TOF mass spectrometer, however, indicates enough mass resolution and detection efficiency for cluster ion impacts.

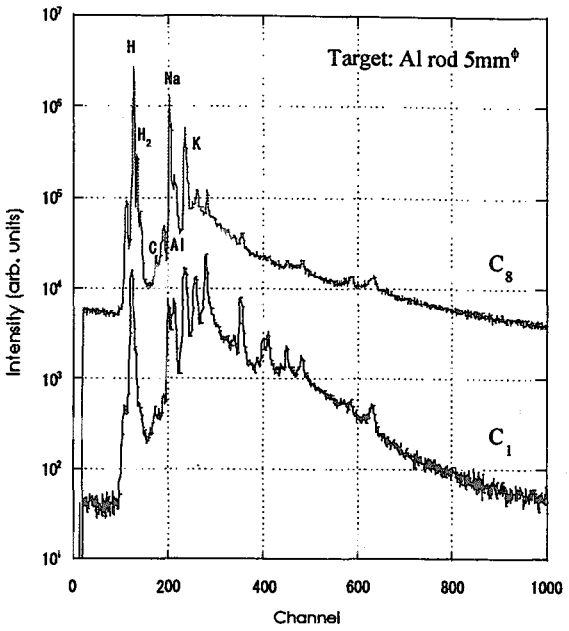

Fig.2. Secondary ion mass spectra for C_1^+ and C_8^+ ion bombardment on Al rod target.

The problems remain as follows; 1) the cleaning of the target surface is needed, because the surface condition sometimes changes the profiles of spectra, 2) the pulse width would be narrowed to get higher mass resolution, and 3) the normalization of mass spectra to the fluence of the cluster ion beam is needed for the comparison of different cluster ion impacts.

References

1) Y. Le Beyec, Int. J. Mass Spectrom. Ion Proc. **174** (1998) 101.
2) M. Döbeli et al., Phy. Rev. B**94** (1994) 388.
3) K.Boussofiane-Baudin et al., Int. J. Mass Spectrom. Ion Proc. **130** (1994) 73.
4) M.Toulemonde et al,Nucl. Instrum. Meth. B **112** (1996) 26.

9.3 Development of a Magnetic Field Monitoring System for the JAERI AVF Cyclotron

S. Okumura*, W. Yokota*, K. Arakawa*, Y. Nakamura*, T. Nara*. T.Agematsu*
I. Ishibori*, S. Kurashima*, M. Fukuda*, T. Ishimoto**, T. Nakajima***,
Advanced Radiation Technology Center, JAERI*
Department of Material Development, JAERI**
Echo Electronics Co.,Ltd.***

1. Introduction

In the JAERI AVF cyclotron, unstable phenomena, such as beam intensity decrease, were observed after starting up the cyclotron or changing an excitation level of the magnet. The magnetic field correction of dB/B = 1×10^{-4} every tenth hours was needed over a few days. We found that an increase in temperature of the iron body of the magnet induced the unstable phenomena[1-2]. Stabilization of the iron body temperature was achieved by precise temperature control of the cooling water for thermal isolation plates installed between the iron body and a main coil[3]. The beam intensity was stabilized within 10 % decrease in 50 hours[4-5]. The stability of the magnetic field seems to be in the order of 10^{-5}, while the accuracy of the magnetic field measurement was not so good for harsh environments in the cyclotron.

While microbeams using the 3 MV tandem and the single-ended accelerators are widely used, higher beam energy for microbeams are required for bio-medical applications. Collimated beams using the cyclotron are applied but the beam size is around several μm. A microbeam production system by focusing, therefore, has been constructed. Reduction of the energy spread of the beam, from dE/E = 1-5 $\times 10^{-3}$ to 2×10^{-4}, is required to achieve the microbeam production. We are developing the flat-top acceleration for this reason. High stable magnetic field, dB/B < 2.0×10^{-5}, is needed for the flat-top acceleration.

2. NMR Magnetic Field Monitoring System

We have developed a nuclear magnetic resonance (NMR) magnetometer with an accuracy of the order of 1×10^{-6} to measure the stability of the cyclotron magnetic field (≈ 2T) with a large gradient.

The NMR probe, including a proton sample and an oscillation circuit, was installed on the surface of the lower earth plate in between dee electrodes in vacuum chamber. The signal cable runs between the dee electrode and the dummy dee and reaches the feed-through connector. The NMR signal is fed into the head amplifier and the magnetic field is evaluated from the resonance frequency.

Although the magnetic field of the cyclotron has a complex distribution: the radial change for the isochronous acceleration and the azimuthal change for beam focusing, a homogeneous magnetic field, dB/B < 1×10^{-4} / cm^3, is required for the precise measurement with the NMR magnetometer. The optimum position of the NMR probe, where the magnetic field in the proton sample is the most homogeneous distribution, was searched by shifting the probe, but the NMR signal level was not enough. To obtain enough homogeneity of the magnetic field at the probe, a pair of correction coils was applied. The correction coils were designed to compensate the field gradient (≈10G/cm) along one direction. Each coil, 1 mm thick, was fabricated with polyimide copper wire of 0.3 mm diameter and epoxy resin (Torr Seal) so as to use in narrow vacuum space. The NMR probe was sandwiched with the correction coils and the direction of the compensation was optimized by rotating the correction coils.

In an NMR magnetometer normally used, the signal cable from the probe runs through low electromagnetic noise environments. In case of the cyclotron, the signal cable is exposed by RF and high magnetic field, because the probe is mounted in the acceleration area to measure the true magnetic field. A weak NMR signal, especially in case of the cyclotron, is disturbed by these electromagnetic fields.

To eliminate the effect of the RF, which heats the signal cable of the NMR and disturbs the NMR signal seriously, the cable was specially manufactured with the following

specifications:

1) Double shield with a mesh and a tube.
2) Polyimide copper wire.
3) Coaxial cable with a copper tube.
4) Filler (Torr Seal) into the tube.
5) Twist pair cable.

3. Measurement of the Magnetic Field

We have measured the magnetic field with the NMR magnetometer in a 195 MeV $^{36}Ar^{8+}$ beam, as shown in Fig.1. The stability of the magnetic field dB/B was within 1×10^{-5} in 45 hours. It indicates that the stability of the magnetic field is enough for the flat-top acceleration.

Reference

1) M.Fukuda et. al., JAERI Review 99-025, 251-253.
2) S.Okumura et. al., The 12th Symp. On Accel. Sci. and Tech., Wako, Japan (1999) 78-80.
3) Y.Nakamura, et al., JAERI-Review 2000-024, 282-284.
4) S.Okumura, et al., JAERI-Review 2001-039, 290-292.
5) S.Okumura, et al., Proceedings of the 16th International Conference on Cyclotrons and their Applications, East Lansing, USA 2001, 330-332.

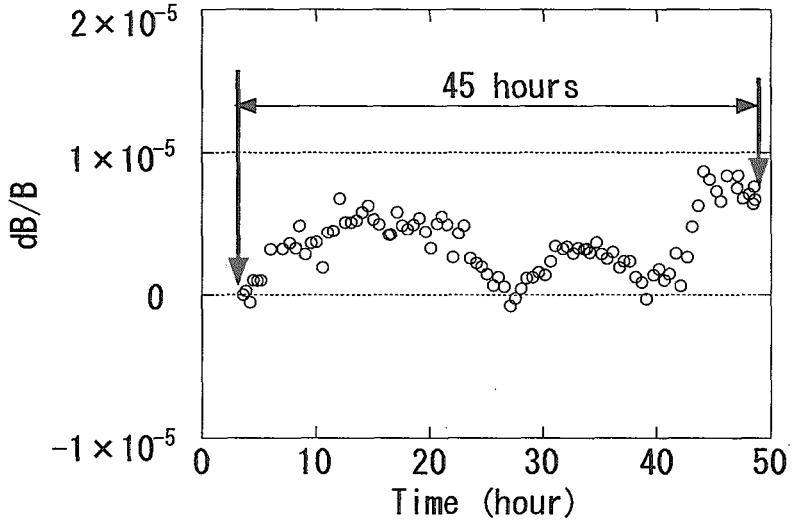

Fig. 1 Stability of the magnetic field measured with the NMR magnetometer.

9.4 Development of the Flat-Top Resonator for the JAERI AVF Cyclotron

S. Kurashima, M. Fukuda, N. Miyawaki, Y. Nakamura, T. Nara
T. Agematsu, I. Ishibori, W. Yokota, S. Okumura and K. Arakawa
Advanced Radiation Technology Center, JAERI

1 Introduction

A flat-top (FT) acceleration system for the JAERI AVF cyclotron has been designed to minimize the energy spread mainly for a microbeam production. The size of the microbeam spot needs to be 1 μm to perform a precise biological experiment. The energy spread of the cyclotron beam is required to be reduced to $\Delta E/E = 2 \times 10^{-4}$ to focus the beam with quadrupole magnets.

The cyclotron has a pair of quarter-wavelength ($\lambda/4$) coaxial type resonators with a movable-short. A resonance frequency varies with changing position of the movable-sort. Figure 1 shows an outline of the cyclotron resonator. The diameters of inner and outer tubes of the main cavity are 300 mm and 1000 mm, respectively. The range of the fundamental frequency is 11 to 22 MHz. A maximum acceleration voltage is 60 kV in a CW mode.

In general, the third- or fifth-harmonic of the fundamental frequency is used for the flat-top acceleration [1, 2] and the harmonic voltage can be obtained with installing an additional resonator. The amplitude of the higher harmonics superimposed on the fundamental waveform is estimated to be $1/N^2$ times the fundamental voltage, where the N is the order of the harmonics. We have adopted the fifth harmonics to save output power of an amplifier. The fifth-harmonic frequency of 55 to 110 MHz is required to be covered to apply the flat-top acceleration to a wide range of energy.

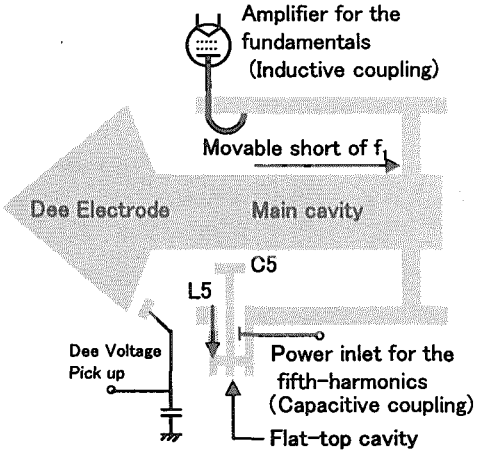

Figure 1: Outline of the cyclotron resonator (including the fifth-harmonic resonator).

2 Design of the Flat-Top Resonator

To determine parameters of the FT resonator, a cold model test was carried out [3] using the model of an FT resonator preliminarily designed for the RIKEN AVF cyclotron [4]. The model of the FT resonator was mounted on the main resonator of the CYRIC 930 cyclotron in Tohoku university. The RF system is basically the same as that of the JAERI AVF cyclotron. The main cavity of the CYRIC cyclotron has a preparatory port to install the model of the FT resonator. The induced FT waveforms were observed successfully at the dee voltage pick-up of the main resonator when the fundamental frequency were tuned to 11, 13, 15 and 20 MHz. Power dissipations for the fifth-harmonic frequencies were estimated from the amplitude levels of the source and the pick-up signals. Assuming that the fundamental voltage was 30 kV, output power of the amplifier was estimated to be about 1 kW.

In order to improve the design of the FT resonator, optimum parameters for downsizing

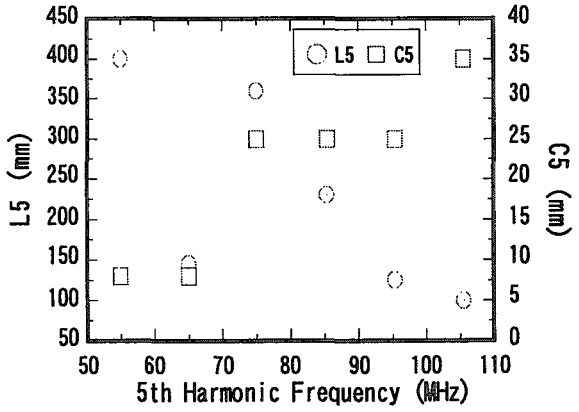

Figure 2: Parameters of the FT resonator calculated with the MAFIA. C5 is the gap of the coupling capacitor. L5 is the position of the movable-short.

the FT resonator itself and for decreasing power dissipation were investigated using the MAFIA code [5]. The compactness of the resonator is indispensable condition due to the limited space for mounting the FT resonator.

The power dissipation at the fundamental frequency of 15 MHz was found to be minimized using the FT resonator consisting of a 70 mm diameter inner- and a 300 mm diameter outer-tubes. The power consumption was estimated to be 80 % of the result in the cold model test. Figure 2 shows a correlation between the gap of C5 and the position of L5 to obtain the fifth-harmonic frequencies. The maximum length of L5 was limited to 400 mm for the compactness, and the minimum length was fixed at 100 mm to keep enough space for mounting a power feeder and a compensation tuner.

3 Manufacturing and performance

The newly developed FT system has been installed in March, 2002. The FT system consists of the resonator, amplifier, low-level devices and an overall controller. Specification of the system is shown in Table 1. The required range of the fifth-harmonic frequency is fully covered by the resonator. The power test at the fundamental frequency of 17.4 MHz has been carried out, and the flat-top waveform was successfully observed at the dee voltage pick-up as shown in Figure 3.

Table 1: Specification of the FT system.

Resonance frequency	55 ~ 110 MHz
Movable gap range of the coupling capacitor (C5)	6 ~ 50 mm
Movable range of the shortoing plate (L5)	250 mm
Inner tube diameter	70 mm
Inside diameter of outer tube	300 mm
Relative frequency change $\Delta f/f$	Maximum of 2 %
Power feeder	Capacitive coupling
Maximum output power of amplifier	3 kW (50 Ω)
Voltage stability	$\pm 5\times10^{-4}$
Phase stability	0.1 deg

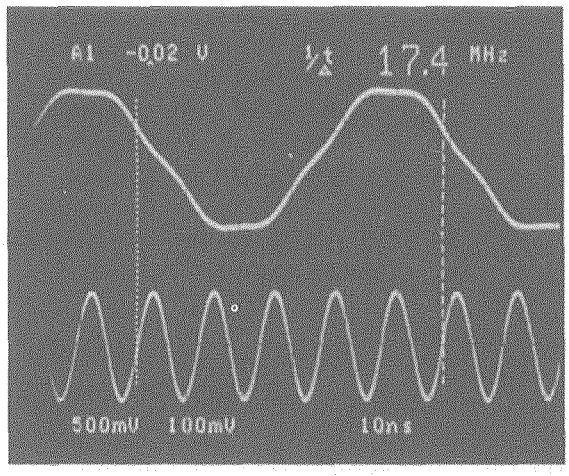

Figure 3: Waveforms observed at the dee voltage pick-up when the fundamental frequency and voltage are 17.4 MHz and 25 kV, respectively. The upper waveform is the combined waveform of the fundamental and the fifth-harmonic frequencies, and the lower is the fifth-harmonic waveform separated with a high-pass filter.

REFERENCES

[1] B. Bischof, "The RF-System of the Flattop-Acceleration Structure in the SIN 590-MeV-Ring-Cyclotron," IEEE Trans. Nucl. Sci. NS-26, 2186 (1979).

[2] J. L. Conradie, et al., "A Flat-Top Acceleration Systems for the NAC Light Ion Injector Cyclotron," Proc. 14th Int. Conf. on Cyclotron and their Applications, Cape Town, South Africa, 249 (1995).

[3] Y. Kumata, et al., "Model Test of the Flat Top cavity for the JAERI AVF Cyclotron" TIARA Annual Report 1999 (JAERI-Review 2000-024), 285 (2000)

[4] S. Kohara, et al., "Model Test of a Resonator for Flat-Top Acceleration System in the RIKEN AVF Cyclotron," Proc. 12th Symp. on Accelerator Science and Technology, Wako, Japan, 227 (1999).

[5] S. Kurashima, et al., "Design of the Flat-top Resonator for the JAERI AVF Cyclotron," Proc. 13th Symp. on Accelerator Science and Technology, Suita, Japan, 232 (2001).

9.5 Present Status of JAERI AVF Cyclotron System

Y. Nakamura*, T. Nara*, T. Agematsu*, I. Ishibori*, S. Kurashima*, W. Yokota*, M. Fukuda*, S. Okumura*, N. Miyawaki*, K. Arakawa*, K. Akaiwa**, To. Yoshida**, S. Ishiro**, A. Matsumura**, Y. Arakawa**, Tu. Yoshida**, S. Kanou**, A. Ihara** and K. Takano**

Advanced Radiation Technology Center, JAERI*
Beam Operation Service, Co., Ltd.**

1. Introduction

The JAERI AVF cyclotron system[1)-3)] in TIARA facility has been operated smoothly without serious troubles since the start of utilization in March, 1992. A total operation time of the cyclotron system reached to 30000 hours at the middle of May in 2001, then amounted to 32800 hours at the end of March in 2002. An yearly operation time of 3271 hours was close to it in the past several years. Especially, during several national holidays located among the weekdays through last year, cyclotron system was operated continuously. An efficiency of the machine time, which is defined as the ratio of allotted beam time to usable one, has decreased gradually as shown in Fig. 1.

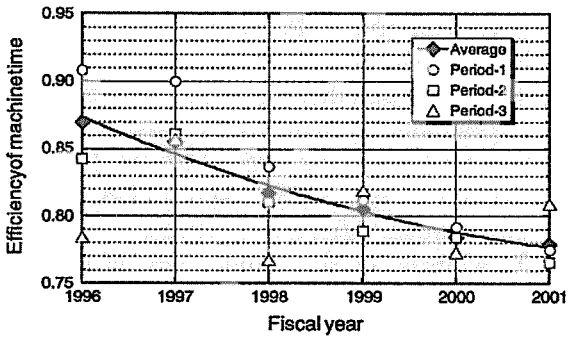

Fig. 1 Change of the efficiency of machine time for recent 6 years.

2. Present Status

2.1 Development and Improvement

A flat-top (FT) acceleration system[4), 5)] using the fifth harmonic of the main RF frequency was installed in last March. The resonant frequency range of the FT system is 55-110 MHz and its maximum input power is rated at 3 kW.

The measurement to confirm the stabilization[6), 7)] of the cyclotron beam has been continued after taking measures for adiabatic treatment and installing an exclusive cooling system. The optimum condition of the cooling system has been investigated to maintain temperature of a magnet yoke invariably during actual cyclotron operation.

A pair of cryogenic pumps installed on two RF resonators were replaced by the FT cavities. One of two pumps was moved to the lower part of a large rectangular duct through the vacuum chamber. A new cryogenic panel was installed inside the vacuum chamber to keep equivalently the vacuum performance.[8)]

In order to observe a precise beam profile at the entrance of a deflector in a flat-top acceleration mode, a new probe with high position-resolution was installed. Either a thin tungsten plate 0.5 mm thick or a slender graphite rod 0.5 mm in diameter as the head of this probe can be chosen.

A chamber equipped with three SSD's placed in a row and a plastic scintillator is shown in Fig. 2. The chamber is installed at CS0 station in the trunk beam transport line. These detectors are used mainly to identify ion species in cocktail beam acceleration.

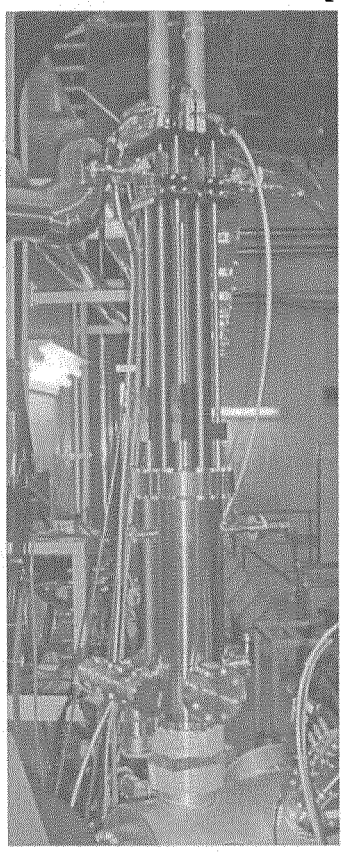

Fig. 2 A tall chamber in which particle identification detectors are included.

2.2 Maintenance and Repair

An air leak was caused at the stainless shield case of the magnetic channel (MC). A small penetrating hall through the case was formed during the cyclotron tuning by bombardment of the intense beam of 70 MeV H^+ as illustrated in Fig. 3. Normal high vacuum condition in the cyclotron chamber became worse due to the air leakage. This MC was replaced with spare MC. Two months later, this small hall was repaired carefully at Takasaki site by the TIG welding. And the soundness of the MC was also confirmed by the measurements of magnetic field and resistance of the molded coils.

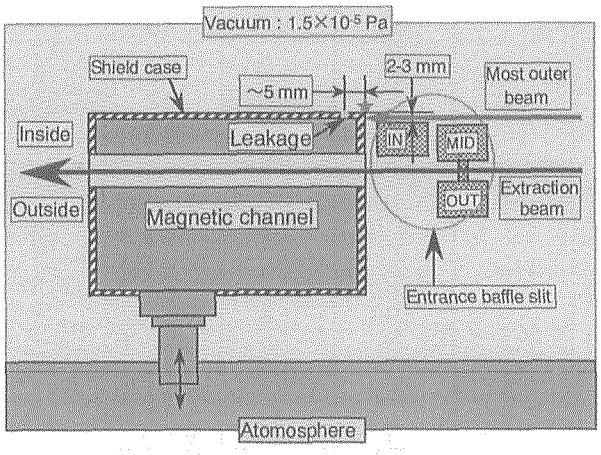

Fig. 3 Prediction of beam bombardment at the MC case. The entrance baffle slit "IN" had been placed outside by 2-3 mm from the designed position.

In early April in 2001, the cyclotron was barely operated for about 2 weeks under serious condition that the beam extracted from cyclotron was fluctuated. As a result of our energetic investigation, the deterioration of the high-voltage wire connected to the inflector electrode was discovered. We repaired the wire temporarily and it was replaced with new one later.

Several mass flow controllers for gas feeding of OCTOPUS using the piezo-element were replaced by precise needle valves with wide dynamic range.

Eight fast closing valves with closing speed of 16 msec were overhauled to keep good conditions.

In July 2001, two weeks before periodical maintenance in summer, a main RF vacuum tube suddenly fell into the fatal condition due to poor electrical conduction between a control grid and an anode. We exchanged it for a used tube tentatively.

The connecting ways related to cooling water, compressed air and electric wires for beam diagnostic devices in the injection line were improved so as to be able to replace easily.

Several power supplies were overhauled to maintain good performances and conditions. Shunt resistors in the power supplies were also replaced.

A storage box enclosed with shielding wall, which is composed of lead block 5 cm thick, was assembled on the floor in the radioactivity cooling room. A lot of radioactivated electrodes and septums for the deflector are stocked in the box as shown in Fig. 4.

In the periodical maintenance of 2001, principal items performed were as follows:

(1) Adjustment and assembling of the No.1 deflector,
(2) Change of the top head of a magnetic channel probe,
(3) Replacement of X-ring fitted up around the driving shaft of a shorting plate in the RF resonator,
(4) Inspection of RF system and evaluation of RF characteristics,
(5) Periodical inspection for a sinusoidal chopper in the trunk beam transport line,
(6) Routine maintenance for five cryogenic pumps in the injection line, each of which is the capacity of 1.6 m^3/s,
(7) Exchange of lubrication oil for about 50 rotary pumps.

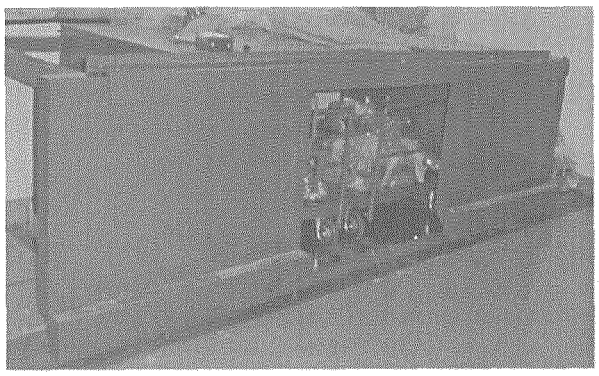

Fig. 4 A storage box enclosed with lead block for radioactivated parts. Internal cubic volume: 1.7 m wide x 0.9 m deep x 0.8 m high.

3. Beam Acceleration Test

A series of neon ion beams including 350 MeV $^{20}Ne^{8+}$, 270 MeV $^{20}Ne^{7+}$ and 200 MeV $^{20}Ne^{6+}$ was developed by a "scaling method". This method is based on the fundamental principle that the momentum is proportional to the charge state under constant magnetic field. These ion beams can be changed within about 10 minutes each other by the same manner as the cocktail beam by adjusting mainly RF frequency and by correcting trim coil field.

The series of $^{4}He^{+}$(25 MeV), $^{12}O^{3+}$(75), $^{16}O^{4+}$(100), $^{22}Ne^{6+}$(165), $^{40}Ar^{10+}$(250), $^{58}Ni^{15+}$(390) and $^{82}Kr^{20+}$(490) has become available as the cocktail beam with M/Q=4. Three kinds of isotope ions were selected intentionally because of the reduction of impurity ions although the ratios of M/Q are rather far from 4.

Helium-3 ion was accelerated up to 60 MeV for the first time in JAERI AVF cyclotron for the purpose of substitutive ion to $^{4}He^{2+}$(100). Furthermore, a metallic $^{56}Fe^{11+}$(210) ion was added on the existing series of the cocktail beam with M/Q=5.

Finally, a number of ion species accelerated by JAERI AVF cyclotron so far are listed in Table 1.

Table 1 The list of ion species accelerated by JAERI AVF cyclotron. The symbol of "Text" in Table 1 is defined by a ratio of the beam current at the Faraday cup just behind the cyclotron to that at 900 mm of the cyclotron radius. The "Tall" is a ratio of the beam current extracted from the cyclotron to that injected into.

Ion species	Energy (MeV)	Intensity (eμA)	Text (%)	Tall (%)
H^+	10	12	80	27
	20	5	77	23
	30	5	67	22
	45	30	79	14
	50	5	44	14
	55	5	63	14
	60	5	57	22
	65	7	62	12
	70	5	42	12
	80	3	47	13
	90	10	48	7.7
D^+	10	11	29	3.7
	20	5.6	80	16
	25	15	88	31
	35	40	59	13
	50	20	49	7.2
$^{3}He^{2+}$	60	8.2	68	18
$^{4}He^{+}$	25	3.6	M/Q=4	13
$^{4}He^{2+}$	20	5.5	69	12
	30	10	42	10
	50	20	62	22
	100	10	32	10
	108	1.6	M/Q=2	
$^{12}C^{3+}$	75	2	M/Q=4	
$^{12}C^{5+}$	220	0.25	77	22
$^{12}C^{6+}$	320	0.0025	M/Q=2	
$^{14}N^{3+}$	67	4	43	10
$^{15}N^{3+}$	56	0.70	M/Q=5	5.0
$^{16}O^{4+}$	100	5	M/Q=4	22
$^{16}O^{5+}$	100	4	34	21
$^{16}O^{6+}$	160	1.9	58	21
$^{16}O^{7+}$	225	1	82	13
$^{16}O^{7+}$	335	0.1	41	6
$^{16}O^{8+}$	430	0.0045	M/Q=2	
$^{20}Ne^{4+}$	75	1.5	M/Q=5	6.6
$^{20}Ne^{5+}$	125	0.01	M/Q=4	
$^{20}Ne^{6+}$	120	1.6	53	18
$^{20}Ne^{6+}$	200	0.8	Scaling	10
$^{20}Ne^{7+}$	260	0.33	70	19
$^{20}Ne^{7+}$	270	0.28	Scaling	14
$^{20}Ne^{8+}$	350	1.5	63	23
$^{20}Ne^{10+}$	540	10^5 cps	M/Q=2	
$^{22}Ne^{6+}$	165	0.007	M/Q=4	
$^{36}Ar^{8+}$	195	2.5	73	13
$^{36}Ar^{10+}$	195	0.1	43	1.2
$^{36}Ar^{18+}$	970	10^5 cps	M/Q=2	
$^{40}Ar^{8+}$	150	2.4	M/Q=5	6.2
	175	3	73	15
$^{40}Ar^{10+}$	250	0.2	M/Q=4	
$^{40}Ar^{11+}$	330	0.7	86	22
$^{40}Ar^{13+}$	460	0.03	63	24
$^{40}Ca^{9+}$	200	2	61	11
$^{56}Fe^{11+}$	210	1.4	M/Q=5	16
$^{56}Fe^{15+}$	400	0.59	66	28
$^{58}Ni^{15+}$	390	0.012	M/Q=4	
$^{82}Kr^{20+}$	490	10^7 cps	M/Q=4	
$^{84}Kr^{17+}$	320	0.08	M/Q=5	5.0
$^{84}Kr^{18+}$	400	0.04	60	2
$^{84}Kr^{20+}$	520	0.06	72	22
$^{84}Kr^{21+}$	525	0.0032	M/Q=4	
$^{129}Xe^{23+}$	450	0.2	72	11
$^{197}Au^{31+}$	500	0.023	49	3

M/Q =2, 4 and 5 : Cocktail beams
Woven pattern : modified data on previous table

References

1) Y. Nakamura, T. Nara, *et al.*, TIARA Annual Report 2000 (JAERI-Review 2001-039) pp. 293-295
2) Y. Nakamura, T. Nara, *et al.*, Proc. 16th Int. Conf. Cyclo. Their Applic., East Lansing, MI, USA (2001) pp. 129-132
3) Y. Nakamura, T. Nara, *et al.*, Proc. 13th Sympo. Accel. Sci. Technol., Suita, Osaka, Japan (2001) pp. 193-195
4) S. Kurashima, M. Fukuda, *et al.*, Proc. 16th Int. Conf. Cyclo. Their Applic., East Lansing, MI, USA (2001) pp. 303-305
5) S. Kurashima, M. Fukuda, *et al.*, this annual report
6) S. Okumura, K. Arakawa, *et al.*, Proc. 16th Int. Conf. Cyclo. Their Applic., East Lansing, MI, USA (2001) pp. 330-332
7) S. Okumura, K. Arakawa, *et al.*, this annual report
8) I. Ishibori, Y. Nakamura, *et al.*, this annual report

9.6 The Number of Operations for Auxiliary Safety Devices

Y. Nakamura* and Y. Arakawa**

Advanced Radiation Technology Center, JAERI*
Beam Operation Service, Co., Ltd.**

1. Introduction

Cyclotron facility in TIARA[1] is equipped with many kinds of auxiliary safety devices, such as safety interlock and display system[2], radiation monitoring system, entrance doors and so on. These devices connected with the cyclotron system[3),4)] are needed especially to be always maintained their reliability and durability. Therefore, we have accumulated so far the number of operations since the installation of 1991 for drafting the maintenance and overhaul plan.

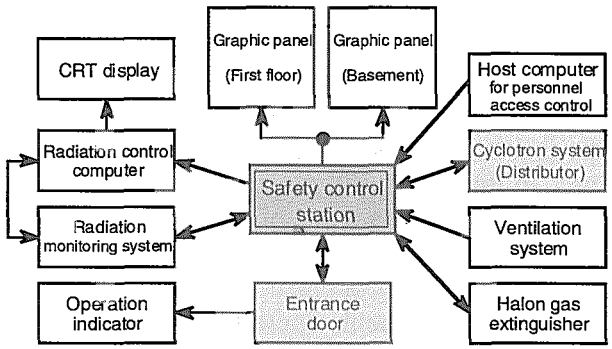

Fig. 1 Relationship between safety control station and their related devices.

2. Counting Method

Apart from the control system of cyclotron, the number of operations (NOO) has been counted up mainly by a programmable controller (C2000H) in the safety control station (SCS) which collects comprehensively various signals related to the safety devices. The relationship between the SCS and their related devices is shown in Fig. 1. The SCS always governs a lot of information for operational condition and status. For examples, the SCS deals with the input signal of 39 points from the entrance doors, on the other hand, it delivers contrarily output signal of 89 points to them.

3. Result of the Number of Operations

We are adding up the NOO for 14 entrance doors and 9 rotary shutters for a year between two overhauls in summer. Besides, the NOO in regard to 34 gate valves, 6 Faraday cups and 6 profile monitors is also monitored by electronic counters.

As an example of these results, the number of cumulative and yearly operations for ten years is shown in table 1 about entrance doors in the cyclotron facility.

Table 1 The number of cumulative and yearly operations about entrance door for ten years. Notation of name means as followings, L:Light ion room, H:Heavy ion room, CY:Cyclotron vault, CP:Cyclotron Pit room, CT:Cable Transit room, M:Master and S:Servant.

Name	JFY	1992	1993	1994	1995	1996	1997	1998	1999	2000	2001	Average
L1M	Accum.	204	347	461	534	662	774	873	982	1100	1283	/ year
	/ year	204	143	114	73	128	112	99	109	118	183	128
L1S	Accum.	14	15	22	30	39	60	63	163	188	191	
	/ year	14	1	7	8	9	21	3	100	25	3	19
L2	Accum.	188	249	395	420	474	541	578	611	661	896	
	/ year	188	61	146	25	54	67	37	33	50	235	90
L3M	Accum.	374	1045	1493	1969	2421	2735	2999	3330	3594	4116	
	/ year	374	671	448	476	452	314	264	331	264	522	412
L3S	Accum.	22	159	166	203	254	261	264	290	297	300	
	/ year	22	137	7	37	51	7	3	26	7	3	30
H1	Accum.	255	362	475	639	862	980	1062	1139	1193	1269	
	/ year	255	107	113	164	223	118	82	77	54	76	127
H2	Accum.	220	899	1232	1613	2229	2844	3395	4019	4529	5238	
	/ year	220	679	333	381	616	615	551	624	510	709	524
H3M	Accum.	256	581	812	1001	1162	1263	1505	1667	1866	2468	
	/ year	256	325	231	189	161	101	242	162	199	602	247
H3S	Accum.	19	37	54	59	70	83	88	105	110	117	
	/ year	19	18	17	5	11	13	5	17	5	7	12
H4	Accum.	273	466	653	894	1084	1407	1772	2001	2204	2400	
	/ year	273	193	187	241	190	323	365	229	203	196	240
H5	Accum.	204	297	357	527	816	1148	1508	1705	1866	2099	
	/ year	204	93	60	170	289	332	360	197	161	233	210
CY	Accum.	25	33	48	62	83	111	133	183	227	247	
	/ year	25	8	15	14	21	28	22	50	44	20	25
CP	Accum.	626	884	1155	1413	1646	1878	2112	2425	2732	3115	
	/ year	626	258	271	258	233	232	234	313	307	383	312
CT	Accum.	264	382	488	560	677	752	836	919	1007	1097	
	/ year	264	118	106	72	117	75	84	83	88	90	110
Woven pattern			: safety door			: shielding door						

The light-weight safety door H2 of heavy ion room 2 where is utilized to irradiate mainly many seeds of various plants and organic samples is the busiest one among 14 doors. The NOO of this door for a year amounts to more than 500 on an average. These 14 doors are inspected periodically every year or two years by their makers.

If two entrance doors are around a room, one is a master door which is used to usually enter in the room, the other is a servant one. The door of H3M, one of which is heavy-weight shielding door and belongs to master one, sometimes occurs worse condition because of frequent operation. For eight shielding doors, the horizontal level of the rail where four iron wheels of the door rotate, is measured with good precision. A little serious sinkage of 3 mm maximum has been observed at the edge on the rail.

Furthermore, the NOO for nine rotary shutters (RS's) imbedded into the shielding wall is listed in Table 2. The allowable cumulative NOO for these RS's was designed about 2000 times in consideration of the actual result at other cyclotron facility. However in actual, some busier RS's are driven around 400 times for a year. A few of them are promoted the deterioration of double vacuum seals around the driving shaft. The busiest TRHB was already renewed to modified one at the stage of 3500 operations in March, 2000.[5)]

In case of the gate valves (GV's), the most frequent GV, which is named TGVLD2, is equipped at the end of the beam course LD. It amounted to 1150 operations at the end of March, 2002. And, eight fast closing GV's were overhauled last year because the NOO had already reached several hundreds.

The NOO per one year for the busiest Faraday cup which is put at the end of HY course, is added up about 5000. The second busiest FC set up at just behind the cyclotron is operated about 3500 times for a year so far. This FC has been already replaced twice with a spare FC owing to air leakage from its stainless steel bellows.

The NOO for auxiliary devices will be rather useful from the viewpoint of future plan and design in similar system.

References

1) H. Watanabe, S. Tanaka, *et al.*, TIARA Annual Report 1992 (JAERI-Review 93-241) pp. 211-220
2) Y. Nakamura, H. Watanabe, *et al.*, TIARA Annual Report 1992 (JAERI-Review 93-241) pp. 227-231
3) Y. Nakamura, T. Nara, *et al.*, Proc. 16th Int. Conf. Cyclo. Their Applic., East Lansing, MI, USA (2001) pp. 129-132
4) Y. Nakamura, T. Nara, *et al.*, Proc. 13th Sympo. Accel. Sci. Technol., Suita, Osaka, Japan (2001) pp. 193-195
5) I. Ishibori, Y. Nakamura, *et al.*, TIARA Annual Report 1999 (JAERI-Review 2000-024) pp. 296-298

Table 2 The number of cumulative and yearly operations about nine rotary shutters for ten years. LA, LB, LC and so on mean their names of the beam transport lines.

Name	JFY	1992	1993	1994	1995	1996	1997	1998	1999	2000	2001	Average
TRLA	Accum.	237	332	559	652	763	883	979	1103	1241	1409	/year
	/year	237	95	227	93	111	120	96	124	63	168	141
TRLB	Accum.	150	213	279	308	342	370	388	417	441	457	
	/year	150	63	66	29	34	28	18	29	8	16	46
TRLC	Accum.	260	630	914	1173	1482	1634	1804	2045	2306	2656	
	/year	260	370	284	259	309	152	170	241	125	350	266
TRLD	Accum.	268	468	769	972	1181	1331	1454	1604	1730	1857	
	/year	268	200	301	203	209	150	123	150	126	127	186
TRHA	Accum.	172	250	444	626	914	1152	1308	1436	1564	1649	
	/year	172	78	194	182	288	238	156	128	64	85	165
TRHB	Accum.	387	786	1100	1412	1874	2265	2671	3203	3697	4395	
	/year	387	399	314	312	462	391	406	532	494	698	440
TRHC	Accum.	211	347	596	907	1287	1889	2605	3083	3474	3971	
	/year	211	136	249	311	380	602	716	478	129	497	397
TRHD	Accum.	193	292	428	509	574	632	714	755	837	1256	
	/year	193	99	136	81	65	58	82	41	41	419	126
TRHE	Accum.	219	360	640	971	1372	1958	2614	3009	3317	3708	
	/year	219	141	280	331	401	586	656	395	98	391	371

9.7 Modification of the vacuum system for AVF cyclotron

I. Ishibori, Y. Nakamura, T. Nara, T. Agematsu, S. Kurashima, W. Yokota, M. Fukuda, S. Okumura and N. Miyawaki

Advanced Radiation Technology Center, JAERI / Takasaki.

1. Introduction

A flat top (FT) acceleration system[1] was installed in the cyclotron for the purpose of the formation of micro beam in March, 2002. A pair of FT cavity was attached to the flanges where two cryogenic pumps had been connected. In order to maintain the vacuum performance of the cyclotron, one of two cryogenic pumps and a new cryogenic panel were assembled to the evacuation chamber which was also reconstructed. The vacuum pressure after the modification was maintained certainly as well as the former condition.

2. Examination and modification

An outline of the vacuum system for the cyclotron before the modification is shown in Fig.1. The vacuum system consists of four main cryogenic pumps, a turbo molecular and a rotary pump. The FT system has a pair of own cavities. There were no spare flanges to install the FT cavities, although these cavities were required to connect directly around the main resonator. Before the removal, we measured the vacuum pressures at several points around the vacuum chamber and the resonator when two cryogenic pumps of CCP_1 and CCP_4 were stopped and the other two pumps of CCP_2 and CCP_3 were operated. The measurement result is shown in Table 1. The vacuum pressure was measured using "cold cathode gauge" made by Balzers.

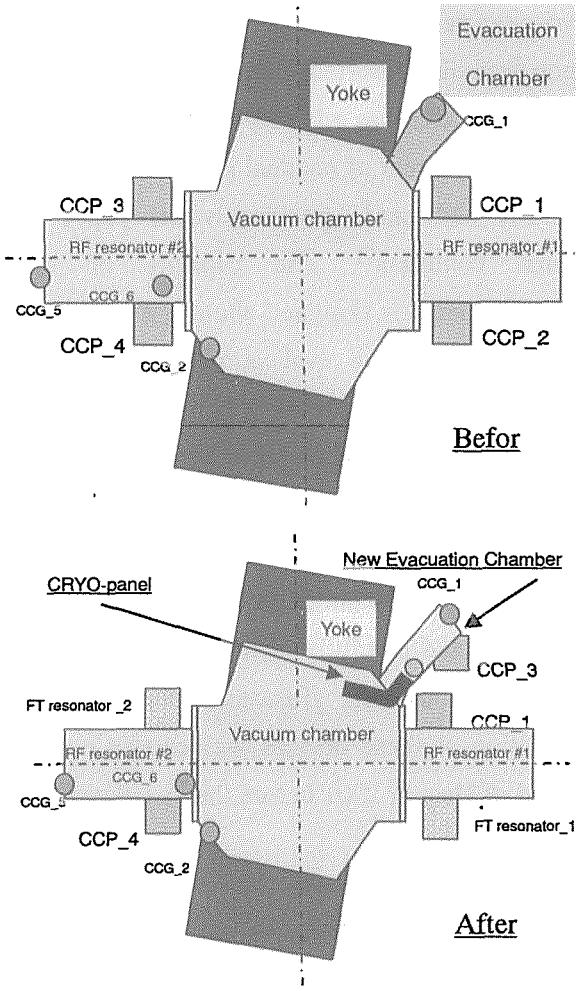

Fig. 1 An outline of the vacuum system for the cyclotron before and after the modification.
CCP1-4: cryogenic pump №1-4,
CCG_1,2,5 and 6: cold cathode gauges

The measured pressures in the resonator

slightly depend on the position of shorting plate in the main resonator and the pressure in the cyclotron become twice as high by stopping two cryogenic pumps.

Therefore two pumps needed to be moved to the evacuation chamber, but it was impossible because of the limitation of the evacuation chamber size. Consequently, the evacuation chamber was reconstructed to a larger one, then one cryogenic pump was moved there and a new cryogenic panel instead of the other cryogenic pump was also inserted into the chamber. This cryogenic panel was adopted by the reason why a main component of residual gas in the vacuum chamber had been specified water vapor at normal condition[2]. The capacity of the cryogenic panel is designed about 8 m^3/s which is the almost same evacuation speed as the existing cryogenic pump for water vapor.

An appearance of the cold absorbing panel inserted into the vacuum chamber is shown in Fig. 2.

The evacuation chamber and cryogenic panel were inspected carefully at the factory prior to the installation in Takasaki site. The installation of these devices was carried out at the end of Dec. in 2001 before the installation of the FT system.

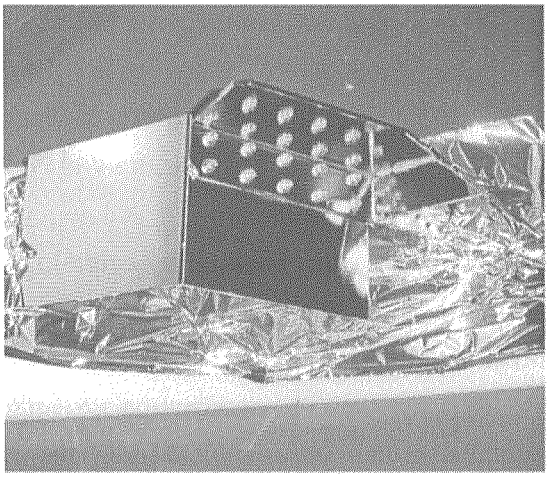

Fig. 2 The cold adsorbing panel plated by nickel on the cupper surface.

3. Performance and operation

In actual, both cryogenic pumps of CCP_2 and CCP_3 were replaced by two FT cavities. After the modification, the pressure indicated at the position of CCG_2 gauge was 1.9 x 10^{-5} Pa when three cryogenic pumps and a new cryogenic panel were operated simultaneously, while the pressure at same position before the modification was 1.6 x 10^{-5} Pa in case of the operation of four cryogenic pumps. Therefore, it seems that the performance of the new cryogenic panel is satisfied its designing specification from above data.

The cryogenic pumps have double stage cold panels, and there were difficult influence of

Table 1 Measurement of vacuum pressure around the cyclotron.

Cryogenic pump	CCP 1 and CCP 4			CCP 1,CCP2,CCP3 and CCP 4		
Position of shorting plate (mm)	0	675	1345	0	675	1345
Vacuum gauge	Pressure (Pa)					
CCG_1	8.3E-5	7.3E-5	7.4E-4	4.7E-5	4.5E-5	4.3 E-5
CCG_2				1.6E-5	1.6E-5	1.6E-5
CCG_5	1.6E-4	1.3E-4	1.,2E-4	1.2E-5	1.1E-4	7.2E-5
CCG_6	8.5E-5	8.3E-5	8.5E-5	3.9E-5	3.7E-5	3.5E-5

warm up. But the cryogenic panel has a single stage cold panel, because the cryogenic panel is under the influence of warm up in the vicinity.

An example of the temperature rise of the cryogenic panel after the start of the continuous operation is shown in Fig. 3.

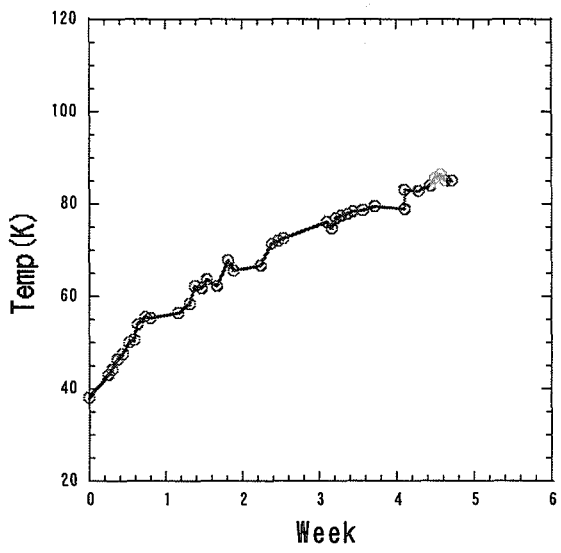

Fig. 3 An example of the temperature rise of the cryogenic panel.

The temperature at the cold panel increased approximately 10 K for a week although generally it depends on the condition in the vacuum chamber, after the lowest temperature at the panel reached to about 40 K. We usually take care of regeneration of the cryogenic panel if the temperature of the cold panel exceeds to 110 K. So far, the regeneration of the panel has been done once for 6-7 weeks in operation. An automatic sequence of the regeneration for the cryogenic panel will be added on the present one in near future.

References

1) S. Kurashima, M. Fukuda, *et al.*, "DESIGN OF THE FLAT-TOP ACCELERATION SYSTEM FOR THE JAERI AVF CYCLOTRON", Proc. 16th Int. Conf. on Cyclo. and Their Applic., East Lansing, Michigan, USA (2001) pp. 303-305

2) Y. Nakamura, I. Ishibori, *et al.*, "Vacuum System for JAERI AVF Cyclotron", JAERI-M 94-007 (1994) 77p.

9.8 Energy Stabilization of TIARA 3 MV Single-ended Accelerator

Takuro Sakai and Sadanori Uno

Advanced Radiation Technology Center, JAERI

1. Introduction

Instability of a terminal voltage for electrostatic accelerator is one of the serious problems in accelerator operations. The instability expands an ion beam energy spread that decrease the transmission of the energy analyzing section and increase the fluctuation of beam current on targets. We have previously reported that, precise energy analyzing slits and a new feedback loop were installed to stabilize the terminal voltage of TIARA 3 MV single-ended accelerator[1]. The system was effective to stabilize the voltage fluctuation in a frequency range of a few Hz. However, a voltage drift extended over a few minute was still unsettled. To suppress the voltage drift, a low-pass filter and additional amplifier circuits were designed and installed to the voltage control circuit.

2. Instruments

The terminal voltage of the single-ended accelerator is sensed by the amount of down-charge current through high precision resistors which are located parallel to Schenkel type high voltage multipliers[2]. However these resistor were degraded by a breakdown in the high voltage column, so a precise current source (Keithley, model 263) was used in this work. The direct momentum analyzing of accelerated ions is another reliable method to know the beam energy.

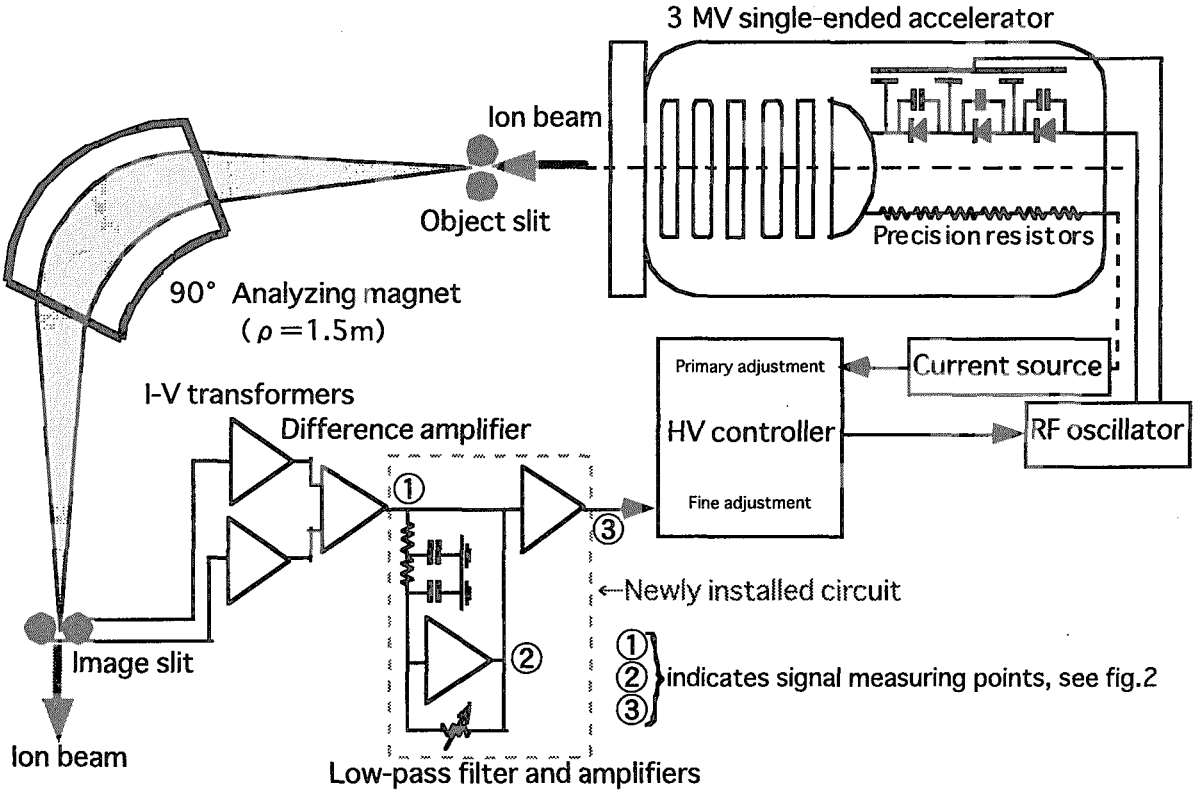

Fig.1 Schematic diagram of voltage control system for the single-ended accelerator

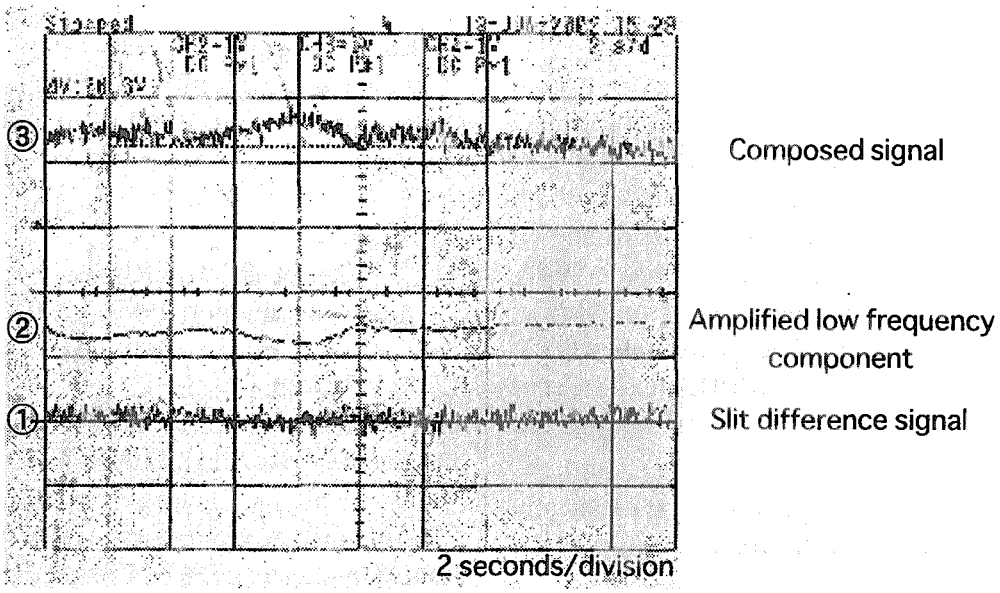

Fig.2 Oscillographic traces of the slit difference signal, its low frequency component and composed control signal

The energy analyzing system is consists of the 90° analyzing magnet and two pairs of slits[1]. Both low-energy and high-energy slit currents are amplified and fed into a differencial amplifier. The difference signal is branched off two signals. High frequency component of one signal is filtered by a low-pass filter (F_{cutoff} = 0.16 Hz) and its low frequency component is amplified to suppress the voltage drift. The voltage control feedback signal is formed by adding the original signal to the modified one. This signal is used for fine control of up-charge to the terminal. Figure 1 shows a schematic diagram of the energy stabilizing systems, and the composed signals are indicated in figure 2.

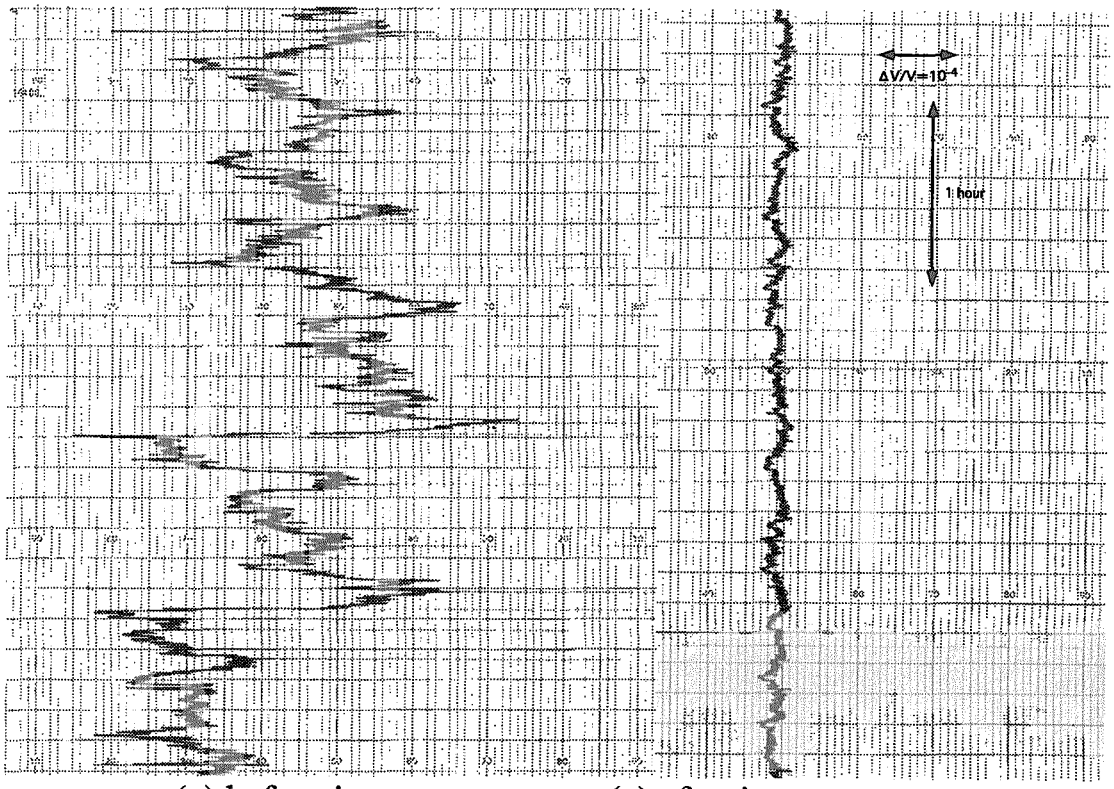

(a) before improvement (a) after improvement

Fig. 3 Traces of the slit difference signal

3. Results

The performance of the new system was tested with 2.6 MV terminal voltage, extracting proton beam current of 10 μA. Traces of the slit difference signals both before and after the improvement are shown in figure 3. The fluctuation was successfully reduced to below a tenth part of initial one. The trial operation has been started to provide a stable beam to micro-PIXE experiment which requires very narrow energy spread ($\Delta E/E \sim 10^{-5}$) of the ion beam[3], and the improved system was proved to be drastically effective to suppress the voltage drift over 10 hours.

Next step of the energy stabilization is to minimize the fluctuation for higher frequency range. A terminal stabilizer[4)-6)], that is equipped with a voltage modulator between the ion source and the terminal, is a promising method for this purpose.

Acknowledgement

We are grateful to JAERI electrostatic accelerator group for their continuous assistance.

References

1) T. Sakai et al., JAERI-Review 2000-024 (TIARA annual report 1999) p239
2) Y. Saitoh et al., Nucl. Instr. and Meth. B89 (1994) 23.
3) T. Kamiya, T. Suda and R. Tanaka, Nucl. Instr. and Meth. B118 (1996) 447.
4) J. Takács, Energy Stabilization of Electrostatic Accelerators, (John Wiley & Sons, Chichester, 1997)
5) G. W. Roth and W. G. Weitkamp, Nucl. Instr. and Meth. 115 (1974) 501.
6) J. E. Cairns, M. W. Greene and J. A. Kuehner, Nucl. Instr. and Meth. 114 (1974) 489.

9.9 Increase of a negative heavy ion source for the 3MV tandem accelerator

K. Mizuhashi*, A. Chiba*, A. Santoso** and S. Tajima*
Advanced Radiation Technology Center, JAERI*
National Nuclear Energy Agency, INDONESIA**

1. Introduction

The 3MV tandem accelerator has completed in March 1991 and started operation for the experiments in November 1991. The injector of the tandem accelerator system was designed according to the plan of operating time that is from 9:00 a.m. to 6:00 p.m. of the weekdays. Since the number of user increased year after year, beam time was not enough for the users. So operating time of tandem accelerator was extended by user's request in 1996. The tandem accelerator is operated from 8:30 a.m. to 11:00 p.m. on the weekdays from 1996. We could not maintain the ion-source on the weekdays by those circumstances. To keep the maintenance time on the weekdays, a negative heavy ion source (Source of Negative Ion by Cesium Sputter, SNICS) that is used over 90% of all of operating time was increased. Now the tandem accelerator has two SNICSs and one Alphatross ion-source that is for negative helium ion.

2. Increase of negative heavy ion source

SNICS can generate the many kinds of negative ion from hydrogen to gold except helium. We began to generate cluster ions of some kinds of chemical element from 1996. As the operation condition for generating cluster ion is very hard, it tend to spoil the inside of the ion source. Therefore two SNICSs are used properly as follows, a new one for the normal ions and the other for the cluster ions. Fig. 1 shows a new injector system having three ion sources. By increase of SNICS, it is possible to condition an ion source independently of the routine operation. When an ion source suddenly has any trouble, some user must to do experiment under the bad conditions of the beam. A dual SNICS system will solve this kind of problem too, because we can quickly change the ion source.

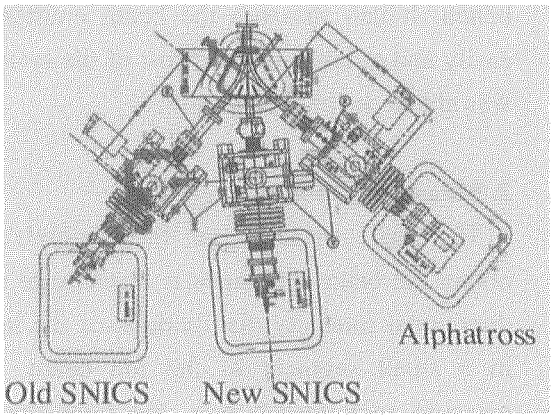

Fig.1 Injector with three ion sources
Three ion sources are connected with tandem accelerator via a switching magnet. Old SNICS joined to 40 degrees port at left side, New SNICS and Alphatross joined to 5 degrees and 50 degrees port at right side.

9.10 Development of Image Analysis Type Emittance Monitor

Atsuya CHIBA, Yasuyuki ISHII and Satoshi TAJIMA
Advanced Radiation Technology Center, JAERI/Takasaki

1. Introduction

When we discuss the beam quality of the electrostatic accelerator, the high voltage stability and the emmitance of the beam extracted from the ion source are important parameters in respect with formation of the high intensity microbeam and effective beam transportation through the beam line. Generally, a measurement of the emittance takes long time, because the measurement points were so many and also current intensity at the point was very little.

We developed a new measuring device consisted of a slit of the multiple clearance type, an illuminant and a CCD camera, and the measurements was carried out for Helium beam extracted from RF ion source at the test bench. It can measure the beam emittance easily and quickly, and the cost of the system was able to be held down low.

2. Measuring method

The basic principle of the methods to obtain the beam emittance is to measure the directional intensity distributions of the ions in a small segment of the ion beam. To measure such distribution, the light image activated by the collimated beam on the illuminant was taken twice time into the personal computer at the different positions of the illuminant by CCD camera put at the rear of the illuminant. The width on the image was analyzed using the gray scale, and the divergence angle was calculated in comparison with the width of the images on the illuminant at two positions. Fig.1 shows how to measure the divergence angle with a pair of the light images.

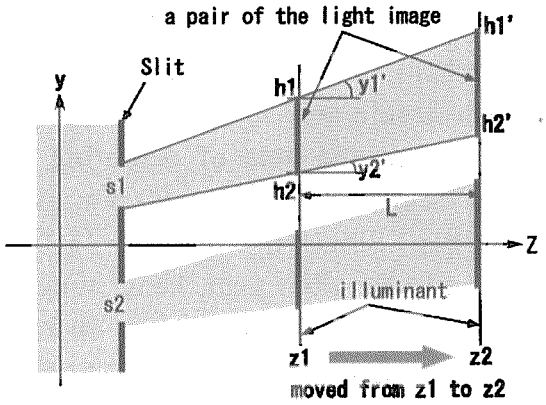

Fig.1. Schematic view of the slit and the illuminant

Maximum value (y1') and minimum value (y2') of the divergence angle for the beam passed through the clearance S1 is shown as equation (1) and (2).

$$y1' = \frac{h1' - h1}{L} \qquad (1)$$

$$y2' = \frac{h2' - h2}{L} \qquad (2)$$

Where h1, h2 and h1', h2' are the positions of the both edges for a pair of the light images at the illuminant position z1 and z2, and L is a moving distance of the illuminant.

3. Outline of the equipment

An outline of the measuring device is

shown in Fig.2. The Helium beam extracted from ion source that is being used for the single-ended accelerator at present is transported to the illuminant through the slit. The illuminant is a thin-sheet of 12 μ m thick of ZnS(Ag) that is bonded on the glass of 1.0 cm thick by the optics adhesive. The light image on the illuminant is digitized by CCD camera at just behind the illuminant by the personal computer, and the emittance is analyzed. The unit of illuminant and camera can slide together to another position on the beam axis.

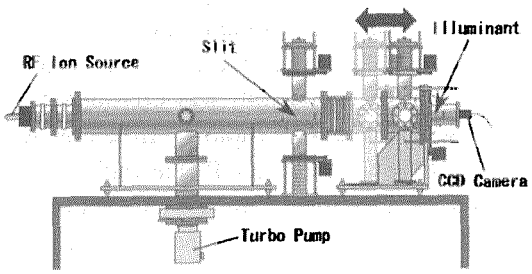

Fig.2. Outline of the measuring device

4. Measurement result

Fig.3 is monochrome image on the illuminant, and Fig.4 is the gray scale distribution on the dotted line of the image.

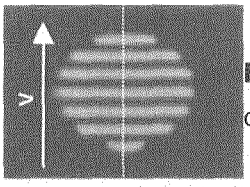

Fig.3. Monochrome image on the illuminant

The gray scale is an index of the luminosity, and it will be proportional to the beam intensity. The beam emittance was obtained by the relation of two gray scale distributions at illuminant position z1=0mm and z2=120 mm. In this measurement, the beam size from the RF source was so large for this device, that a result was limited to upper half.

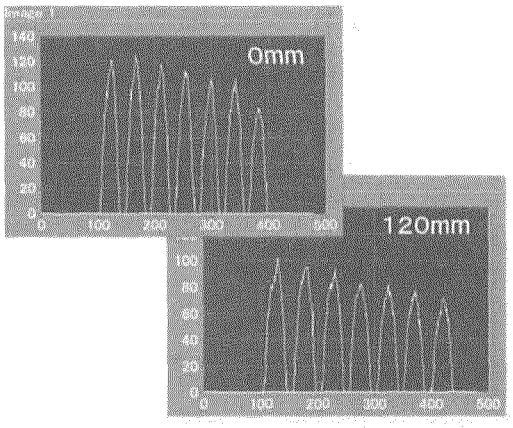

Fig.4. The gray scale distribution on the dotted line. The horizontal axis has shown the y position of the beam. Upper was obtained position at standard position and lower was obtained at 120mm far from above .

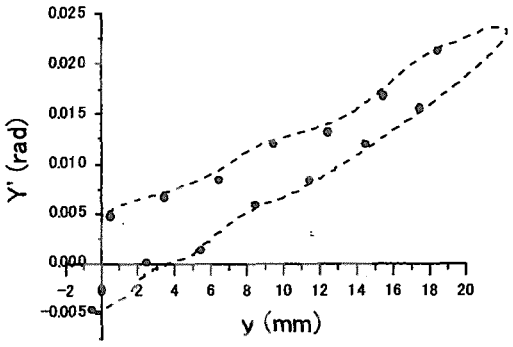

Fig.5. Beam emittance of 8keV Helium ion from RF source. The vertical axis means a divergence angle, and the horizontal axis is the perpendicular position in the beam.

5. Summary

In present measurement, it was possible to distinguish the light image clearly, and also there were no fuzziness and slippage of the borderline by moving of the illuminant. The measurement of the 100% emittance was easily obtained by the simple system with short measurement time (about 20 sec/a measurement).

9.11 Improvement of the injection electrode system for forming a submicron ion beam

Yasuyuki Ishii, Akira Isoya and Kazuo Arakawa
Advanced Radiation Technology Center

1 Introduction

The submicron ion beam system has been developed to produce a several tens keV H_2^+ with 0.1 μm width. The system consists of the duoplasmatron-type ion source [1], the acceleration lens system [2] and the submicron beam measurement system [3]. The beam width was produced about 0.5 μm when the system was developed. The beam width was gradually reduced by improving various parts. Especially the smaller beam width was formed by reducing the beam divergence angle injected in the acceleration lens system. So far, about 30 keV H_2^+ beam with 0.28 μm width has been formed using the system [4]. The beam width was, however, about 2.5 times larger than that of the beam trajectory calculations. In addition, the beam focused by the acceleration lens system (hereafter beam spot) was fluctuated within about 0.4 μm per 20 min. Since the movement of the beam spot was slow, it was considered to be negligible in order to measure the beam width.

The beam width difference between the calculated and the formed beam width was considered to lie in the distinction of the beam divergence angle injected in the acceleration lens system because of the usage of the ion beam generation method from the unstable plasma beam in the ion source (hereafter plasma beam method). The method was used to generate the ion beam with the reduction of the beam divergence angel and the about 100 eV beam with the small beam energy spread within 2 eV. The plasma beam was extracted in the high vacuum space of about 6×10^{-4} Pa on the basis of employing the non-magnetic anode to reduce the collision of ion-neutral gas and/or ion-ion. Some electrodes were introduced between the anode and the extraction electrode or the plasma beam was actively diverged in that same space to stabilize the plasma beam. These efforts could not, however, improve on the beam divergence angle.

The other beam extraction method was introduced to break through this difficulties. The method was the one extracting ion beam from the neighborhood of the small single anode hole without using plasma beams in the ion source (hereafter anode extraction method). Although the beam divergence angle using the anode extraction method was not expected to be reduced in the demagnification rate of more than the plasma beam method, the object point width could be shorter than that of plasma beam method at the 1st acceleration lens. Thereby beam spot width was considered to reduced within 0.2 μm width. An anode with a 0.2mmϕ hole tapered at the Pierce angle was introduced by performing this method in the ion source. The experimental results of the characteristics of ion beam generation were represented in this report. The results show that the divergence angle was reduced in about 3×10^{-3} rad, which is about $\frac{1}{5}$ times shorter than the previous injection divergence angle. This ion beam generation method could lead us to form the 0.1 μm beam width.

2 Ion beam generation system

The schematic diagrams of the submicron ion beam system with the anode of a 0.2mmϕ hole tapered at the Pierce angle and the enlarged illustration of its anode were shown in Fig. 1 and Fig. 1 (A), respectively. The anode was made of Cu as the non-magnetic and thermal conductive material. The distance between the anode and the extraction electrode was shortened from over 15 mm of the previous setting condition to about 8 mm in order to make the electric field strength. The plasma sheath was generated in the neighborhood of anode hole by applying over 300 V to the extraction electrode. The divergence angle of the beam was reduced by the 0.2mmϕ hole of the extraction electrode. The parallel acceleration electrode was placed down stream of the extraction electrode to reduce the divergence angle more. Finally, the

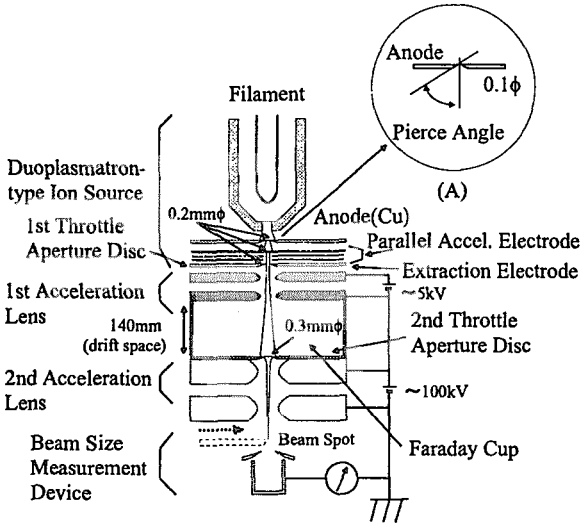

Figure 1: Schematic diagram of the submicron ion beam system of the anode with a 0.2mmϕ hole tapered at Pierce angle.

throttle electrode with a 0.2mmϕ hole was set in 18 mm under the parallel acceleration electrode as the throttle aperture of 1st acceleration lens. The extraction and the throttle electrode currents were measured as I_{ext} and I_{inj}, respectively. The beam current passing through the 1st acceleration lens was also measured by Faraday cup placed on the downstream of its lens.

3 Performance of the beam generation system

The experimental data of beam current extracted from the ion source is shown in Fig.2. The

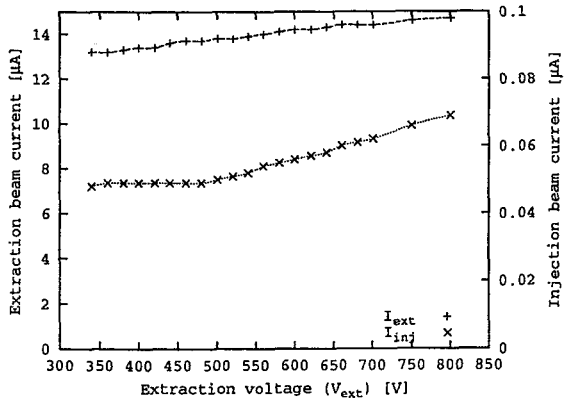

Figure 2: Relation between extraction current (I_{ext}) and the injection current (I_{inj}) as a function of the extraction voltage (V_{ext}).

vacuum in the ion source, the voltage of parallel acceleration electrode and the 1st acceleration lens voltage were about 8 Pa, 350 V and 6 kV, respectively. The beam current gradually increased from about 13 μm to about 15 μA by applying the extraction voltage form 300 V to 800 V (I_{ext}). The beam current passing through the extraction electrode with 0.2mmϕ extraction hole and the parallel acceleration electrodes also increased from about 0.05 μA to about 0.07 μA (I_{inj}) on the 1st throttle aperture disk. The ratio of $\frac{I_{inj}}{I_{ext}}$ was almost constant in 4×10^{-3} order. After the beam passed through this throttle aperture with 0.2mmϕ hole, the beam was injected in the 2nd throttle aperture disk in front of the 2nd acceleration lens. The beam current (I_{acc}) was measured using Faraday as shown in Fig.1. The ratio of I_{inj} and I_{accel} was changed as shown in Fig.3 as a function of extraction voltage (V_{ext}). The maximum ratio was about 38% at

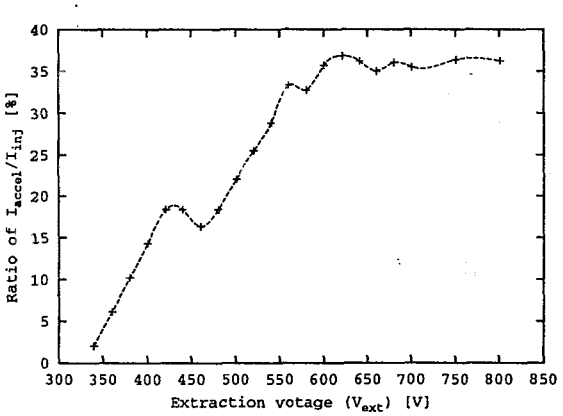

Figure 3: Ratio of the transit current as a function of V_{ext}

V_{ext} of about 620 V. The beam width on the throttle electrode was calculated in about 0.17mmϕ at this point from relation between the ratio and planar dimension of throttle hole as the beam with the disk-like ion density approximately. The beam divergence angle injected in the acceleration lens system was calculated on the basis of the geometrical of the electrodes as shown in Fig.4. The minimum beam divergence angle injected in the acceleration lens was estimated in 3×10^{-3} rad order form the geometry of the electrodes. The divergence angel was about $\frac{1}{5}$ times shorter than that of the previous ion beam generation system This beam divergence angle is sufficient to form the beam width within 0.28 μm. This incident angle lead us to from the beam width of less than 0.28 μm.

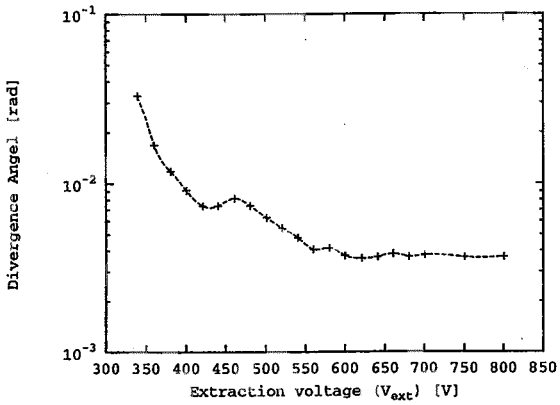

Figure 4: Relation between the beam current in front of the acceleration lens system and the transit current injected in its lens system as a function of V_{exit}.

References

[1] Y. Ishii et. al, Nucl. Instr. and Meth. B113(1996) 75.

[2] A. Isoya, Ulvac Technical Journal No.44(1996) p.42.

[3] Y.Ishii. et. al, JAERI-Review 99-025, P.25.

[4] Y. Ishii, et,al., Nucl. Instr. and Meth. B181(2001)71

10. Status of TIARA 2001

This is a blank page.

10.1 Utilization of TIARA Facilities

Utilization and Coordination Division,

Advanced Radiation Technology Center, JAERI

1. Introduction

TIARA is a center of the ion accelerator facilitie composed of four ion accelerators, the AVF cyclotron, the 3MV tandem accelerator, the 3MV single-ended accelerator, and the 400kV ion implanter. These accelerators have been fully served for ion beam applications since January 1994.

2. Utilization System

TIARA is opened for public use: it receives applications of the experimental subjects in wide areas once a year from outside users as well as JAERI staffs. The subjects and these own utilizable beam times are approved after the official investigation by Subcommittee for TIARA under Advisory Council for JAERI's Research Facilities, which are both publicly organized since 1999. To attain an effective outcome of the research program, the utilization time of each accelerator is fairly allotted to the subjects three times in a year based on the approved beam time.

Charges for the utilization are remitted in the case that a contract of the joint research between JAERI and a university or a company or that of the projective joint research between JAERI and universities is made. The results of research have to be published at the TIARA Research Review Meeting and in the JAERI TIARA Annual Report. There is another system of visitor use with charges but without the publication duty.

3. Experimental subject approved

Number of subjects using cyclotron approved in FY2001 for the experiment was 48 while the total number using three electrostatic accelerators was 51 as shown in Table 1. Table 2 shows the number allotted to users under various contracts.

4. Allotted time to users

The cyclotron has been continuously operated from Monday to Friday. The utilization time for the cyclotron is allotted with unit of the hour. In case of the electrostatic accelerators, on the other hand, the utilization time is allotted with unit of the day either from 9 a.m. to 7:30 p.m. (A mode), or from 9 a.m. to 10 p.m.(B mode).

As shown in Table 3, the cyclotron was used

Table 1 Number of experimental subjects at various research fields.

Accelerators / Fields of research	Number of subjects: Cyclotron	Electrostatic accelerators
Materials for space	4	5
Materials for fusion	1	11
Biotechnology	30	2
Inorganic material	0	24
RI & nuclear sci.	1	0
Organic material & Radiation chemistry	7	0
Basic technology	5	9
Total	48	51

Table 2 Number of experimental subjects at various relations with users.

Accelerators / Relations with visitors		Number of subjects: Cyclotron	Electrostatic accelerators
JAERI only	Takasaki Establishment	9	12
	Others	0	9
Cooperative research with university		14	16
Projective joint research between JAERI and universities		9	9
Joint research with private company or governmental institute		16	5
Total		48	51

at the various research fields, while the electrostatic accelerators were mainly used in the field of inorganic material and material for fusion. The ratios of allotted time for JAERI staffs to whole utilization time were 31% for the cyclotron and 50% for the other electrostatic accelerators as shown in Table 4.

Table 3 Utilization of the accelerators in FY2001 at various research fields.

Accelerators / Fields of research	Utilization time at each period															
	Cyclotron (hours)				Tandem accelerator (days)				Single-ended accelerator (days)				Ion implanter (days)			
	01-1	01-2	01-3	total	01-1	01-2	01-3	total	01-1	01-2	01-3	total	01-1	01-2	01-3	total
Material for space	203	106	131	440	12	15	4	31	-	-	-	-	12	11	7	30
Material for fusion	0	0	64	64	11	17	19	47	10	9	10	29	7	10	10	27
Biotechnology	410	354.5	126.5	891	3	4	0	7	-	-	-	-	-	-	-	-
Inorganic material	-	-	-	-	13	11	11	35	21	25	20	66	22	22	18	62
RI & nuclear science	12	12	0	24	-	-	-	-	-	-	-	-	-	-	-	-
Organic material & Radiation chemistry	82	67.5	42.5	192	-	-	-	-	-	-	-	-	-	-	-	-
Basic technology	125	59	20	204	9	8	6	23	18	15	12	45	0	0	0	0
Machine study	125	80	79	284	4	6	3	13	4	4	4	12	3	3	2	8
Visitors use with charges	204.5	140	85	429.5	3	2	1	6	0	0	0	0	5	3	3	11
Total	1161.5	819	548	2528.5	55	63	44	162	53	53	46	152	49	49	40	138

Table 4 Utilization of the accelerators in FY2001 at various relations with users.

Accelerators / Relation with visitors		Utilization time at each period															
		Cyclotron (hours)				Tandem accelerator (days)				Single-ended accelerator(days)				Ion implanter (days)			
		01-1	01-2	01-3	total	01-1	01-2	01-3	total	01-1	01-2	01-3	total	01-1	01-2	01-3	total
JAERI Only	Takasaki Establishment	233	169	102.5	504.5	22	21	5	48	6	8	11	25	26	22	16	64
	others	0	0	0	0	3	5	4	12	15	8	8	31	3	3	5	11
Cooperative research with universities		101.5	97	49.5	248	13	13	11	37	9	14	6	29	6	10	8	24
Projective joint research between JAERI and universities		256	149	78	483	7	9	14	30	19	18	16	53	4	7	5	16
Joint research with company or governmental institute		241.5	184	154	579.5	3	7	6	16	0	1	1	2	2	1	1	4
Machine study		125	80	79	284	4	6	3	13	4	4	4	12	3	3	2	8
Visitors use with charges		204.5	140	85	429.5	3	2	1	6	0	0	0	0	5	3	3	11
Total		1161.5	819	548	2528.5	55	63	44	162	53	53	46	152	49	49	40	138

10.2 Operation of JAERI AVF Cyclotron System

Y. Nakamura*, T. Nara*, T. Agematsu*, I. Ishibori*, S. Kurashima*, W. Yokota*, M. Fukuda*, S. Okumura*, K. Akaiwa**, To. Yoshida**, S. Ishiro**, A. Matsumura**, Tu. Yoshida**, Y. Arakawa**, S. Kanou**, A. Ihara** and K. Takano**

Advanced Radiation Technology Center, JAERI*
Beam Operation Service, Co., Ltd.**

The JAERI AVF cyclotron system was smoothly operated according to a beam time schedule. The total operation time through JFY 2001 amounted to 3271 hours.

Cumulative and yearly operation time since the start of operation is shown in Fig. 1. The fact that a very fairly step-wise feature is seen, means clearly that the cyclotron system has been in steady operation for 10 years since 1992.

The ratios of operation time used for experiments including visitor's use with charge, machine tuning, beam development and machine study were 68.6%, 19.1% and 12.3%, respectively. Twenty-six kinds of ion species, which are the almost same as last year, were also delivered for various experiments.

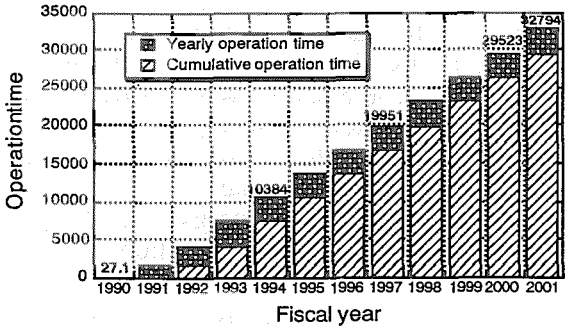

Fig. 1 Cumulative and yearly operation time.

Regular yearly overhaul was performed for four weeks in summer, 2001.

In order to confirm the stabilization of the cyclotron beam, a precise NMR probe installed inside of the cyclotron chamber to monitor variation of the magnetic field during cyclotron operation.

The flat-top acceleration system with frequency range of 55-110 MHz was installed in March, 2001 after careful design. A high-position resolution deflector probe equipped with either a thin tungsten plate or a slender graphite rod was installed to observe the turn separation.

In October 2001, an air leakage through a little hole of the stainless case enclosed the magnetic channel (MC) coils was caused during the tuning by intense beam of about 6 μA of 70 MeV proton. This MC was replaced with spare MC quickly.

Figure 2 shows the percentages of accelerated ions. The summed rate of heavy ions and cocktail ones occupied 67.1 % to total time, while the beam time for light ions was 31.6 % of all.

Another series of M/Q=4 cocktail beam consisted of $^{4}He^{+}$, $^{12}C^{3+}$, $^{16}O^{4+}$, $^{22}Ne^{6+}$, $^{40}Ar^{10+}$, $^{58}Ni^{15+}$ and $^{82}Kr^{20+}$ was developed for practical use. Furthermore, helium-3 ion was accelerated first up to 60 MeV.

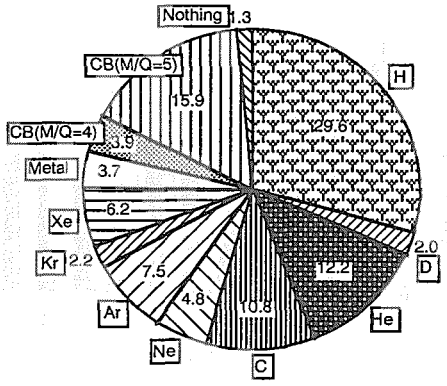

Fig. 2 The percentages of accelerated ion species during JFY 2001.

The frequencies of the change of ion species, energy and beam course are shown in Fig. 3. The number of the beam course alterations amounted to more than 260 in last two years. And the frequencies of particle and energy changes also increase gradually year by year.

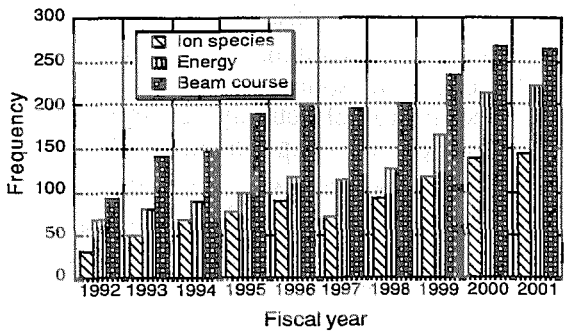

Fig. 3 Frequencies of the change for particle, energy and beam course since 1992.

10.3 Operation of the Electrostatic Accelerators

I. Takada*, K.Mizuhashi*, S. Uno*, K. Ohkoshi*, A.Chiba*,
Y. Saitoh*, Y. Ishii*, T. Kamiya *, T. Sakai*, M.Ishii**, T.0rimo**,
T.Takayama**, M.Kouka**, A.Ohmae**, T.Kitano** and S.Kanai**

Advanced Radiation Technology Center, JAERI *
Beam Operation Service, Co., Ltd.**

1. Operation

The electrostatic accelerators were operated smoothly for various experiments in FY 2001. The total operation time for each accelerator in this fiscal year was 2,036 hours for the tandem accelerator, 2,420 hours for the single-ended accelerator and 1,859 hours for the 400kV ion implanter, respectively. Monthly operation time for each accelerator are shown in Fig.1 .

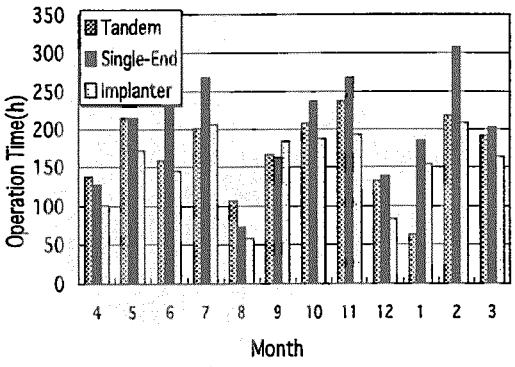

Fig. 1 Monthly operation time for each accelerator in FY 2001.

2. Maintenance

The maintenance for the accelerators were carried out in April, August and December. During these terms several improvement and renewals were performed as follows;

For the tandem accelerator; 1) A second ion source was installed in the injector to effectively promote the operation for experiments in January. 2) A high-voltage on the terminal could not be kept stable several times a year. This trouble similarly occurred in other pelletron accelerator in japan and cause of it has not defined. For the single-ended accelerator; 3) The ion source which was cracked at the joint of glass was exchanged thrice with new ones . 4) A HV stabilizer was exchanged with new one in August because the noise increased, and precise control could not be done by operating for about seven years.

For the 400kV ion implanter ; 5) A burned power supply of TMP exchanged with spare one . 6) The gauss meters of BMI-1,BMI-2 and BMI-3 were renewed with high-resolution one in August.

3. Development

A performance generating the single charged ions of MINI-ECR source was tasted and confirmed that the beam intensities of MINI-ECR were much than it of freeman source for some ion species. In order to decrease the damages for the high-voltage measuring resistors, the demonstration of the non-inductive type resistors were carried out by the single-ended accelerator, and we could confirm they have a durability for the high-voltage sparks. In order to develop the beam energy stabilizing system for micro-beam operation, the slit control system which consists of two precise pair slits set at front and behind of the 90° energy analyzing magnet was demonstrated by the single-ended accelerator. By using the low-pass filter with the signal from the slit, 4×10^{-5} of energy stability ($\Delta E/E$) was obtained at 2.6MV proton operation.

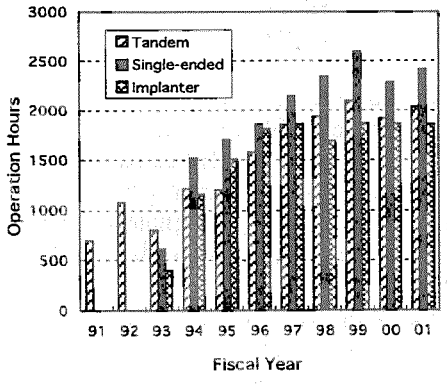

Fig.2 Yearly operation time for each accelerator since 1991

10.4 Radiation Control & Radioactive Waste Management in TIARA

Safety Division & Utilities and Maintenance Division
Department of Administrative Services, JAERI

1. Radiation Control

1.1 Individual monitoring

(1) Individual monitoring for the radiation workers

Table 1 shows a distribution on effective dose equivalent of the radiation workers in FY 2001. The effective dose equivalent values of almost workers were less than 0.1 mSv (minimum detectable dose equivalent).

Maximum dose equivalent was 1.6 mSv/y due to the overhauling of the cyclotron.

(2) Individual monitoring for the visitors and others

Table 2 shows number of persons who have been temporally entered the radiation controlled areas. The effective dose equivalent of all persons was less than 0.1 mSv.

Table1. Distributions on the effective dose equivalent in FY2001.

Persons / Items \ Periods		Number of persons			
		1st quarter	2nd quarter	3rd quarter	4th quarter
Distribution range on effective dose equivalent HE:Effective dose equivalent*1(mSv)	HE < 0.1	539	561	553	599
	0.1 ≦ HE ≦ 1.0	1	11	21	10
	1.0 < HE ≦ 5.0	0	0	0	0
	5.0 < HE ≦ 50.0	0	0	0	0
	50.0 < HE	0	0	0	0
Persons for radiation control(A)		540	572	574	609
Exposure above 1mSv	Persons(B)	0	0	0	0
	(B)/(A)×100(%)	0	0	0	0
Mass effective dose equivalent (Persons·mSv)		0.1	2.4	4.7	1.9
Mean dose equivalent (mSv)		0.00	0.00	0.01	0.00
Maximum dose equivalent (mSv)		0.1	0.6	0.7	0.3

*1 Not detected according to internal exposure.

Table 2. Number of temporary entrance persons to radiation controlled areas in FY2001.

Persons / Periods	Number of persons				
Temporary entrance persons	1st quarter	2nd quarter	3rd quarter	4th quarter	Total
	401	345	563	313	1622

1.2 Monitoring of radioactive gases

Table 3 shows the maximum radioactive concentrations and total activities for radioactive gases released from TIARA's stack, during each quarter of FY 2001.

The least amount of ^{41}Ar, ^{11}C, ^{13}N and ^{18}F were detected for some time during operation of the cyclotron, but the pulverized substance (^{65}Zn, etc) were not detected

Table 3. Monitoring results of released gaseous radioactivity in FY 2001.

Nuclide	Items / Periods	1st quarter	2nd quarter	3rd quarter	4th quarter	Total
^{41}Ar	Maximum concentration (Bq/cm^3)	1.6×10^{-4}	$<5.4 \times 10^{-5}$	$<5.4 \times 10^{-5}$	$<5.4 \times 10^{-5}$	1.6×10^{-4}
	Activity (Bq)	7.9×10^{8}	6.6×10^{6}	1.7×10^{8}	4.1×10^{7}	1.0×10^{9}
^{11}C	Maximum concentration (Bq/cm^3)	$<5.4 \times 10^{-5}$	$<5.4 \times 10^{-5}$	7.9×10^{-5}	———	7.9×10^{-5}
	Activity (Bq)	7.3×10^{7}	1.3×10^{8}	4.6×10^{8}	———	6.6×10^{8}
^{13}N	Maximum concentration (Bq/cm^3)	$<5.4 \times 10^{-5}$	$<5.4 \times 10^{-5}$	$<5.4 \times 10^{-5}$	———	$<5.4 \times 10^{-5}$
	Activity (Bq)	1.8×10^{8}	7.4×10^{7}	5.9×10^{7}	———	3.1×10^{8}
^{18}F	Maximum concentration (Bq/cm^3)	$<5.4 \times 10^{-5}$	———	———	———	$<5.4 \times 10^{-5}$
	Activity (Bq)	2.6×10^{6}	———	———	———	2.6×10^{6}
^{65}Zn	Maximum concentration (Bq/cm^3)	$<6.5 \times 10^{-10}$	$<5.7 \times 10^{-10}$	$<6.4 \times 10^{-10}$	$<6.1 \times 10^{-10}$	$<6.5 \times 10^{-10}$
	Activity (Bq)	0	0	0	0	0

1.3 Monitoring for external radiation and surface contamination

External radiation monitoring was routinely carried out in/around the radiation controlled areas and surface contamination monitoring was also carried out. Neither unusual value of dose equivalent rate nor surface contamination were detected.

Figure 1 displays a typical example of distribution of the dose equivalent rate at the radiation controlled area in the cyclotron building.

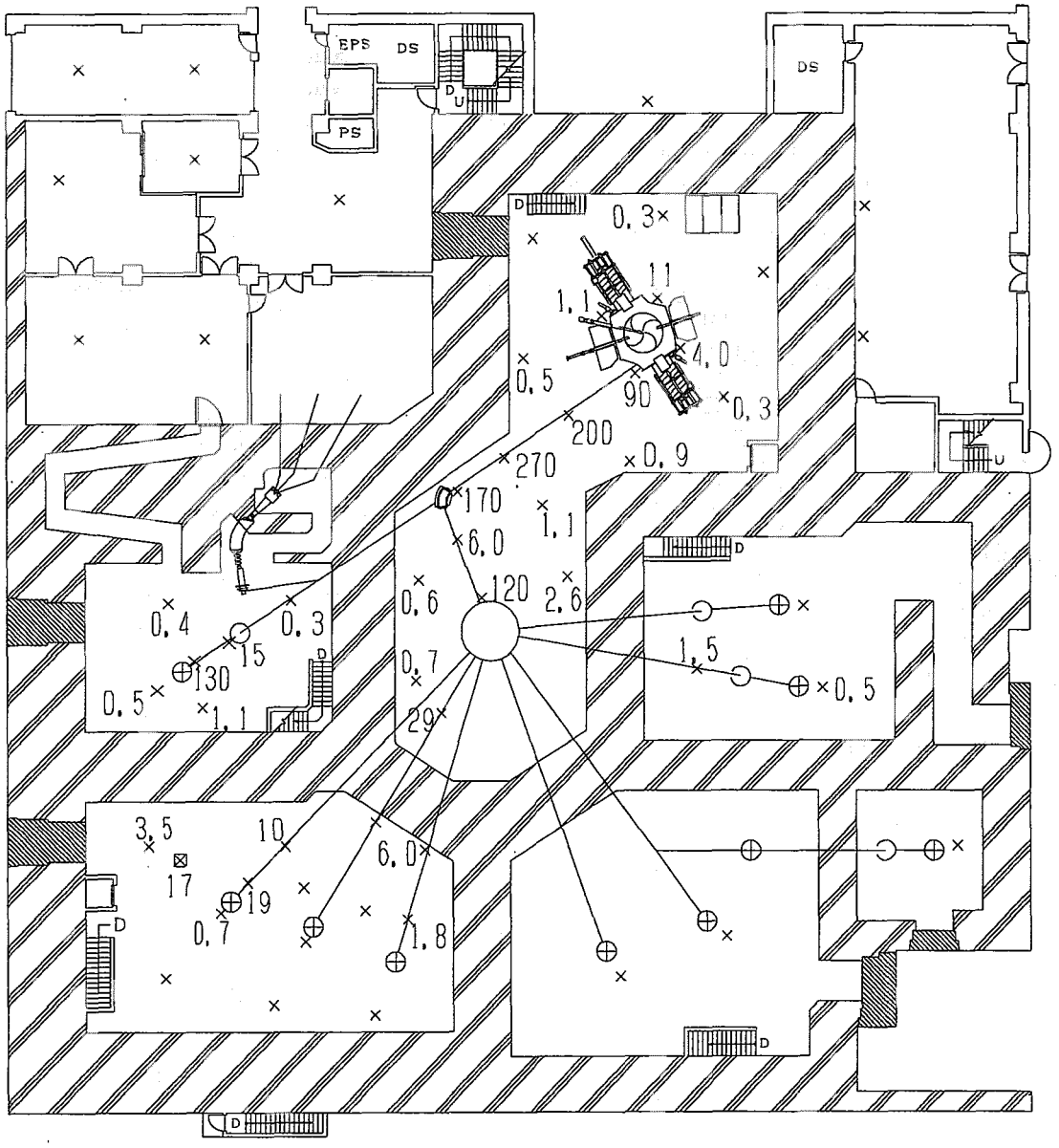

Fig.1 Dose rate distribution at the radiation controlled area in the cyclotron building.
Date measured : March 27, 2002
Measuring position : Indicated with × above 1m from floor
Unit : μSv/h(numeric less than 0.2μSv/h are not indicated)

2. Radioactive Waste Management

2.1 Solid wastes

Table 4 shows the amounts of solid wastes at various properties and kinds generated in each quarter of FY 2001. All wastes were combustible matter such as rubber gloves, compressible matter such as thin metals, and incompressible matter such as contaminated components. Compressible wastes were generated mainly by the cyclotron maintenance.

2.2 Liquid wastes

Liquid waste was almost waste water ("inorganic" in Table 5) generated with chemical experiments and operation of air conditioning units installed in each room of the first class radiation controlled area. Larger quantities of the wastewater in summer season (2nd quarter) are mainly due to condensed water, which is treated by evaporation, and condensed water is reused in the controlled area. Only small amounts of residue are generated by the evaporation because the waste quality is very pure.

The evaporation residue and sludge are solidified by cement in a stainless steel drum. The residue and sludge of ca. 100 liter makes cement solidify of 200-litter drum.

Table 4. Radioactive solid wastes generated in FY 2001.

Items \ Amounts	Amounts of generation in each periods (m^3)					Number of package /drum
	1st quarter	2nd quarter	3rd quarter	4th quarter	Total	
Category A*	0.26	0.36	0.70	5.03	6.35	
1)Combustible	0.16	0.32	0.36	0.34	1.18	7**
2)Incombustible	0.10	0.04	0.34	4.69	5.17	0
Compressible	0.10	0.04	0.08	0.20	0.42	2**
Filters	0	0	0.26	4.29	4.55	0
Incompressible	0	0	0	0.20	0.20	1**
Ion exchange resin	0	0	0	0	0	0
(Cement solidify)	0	0	0	0	0	0
Category B*	0	0	0	0	0	
1)Incombustible	0	0	0	0	0	0

* defined by dose at the outer surface of container : (A) $<$ 2 mSv/h $\leqq$ (B)

** 200-liter drum

Table 5. Radioactive liquid waste generated in FY 2001.

Items \ Amounts	Amounts of generation in each periods (m^3)					Number of package /drum
	1st quarter	2nd quarter	3rd quarter	4th quarter	Total	
Category A*	9.52	14.95	5.53	4.45	34.45	
1)Inorganic	9.52	14.95	5.53	4.45	34.45	treatment
2)Organic	0	0	0	0	0	0
Organic	0	0	0	0	0	0
Oil	0	0	0	0	0	0
3)Sludge	0	0	0.10	0	0.10	1
Category B*	0	0	0	0	0	
1)Inorganic	0	0	0	0	0	0
2)Organic	0	0	0	0	0	
Organic	0	0	0	0	0	0
Oil	0	0	0	0	0	0
3)Sludge	0	0	0	0	0	0
Evaporation residue	0	0	0.10	0	0.10	1

* defined by concentrations in $Bq/cm^3(\beta,\gamma)$: (A) $<$ 3.7×10 $\leqq$ (B) $<$ 3.7×10^4

Appendix

This is a blank page.

Appendix 1. LIST OF PUBLICATION

A.1.1 Publications in Journal

11J01

J.S.Laird, T. Hirao, H. Mori, S. Onoda, T. Kamiya, H. Itoh,

Development of a new data collection system and chamber for microbeam and laser investigations of single event phenomena,

Nuclear Instruments and Methods in Physics Research B 181 (2001) 87-94.

T SCS 12001

11J02

H. Mori, T. Hirao, J.S. Laird, S. Onoda, T. Kamiya, H. Itoh, T. Okamoto, Y. Koizumi,

Investigation of single-event charge collection from angled ion strikes,

Nuclear Instruments and Methods in Physics Research B 181 (2001) 340-343.

T SCS 12001

11J03

J.S.Laird, T. Hirao, H. Mori, S. Onoda, H. Itoh,

A System for Ultra-Fast Transient Ion and Pulsed Laser Current Microscopies as a Function of Temperature,

Solid State Phenomena Vols. 78-79 (2001) pp. 401-406.

T SCS 12001

11J04

T. Hirao, J.S. Laird, H. Mori, S. Onoda, H. Itoh,

The Investigation of Charge Transport Properties of SOI Semiconductor Devices Using a Heavy Ion Microbeam,

Solid State Phenomena Vols. 78-79 (2001) pp. 395-400.

T SCS 12001

11J05

T. Ohshima, H. Itoh, M. Yoshikawa,

Enhancement of Electrical Activation of Aluminum Acceptors in 6H-SiC by Co-implantation of Carbon Ions,

Materials Science Forum Vols. 353-356 (2001) 575-578.

I SCS 12003

11J06

T. Ohshima, H. Itoh, M. Yoshikawa,

Effect of gamma-ray irradiation on the characteristics of 6H silicon carbide metal-oxide-semiconductor field effect transistor with hydrogen-annealed gate oxide,

J. Appl. Phys 90 (2001) 3038-3041.

I SCS 12003

11J07

T. Ohshima, A. Uedono, H. Abe, Z. Q. Chen, H. Itoh, M. Yoshikawa, K. Abe, O. Eryu, K. Nakashima,

Positron Annihilation Study of Vacancy-Type Defects in Silicon Carbide Co-Implanted with Aluminum and Carbon Ions,

Physica B 308-310 (2001) 652-655.

I SCS 12003

11J08

A. Ohi, T. Ohshima, M. Yoshikawa,K.K.Lee, M. Iwami, H. Itoh,
Post-Implantation Annealing Effects on the Surface Morphology and Electrical Characteristics of 6H-SiC Implanted with Aluminum,
Materials Science Forum 389-393 (2002) 831-834.
I SCS 12003

11J09
T. Ohshima, K. K. Lee, A. Ohi, M. Yoshikawa, H. Itoh,
Gamma-Ray Irradiation Effects on the Electrical Characteristics of 6H-SiC MOSFETs with Annealed Gate-Oxide,
Materials Science Forum 389-393 (2002) 1093-1096.
I SCS 12003

11J10
K. K. Lee, T. Ohshima, H. Itoh,
Radiation Response of p-Channel 6H-SiC MOSFETs Fabricated Using Pyrogenic Conditions,
Materials Science Forum 389-393 (2002) 1097-1100.
I SCS 12003

11J11
K. Shimono, N. Shikazono, M. Inoue, A. Tanaka and H. Watanabe,
Effect of fractionated exposure to carbon ions on the frequency of chromosome aberrations in tobacco root cells,
Radiat. Environ. Biophys. 40, 221-225(2001).
C BIT 11006

11J12
S. Kitamura, M. Inoue, N. Shilazono and A. Tanaka,
Relationships among Nicotiana species revealed by the 5S rDNA spacer sequence and fluorescence in situ hybridization,
Theor. Appl. Genet. 103, 678-686(2001).
O BIT 11006

11J13
K. Hamada, M. Inoue, A. Tanaka and H. Watanabe,
Potato virus Y-resistance in the progeny of haploid mutants obtained by the culture of Nicotiana tabacum L. anthers exposed to ion beams,
Plant Biotechnology 18, 251-257(2001).
C BIT 11006

11J14
Y. Nomura, M. Hatashita and M. Inoue,
Production of self-compatible buckwheat by ion exposure,
FAGOPYRUM (2002) in press.
C BIT 11006

11J15
Y. Hase, M. Yamaguchi, M. Inoue and A. Tanaka,
Reduction of surval and induction of chromosome aberrations in tobacco irradiated by carbon ions with different LETs,
Int. J. Radiat. Biol. (2002) in press.
C BIT 11006

11J16
M. Inoue,

Biological actions of ion beams
– Biotechnological approach and utilization-,
Radiation & Industries 92, 30-35 (2001).
O BIT 01009, 02017

11J17
M.Takahashi, Y. Sasaki, S. Ida and H. Morikawa,
Enrichment of nitrite reductase gene improves the ability of Arabidopsis thaliana plants to assimilate nitrogen dioxide,
Plant Physiol., 126(2): 731-741 (2001).
C BIT 11018

11J18
K. Shimizu, M. Takahashi, N. Goshima, S. Kawakami, K. Irifune and H. Morikawa,
Presence of an SAR-like sequence in junction regions between an introduced transgene and genomic DNA of cultured tobacco cells : its effect on transformation frequency,
Plant Journal, 26(4): 375-384(2001).
C BIT 11018

11J19
H. Morikawa and M. Takahashi,
Remediation of Soil, Water and Air by Naturally Occurring and Transgenic Plants,
Gamma Field Symposia, 39: 81-101 (2001).
C BIT 11018

11J20
H. Morikawa, M.Takahashi and G.Arimura. Manipulation of genes for nitrogen metabolism in plants.
In Air Pollution and Biotechnology in Plants. Ed. by K. Oomasa et al.,*Springer-Verlag*, pp. 383-401 (2002).
C BIT 11018

11J21
T. Yoneyama, H.Y.Kim, H.Morikawa and H. S. Srivastava,
Metabolism and detoxification of nitrogen dioxide and ammonia in plants,
In Air Pollution and Biotechnology in Plants ed. by K. Oomasa et al.,
Springer-Verlag, pp. 221-234 (2002).
C BIT 11018

11J22
Y. Kawamura, K. Fukunaga, A. Umehara, M. Takahashi and H. Morikawa,
Selection of Rhododendron mucronatum plants that have a high capacity for nitrogen dioxide uptake,
Acta Biotechnologica, 22:113-120 (2002).
C BIT 11018

11J23
H. Morikawa, M. Takahashi and Y. Kawamura.
Metabolism of nitrogen dioxide in plants-Assimilation, dissimilation and novel metabolites,
Physiology and Molecular Biology of Plants. 8(1) 19-29 (2002).
C BIT 11018

11J24
A. Sakamoto, M. Ueda & H. Morikawa,
Arabidopsis glutathione-dependent formaldehyde dehydrogenase is an S-nitrosoglutathione reductase,

FEBS Lett. 515: 20-24 (2002).
C BIT 11018

11J25
K. Kondo, M. Takahashi and H Morikawa,
Regeneration and transformation of a roadside tree Pittosporum tobira A,
Plant Biotechnol., 19(2) 135-139 (2002).
C BIT 11018

11J26
M. Maekawa, A. Tanaka, N. Shikazono and Y. Hase,
Somatic reversion induced by ion beam irradiation in stable yellow leaf mutant of rice,
Rice Genetics Newsletter 18: 36-39(2001).
C BIT 11021

11J27
Y. Kobayashi, T. Funayama, M. Taguchi, S. Wada, M. Tanaka, T. Kamiya, W. Yokota, H. Watanabe and K. Yamamoto,
Cell Irradiation System with a Single or Precise Numbers of Heavy Ions using a Collimated Heavy Ion Microbeam at TIARA, JAERI Takasaki
J. Radiation Research, 42, 449(2001).
C BIT 11025

11J28
T. Funayama, Y. Kobayashi, M. Taguchi, S. Wada, M. Tanaka and K. Yamamoto,
Irradiation of Collimated Heavy Ion Beams on Individual Cells,
J. Radiation Research, 42, 449(2001).
C BIT 11025

11J29
S. Wada, Y. Kobayashi, T. Funayama and K. Yamamoto,
Detection of DNA damage in the individual cells induced by heavy ion microbeam irradiation with the comet assay,
J. Radiation Research, 42, 449(2001).

C BIT 11025

11J30
T. Kawachi, C. Nishijo, H Fujikake, A. L. Salwa, N. Ohtake, K. Sueyoshi, T.Ohyama, N. S. Ishioka, S Watanabe, A. Osa, T. Sekine, S. Matsuhashim T. Ito, C. Mizuniwa, T. Kume, S. Hashimoto, H. Uchida, and A.Tsuji,
A Effects of anion channel Blockers on xylem nitrate transport in barley seedlings,
Soil Sci. Plant Nutri, 48, 271-277(2002).
C BIT 11030

11J31
N. Bughio, H. Nakanishi, S. Kiyomiya, S. Matsuhashi, N. S. Ishioka, S. Watanbe, H. Uchida, A. Tsuji, A. Osa, T. Kume, S. Hashimoto, T. Sekine, and S. Mori,
Real-time [11C]methionine translocation in barley in relation to mugineic acid phytosiderophore biosynthesis,
Planta, 213, 708-715(2001).
C BIT 11031

11J32
S. Kiyomiya, H. Nakanishi, H. Uchida, A. Tsuji, S. Nishiyama, H. Tsukda, N. S. Ishioka, S. Watanabe, A. Osa, C. Mizuniwa, S. Matsuhashi, S.

Hashimoto, T. Sekine, and S. Mori,
Light activates H215O flow in rice - Detailed monitoring using a positron-emitting tracer imaging system (PETIS),
Physiologia Plantarum 113, 359-367(2001).
C BIT 11031

11J33
T. M. Nakanishi, K. Tanoi, M. Yokota, S. Ueoka, N. S. Ishioka, S. Watanabe, A. Osa, T. Sekine, T.Ito, T. Mizuniwa, S. Matsuhashi, S. Hashimoto, H. Uchida and A. Tsuji,
^{18}F Used as Tracer to Study Water Uptake and Transport Imaging of a Cowpea,
J.Radioanal. and Nucl. Chem. 249(2), 503-507 (2001).
C BIT 11033

11J34
J. Furukawa, H. Yokota, K. Tanoi, S. Ueoka, S. Matsuhashi, N. S.Ishioka, S. Watanabe, H. Uchida, A. Tsuji, T. Ito, T. Mizuniwa, A. Osa, T. Sekine, S. Hashimoto and T. M. Nakanishi,
Vanadium Uptake Manner and an Effect of Vanadium Treatment on 18F-Labeled Water Movement in a Cowpea Plant by Positron Emitting Tracer Imaging System (PETIS)
J.Radioanal. and Nucl. Chem. 249(2), 495-498 (2001).
C BIT 11033

11J35
K. Ogura, M. Asano, N. Yasuda and M. Yoshida,
Properties of TNF-1 track etch detector,
Nucl. instr. and Meth. In Phys. Res. B 185 222-227(2001).
C RCO 11037

11J36
S. Takahashi, M. Yoshida, M. Asano, T. Tanaka, and T. Nakagawa,
Effect of heavy-ion irradiation on the gas permeability of poly(ethylene terephthalate) (PET) membranes,
J. Appl. Polym. Sci., 82, 206-216(2001).
C RCO 11037

11J37
J. Li, Yasunari Maekawa, Tetsuya Yamaki, Masaru Yoshida,
Chemical Modification of a Poly(ethylene terephthalate) Surface by Selective Alkylation of Acid Salts,
Macromol. Chem. Phys., in press(2002).
C RCO 11038

11J38
S. Seki, Y. Matsui, Y. Yoshida, S. Tagawa, J.R. Koe, M. Fujiki,
Dynamics of Cherge Carriers on Poly[bis(*p*-alkylphenyl)silane]s by Electron Beam Pulse Radiolysis,
J. Phys. Chem. B **106** (2002) 6849-6852.
C RCO 11039

11J39
Y. Matsui S. Seki, and S. Tagawa,
Direct Observation of Intra-molecular Energy Migration in s-conjugated Polymer by Femto-second Laser Flash Photolysis,
Chem. Phys. Lett. **357** (2002) 346-350.
C RCO 11039

11J40
F.C. Grozema, L.D.A. Siebbeles, J.M. Warman, S. Seki, S. Tagawa, and U. Scherf,
Hole Conduction along Molecular Wires: s-Bonded Silicon versus p-Bond-Conjugated Carbon,
Adv. Mater. **14** (2002) 228-231.
C RCO 11039

11J41
S. Seki, S. Tsuji, Y. Matui, and S. Tagawa,
Dynamics of Silylenes in Polysilylenes with Structural Defects by Excimer Laser Flash Photolysis,
Chem. Lett. (2001) 1208-1209.
C RCO 11039

11J42
S. Seki, K. Maeda, S. Tagawa, H. Kudoh, M. Sugimoto, Y. Morita, and H. Shibata,
Formation of Quantum Wires along Ion Projectiles in Si Backbone Polymers,
Adv. Mater. **13** (2001) 1663-1665.
C RCO 11039

11J43
Y. Yoshida, Y. Mizutani, T. Kozawa, A. Saeki, S. Seki, S. Tagawa, and K. Ushida,
Development of Laser-synchronized Picosecond Pulse Radiolysis System,
Radiat. Phys. Chem. **60** (2001) 313-318.
C RCO 11039

11J44
K. Maeda, S. Seki, S. Tagawa, and H. Shibata,
Radiation Effects on Branching Polysilanes,
Radiat. Phys. Chem. **60** (2001) 461-466.
C RCO 11039

11J45
S. Seki, Y. Kunimi, K. Nishida, Y. Yoshida, and S. Tagawa,
Electronic State of Radical Anions on Poly(methyl-*n*-propylsilane) Studied by Low Temperature Pulse Radiolysis,
J. Phys. Chem. B **105** (2001) 900-904.
C RCO 11039

11J46
S. Seki, Y. Yoshida, and S. Tagawa,
Charged Radicals of Polysilane Derivatives Studied by Pulse Radiolysis,
Radiat. Phys. Chem. **60** (2001) 411-415.
C RCO 11039

11J47
S. Seki, Y. Kunimi, K. Nishida, K. Aramaki, and S. Tagawa,
Optical Properties of Pyrrolyl-substituted Polysilanes,
J. Organomet. Chem. **611** (2000) 62-68.
C RCO 11039

11J48
Y. Kunimi, S. Seki, M. Tashiro, and S. Tagawa,
Free Volume in Poly(n-alkylphenylsilane) Probed by Positron Annihilation,
J. Photopolym. Sci. Technol. **13** (2000) 723-726.
C RCO 11039

11J49

S. Seki, Y. Sakurai, K. Maeda, Y. Kunimi, and S. Tagawa,
Studies on the Negative Resist Material Based on Polysilanes for EB and X-ray Lithography,
Jpn. J. Appl. Phys. **39** (2000) 4225-4230.
C RCO 11039

11J50
M. Taguchi, M. Moriyama, H. Namba, and H. Hiratsuka,
Yield of acridine C-radical produced by irradiation with energetic heavy ions,
Radiat. Phys. Chem., 64, 115 -122(2002).
C RCO 11040

11J51
H. Koizumi, M. Taguchi, Y. Kobayashi, and T. Ichikawa,
Crossliking of polyimethylsiloxane in heavy ion tracks,
Nucl. Instr. And Meth. B 179 (2001) 530-535.
C RCO 11041

11J52
T.Hirose, H.Tanigawa, M.Ando, A.Kohyama, Katoh and M. Narui,
Radiation effects on low cycle fatigue properties of reduced activation ferritic/martensitic steels,
J. Nucl. Mater., (2002) in press.
C NM 11005

11J53
H. Tanigawa, T. Hirose, M.Ando, S.Jistukawa, Y. Katoh and A. Kohyama,
Microstructural analysis of mechanical-tested reduced activation ferritic/martenstic steels,
J. Nucl. Mater., (2002) in press.
C NM 11005

11J54
E. Wakai, K. Furuya, M. Sato, K. Oka, N. Tanaka Ohnuki, Y. Kato, F. Takada and T. Sawai,
Effect of helium on ductile-brittle transition behavior in reduced-activation 8Cr-2W martensitic steel,
J. Nucl. Mater., accepted.
C NM 11005

11J55
E. Wakai, T. Sawai, A.Naito and S. Jitsukawa,
Microstrucutural development and swelling behavior of F82H steel irradiated by dual ion beams,
J. Electron Microscope, 51(2002)S239.
TS NM 12010

11J56
T. Sawai, E. Wakai, A. Naito and S. Jitsukawa
Swelling behavior of TIG-welded F82H IEA heat,
J. Nucl. Mater., (2002) in press.
TSI NM 12010

11J57
E. Wakai, T. Sawai, K. Furuya, A. Naito, S. Yamashita, S. Ohnuki, S. Yamamoto, H. Naramoto, T. Aruga and S. Jitsukawa,
Effect of Triple Ion Beams in Ferritic/Martensitic Steel on Swelling Behavior,
J. Nucl. Mater., (2002) in press.
TSI NM 12010

11J58

E. Wakai, T. Sawai, M. Ando, T. Aruga, K. Oka, S. Ohnuki, S. Yamamoto, H. Naramoto, H. Tanigawa. K. Kikuchi and S. Jitsukawa,
Swelling behavior of F82H steel irradiated by triple/dual ion beams,
J. Nucl. Mater., (2002), accepted.
TSI NM 12010

11J59
I. Mukouda and Y. Shimomura,
Annihilation of Interstitial Atoms to Dislocations in Neutron-irradiated Cu and Ni at High Temperature,
Materials Science & Engineering: A309-310, (2001) 190-197.
TIS IOM 12008

11J60
N. Sekimura, S. Yonamine, T. Iwai, Y. Arai, A. Naito, Y. Miwa and S. Hamada,
Synergistic Effects of Hydrogen and Helium on Microstructural Evolution in Vanadium Alloys by Triple Ion Beam Irradiation,
Journal of Nuclear Materials 283-287 (2000) pp.224-228.
TSI IOM 12009

11J61
T. Okita, T. Kamada and N. Sekimura,
Effects of Dose Rate on Microstructural Evolution and Swelling under Neutron Irradiation,
Journal of Nuclear Materials 283-287 (2000) pp.220-223.
TSI IOM 12009

11J62
K. Morishita, T. Diaz de la Rubia, E. Alonso, N. Sekimura and N. Yoshida,
A Molecular Dynamics Simulation Study of Small Cluster Formation and Migration in Metals,
Journal of Nuclear Materials 283-287 (2000) pp.753-757.
TSI IOM 12009

11J63
T. Okita, N. Sekimura, T. Satoh, F. A. Garner and L. R. Greenwood,
The Primary Origin of Dose Rate Effects on Microstructural Evolution of Austenitic Alloys during Neutron Irradiation,
to be published in *Journal of Nuclear Materials*.
TSI IOM 12009

11J64
T. Satoh, N. Sekimura and T. Okita,
Effects of Solid Transmutation and Helium on Microstructural Evolution in Neutron-Irradiated Vanadium,
to be published in *Journal of Nuclear Materials*.
TSI IOM 12009

11J65
T. Kamada, Y. Wakasugi, T. Okita, Y. Arai and N. Sekimura,
Irradiation Hardening in Ferritic Steels under Heavy Ion Irradiation by Small Indentation,
to be published in *Journal of Nuclear Materials*.
TSI IOM 12009

11J66
F. A. Garner, M. L. Hamilton, B. H. Sencer, T. Okita, N. Sekimura, D. L. Porter, T. R. Allen and

W. G. Wolfer,
The Surprisingly Large Influence of Displacement Rate on the Swelling of Pure Metals, Fe-based FCC and BCC Alloys, and Vanadium Alloys ,
to be published in *Journal of Nuclear Materials.*
T S I IOM 12009

11J67
F. Kano, A. Naito and I. Ioka,
Effects of Initial Grain Boundary Segregation on Radiation-Induced Segregation in Stainless Steels,
J of Nucl. Mat. To be published.
T IOM 12016

11J68
K. Yasuda, C. Kinoshita and S. Matsumura,
Effects of Simultaneous Displacive and Ionizing Radiation in Ionic and Covalent Crystals,
Defect and Diffusion in Ceramics (2002) p53-74.
I IOM 12020

11J69
K. Yasuda, T. Higuchi. K. Shiiyama, C. Kinosita, K. Tanaka and M. Kutsuwada,
Effects of electric field on the aggregation of point defects in ion-irradiated α-Al_2O_3,
submitted to *Philos. Mag. Lett*.
I IOM 12020

11J70
Y. Nakanishi, A. Wakahara, H. Okada, A. Yoshida, T. Ohshima, and H. Itoh,
Effect of 3MeV electron irradiation on photoluminescence properties ofEu-doped GaN
submitted to *Appl. Phys. Lett.*
I SCS 12004

11J71
H. -S. Lee, H. Okada, A. Wakahara, A. Yoshida, T. Ohshima, H. Itoh, S. Kawakita, M. Imaizumi, and S. Matsuda,
Effect of proton irradiation on electrical properties of CuInSe2 thin films,
Solar energy materials & solar cells in press.
I SCS 12004

11J72
T. Yamaki, T. Sumita, S. Yamamoto,
Formation of TiO2-xFx Compounds in Fluorine Implanted TiO_2,
J. Mater. Sci. Lett., 21 (2002) 33.
ISO IOM 12025

11J73
S. Yamamoto, T. Sumita, T. Yamaki, A. Miyashita, H. Naramoto,
Characterization of Epitaxial TiO_2 Films Prepared by Pulsed Laser Deposition,
J. Cryst. Growth, 237-239(2002) 569.
ISO IOM 12025

11J74
T. Yamaki, T. Sumita, S. Yamamoto, A. Miyashita,
Preparation of Epitaxial TiO2 Films by PLD for Photocatalyst Applications,
J. Cryst. Growth, 237-239(2002) 574.
ISO IOM 12025

11J75
T. Umebayashi, T. Yamaki, H. Itoh, K. Asai,
Band-Gap Narrowing of Titanium Dioxide by Sulfur Doping,

Appl. Phys. Lett., 81 (2002) 454.
ISO IOM 12025

11J76
T. Umebayashi, T. Yamaki, H. Itoh, K. Asai,
Analysis of Electronic Structures of 3d Transition Metal-Doped TiO_2 Based on Band Calculations,
J. Phys. Chem. Solids, in press.
ISO IOM 12025

11J77
T. Sumita, T.Yamaki, S.Yamamoto, A. Miyasita,
Photo-Induced Surface Charge Separation of Highly Oriented TiO_2 Anatase and Rutile Thin Films,
Appl. Surf. Sci., in press.
ISO IOM 12025

11J78
T. Sumita, T.Yamaki, S.Yamamoto, A. Miyasita,
Photo-Induced Surface Charge Separation in Cr-Implanted TiO_2 Thin Film,
Thin Solid Films, in press.
ISO IOM 12025

11J79
R. Shinohara, T. Yamaki, S. Yamamoto, H. Itoh, K. Asai,
High-Quality Epitaxial TiO_2 Films Grown on . -Al_2O_3 Substrates by Purlsed Laser Deposition,
J. Mater. Sci. Lett., in press.
ISO IOM 12025

11J80
D.G Syarif, A. Miyashita, T.Yamaki, T.Sumita, Y. Choi, H. Itoh,
Preparation of Highly Active TiO_2 Photocatalyst Films by Controlling the Oxygen Pressure,
Appl. Surf. Sci., in press.
ISO IOM 12025

11J81
K. Narumi and H. Naramoto,
Modification of C60 Thin Films by Ion Irradiation
Surface and Coatings Technology 158-159C (2002) 363-366.
T IOM, MAN, 12030

11J82
Y. Chimi, K. Adachi, A. Iwase, N. Ishikawa, K. Yamakawa,
Thermal relaxation of hydrogen disorering in Pd-H system irradiated with high energy particles,
J. Alloys and Comounds 330-332 (2002) 187.
S IOM 12032

11J83
Y. Chimi, A. Iwase, N. Ishikawa, T. Kambara,
Defect production induced by electronic excitation in iron,
Nucl. Instrum. Methods B 193 (2002) 248.
S IOM 12034

11J84
S. Ishino,
Historical Survey of the Study of Radiation Damage Mechanisms of Reactor Pressure Vessel Steels,
Kinzoku (Metals & Technologies) 71(2001) 719 (in Japanese)
O IOM 12035

11J85

N. Soneda, S. Ishino, T. Diaz de la Rubia,

Vacancy Loop Formation by 'Cascade Collapse' in α-Fe: A Molecular Dynamics Study of 50 keV Cascades,

Philos. Mag. Lett. 81(2001) 649.

O IOM 12035

11J86

K. Morita, S. Ishino, T. Tobita, Y. Chimi, N. Ishikawa, A. Iwase,

Use of high energy ions for the mechanistic study of irradiation embrittlement in pressure vessel steels using Fe-Cu model alloys,

Journal of Nuclear Materials, (2002) in press.

O IOM 12035

11J87

A. Iwase, T. Hasegawa, Y. Chimi, T. Tobita, N. Ishikawa, M. Suzuki, T. Kambara, S.Ishino,

Hardening of Fe-Cu alloys by swift heavy ion irradiation,

Nuclear Instruments and Methods in Physics Research B, (2002) in press.

O IOM 12035

11J88

M. Ishino, O. Yoda, Y. Haishi, F. Arimoto, M. Takeda, S. Watanabe, S. Ohnuki, H. Abe,

Boundary structure of Mo/Si multilayers for soft X-ray mirrors,

Jpn. J. Appl. Phys. 41 (2002) 3052-3056

I IOM 12019

11J89

H. Abe, S. Yamamoto, A. Miyashita,

In-situ TEM observation of nucleation and growth of spherical graphitic clusters under ion implantation,

J. Electron Microscopy 51 (2002) s183.

I IOM 12019

11J90

D. Huli. ová, K. Hosoi, S. Kuroda, H. Abe, A. Oya,

Carbon nanotubes prepared from polymer microshperes by spinning and carbonizing

Mol. Cryst. Liq. Cryst. Accepted.

I IOM 12019

11J91

Y. Choi, S. Yamamoto, H. Abe, H. Itoh,

Effect of annealing and quenching treatments on reconstruction of rutile thin films on sapphire substrates,

Surface Science, 499 (2002) 203-209.

I IOM 12019

11J92

D. Huli. ová, K. Hosoi, S. Kuroda, H. Abe, A. Oya,

Carbon nanotubes prepared by spinning and carbonizing fine core/shell polymer microspheres,

Advanced Materials 14 (2002) 452-455.

I IOM 12019

11J93

H. Abe, S. Yamamoto, A. Miyashita, K.E. Sickafus,

Formation mechanisms of carbon onions and nanocapsules in C+- ion implanted copper,

J. Appl. Phys 90 (2001) 3353-3358.

I IOM 12019

11J94
H. Abe,
Nucleation of carbon onions and nanocapsules under ion implantation at high temperature,
Diamond and Related Materials 10 (2001)1201-1204.
I IOM 12019

11J95
E. Wakai, A. Hishinuma, H. Abe, S. Takagi, K. Abiko,
Microstructural evolution of Fe-50Cr-xW model alloys during Fe+ ion Irradiation,
Materials transaction JIM vol.41, No.9 (2000) 1176-1179.
I IOM 12019

11J96
Y. Kasukabe, H. Tani, H. Abe, Y. Yamada,
In-situ transmission electron microscopy and electron energy loss spectroscopy observation of TiN grown by N-implantation,
Jpn. J. Appl. Phys. 39 (2000) 4395-4399.
I IOM 12019

11J97
K. Yasuda, C. Kinoshita, M. Ohmura, H. Abe,
Production and stability of dislocation loops in an MgO-Al2O3 system under concurrent irradiation with ions and electrons,
Nucl Instr. and Meth. in Phys. Res. B166-167 (2000) 107-114.
I IOM 12019

11J98
S. Yamamoto, T. Sumita, Sugiharuto, A. Miyashita and H. Naramoto,
Preparation of epitaxial TiO2 films by pulsed laser deposition technique,
Thin Solid Films 401 (2001) 88-93.
S IOM 12023

11J99
S. Yamamoto, T. Sumita, T. Yamaki, A. Miyashita and H. Naramoto,
Characterization of epitaxial TiO_2 films prepared by pulsed laser deposition,
J. Crystal Growth 237-239(2002) 569-573.
S IOM 12023

11J100
S. Yamamoto, H. Naramoto,
RBS/channeling analysis of epitaxial films with Nb buffer layer on sapphire substrate,
Nucl. Instr. Meth. B 190 (2002) 657-660.
S IOM 12023

11J101
Y. Choi, S. Yamamoto, H. Abe, H. Itoh,
Effects of annealing and quenching treatments on reconstruction of rutile thin films on sapphire substrates,
Surface Science 499 (2002) 203-209.
S IOM 12023

11J102
H. Kudo,
Ion-Induced Electron Emission from Crystalline Solids,
(Springer Tracts in *Modern Physics* Vol. 175, 161

pages, 85 figs.) Springer, Berlin, Heidelberg, 2002.
TISO MAN 12026

11J103
Hiroshi Kudo, Katsuhiro Haruyama, Takao Kinoshita, Seiji Seki, Kazumasa Narmi, Hiroshi Naramoto,
Carbon KVV Auger electron emission from highly oriented pyrolytic graphite bombarded by fast ions,
Nucl. Instrum. & Methods B190 (2002) 160-163.
SO MAN 12026

11J104
K. Takahiro, N. Takeshima, K.Kawatsura, S. Nagata, S. Yamamoto, H. Naramoto,
Irradiation-induced improvement of crystalline quality of epitaxial Cu/Si(100) film,
Surface and Coating Technology, in press.
O IOM 12027

11J105
J. Vacik, H.Naramoto, K. Narumi, S. Yamamoto and K. Miyashita,
Pattern Formation Induced by Co-deposition of Ni and C_{60} on MgO(100),
J. Chemical Physics 114 (2001) 9115-9119.
O IOM

11J106
H. Naramoto, X. D. Zhz, J. Vacik, Y. H. Xu, K. Narumi, S. Yamamoto, K. Miyashita,
Allotropic Conversion of Carbon-related Films by Using Energy Beams,
Physics of the Solid State 44 (2002) 668-673.
TS IOM 12029

11J107
H. Naramoto, Y.Xu, K.Narumi, X. Zhu, J. Vacik, S. Yamamoto and K. Miyashita,
Modification of Carbon Related Films with Energy Beams,
Mat. Res. Soc. Proc. 647 (2001) O5. 18. 1-O5. 18. 6.
TS IOM 12029

11J108
X. . Zhu, Y. H. Xu, H. Naramoto, K. Narumi and K. Miyashita,
Role of simultaneous Ne+ ion bombardment in preparing carbon films from C_{60} fullerene,
J. Phys.:Condensed Matter 14 (2002) 5083-5090.
O IOM

11J109
X. D. Zhz, H. Naramoto, Y. H. Xu, K. Narumi, and K. Miyashita,
Tuning Surface Morphologies of Ion-Assisted Diamond-like Carbon Film on Nanometer Scale,
J.Chemical Physics 116 (2002) 10458-10461.
O IOM

11J110
V. Laverentiev, H. Abe, S. Yamamoto, H. Naramoto, and K. Narumi,
Formation of carbon nanotubes under conditions of Co+C_{60} film,
Physica B: Condensed Matter (2002) , in print.
O IOM

11J111
Y. Xu, K. Narumi, K. Miyashita, and H.

Naramoto,
AFM Observation of Nanosized SiC Dots Prepared by Ion Beam Deposition,
Surface and Interface Analysis in press.
O IOM

11J112
V. Laverentiev, H. Abe, S. Yamamoto, H. Naramoto, and K. Narumi,
Formation of carbon nanotubes under conditions of Co+C_{60} film,
Physica B: Condensed Matter (2002), in print.
O IOM

11J113
V. Laverentiev, H. Abe, S. Yamamoto, H. Naramoto, and K. Narumi,
FORMATION OF PROMISING Co-C NANO-COMPOSITIONS,
Suraface and Interface Analysis (2002), in print.
O IOM

11J114
V. Laverentiev, H. Abe, S. Yamamoto, H. Naramoto, and K. Narumi,
Co and C_{60} Interaction under Conditions of Mixture,
MOLECULAR CRYSTALS AND LIQUID CRYSTALS (2002), in press.
O IOM

11J115
K. Hirata, S. Saitoh, K. Narumi, Y. Nakajima, and Y. Kobayashi,
Non-linear effect of cluster irradiation on chemical modification of polycarbonate
Nucl. Instr. and Meth. in Phys. Res. B, in press.
T RCO 12040

11J116
T. Yamaguchi, E. Watanabe, T. Souno, H. Nishikawa, M. Hattori, Y. Ohki, T. Kamiya, K. Arakawa,
Evaluation of silica glasses implanted by high-energy ions using a UV-Excited Microscopy,
Nuclear Instruments and Methods in Physics Research Section B: Beam Interactions with Materials and Atoms,
Vol. 191, Issues 1-4, May 2002, Pages 371-374.
O IOM 12041

11J117
H. Nishikawa, T. Souno, M. Hattori, Y. Nishihara, Y. Ohki, E. Watanabe, M. Oikawa, T. Kamiya, K. Arakawa,
Radiation effects and surface deformation of silica by ion microbeam,
Nuclear Instruments and Methods in Physics Research Section B: Beam Interactions with Materials and Atoms, Vol. 191, Issues 1-4, May 2002, Pages 342-345.
T, S IOM 12041

11J118
M. Hattori, Y. Nishihara, Y. Ohki, M. Fujimaki, T. Souno, H. Nishikawa, T. Yamaguchi, E. Watanabe, M. Oikawa, T. Kamiya, K. Arakawa
Characterization of ion-implanted silica glass by vacuum ultraviolet absorption spectroscopy,
Nuclear Instruments and Methods in Physics Research Section B: Beam Interactions with Materials and Atoms, Vol. 191, Issues 1-4, May

2002, Pages 362-365.
O IOM 12041

11J119
S. Watanabe, N. S. Ishioka, A. Osa, M. Koizumi, T. Sekine, S. Kiyomiya, H. Nakanishi and S. Mori,
Production of Positron Emitters of Metallic Elements to Study Plant Uptake and Distribution,
Radiochim. Acta, 89 (2001) 853.
C NRI 11036

11J120
Y. Suzuki, J. Li, Y.Maekawa, M. Yoshida, K. Maeyama, N. Yonezawa,
Conversion of hydrophilic surface of poly(ethylene terephthalate) filmto hydrophobic one under hydrophilic conditions,
Journal of Chemical Society of Japan, 2, 255-259 (2002).
C RCO 11038

11J121
S. Tsuji, S. Seki, T. Kozawa, and S. Tagawa,
Reaction Mechanisms of Excimer Resists Studied by Laser Flash Photolysis,
J. Photopolym. Sci. Technol. 13 (2000) 729-732.
C RCO 11039

11J122
M. Tashiro, P. K. Pujari, S. Seki, Y. Honda, S. Nishijima, and S. Tagawa,
Studies on Thermally Induced Structural Changes in Silicon Based Polymers by Positron Annihilation,
Radiat. Phys. Chem. 58 (2000) 587-592.
C RCO 11039

11J123
S. Watanabe, N. S. Ishioka, T. Sekine, A. Osa, M. Koizumi, H. Shimomura, K. Yoshikawa and H. Muramatsu,
Production of Endohedral ^{133}Xe-Fullerene by Ion Implantation,
J. Radioanal. Nucl. Chem, in press.
O NRI

11J124
M. Kasahara, C.-J. Ma, T. Kamiya and T. Sakai,
Preliminary studies on applications of micro-PIXE to atmospheric aerosols,
Nuclear Instrument & Methods, B181, 622-627 (2001).
S ACT 12046

11J125
C.J. Ma, M. Kasahara, S. Tohno and T. Kamiya,
A new approach for characterization of single raindrops,
Water, Air, and Soil Poll., 130, 1601-1606 (2001).
S ATC 12046

11J126
M Kasahara, R Höllor, S Tohno, Y Ohnishi and C.-J. Ma,
Application of PIXE Technique to Studies on Global Warming/Cooling Effect of Atmospheric Aerosols,
Nuclear Instruments & Methods B, 204-208 (2002).
S ACT 12046

11J127

T. Satoh, K. Ishii, S. Matsuyama, H. Yamazaki, Ts. Amartivan, A. Tanaka, S. Sugihara, Y. Komori, K. Katoh,
Investigaation on the Influence of Back Scattered Protons PIXE Spectrum,
IJPIXE,, Vol. 11, Nos. 1&2, 2001, 49-59.
S ACT 12048

11J128
T. Ohnuki, F. Sakamoto, N. Kozai, M. Samadfam, T. Kamiya, T. Sakai, T. Satoh and S. Oikawa,
Application of the micro-PIXE technique for analyzing Arsenic in Biomat and Lower Plants of Lichen and Mosses Around An Arsenic Mine Site, Gunma, Japan,
Nuclear Instruments and Method in Physics Research B, 190, 477-481 (2002).
TC IOM 22049

11J129
A. Endo, H. Noguchi, Su. Tanaka, Y. Kanda, Y. Oki, T. Iida, K. Sato, S. Tsuda,
Particle size analysis of radioactive aerosols formed by irradiation of argon using 65MeV quasi-monoenergetic neutrons,
Appl. Radiat. Isotopes, 56, 615-620, (2002).
C ACT 11046

11J130
E. Kim, A. Endo, Y. Yamaguchi, M. Yoshizawa, T. Nakamura and T. Shiomi,
Measurement of Neutron Dose with an Organic Liquid Scintillator Coupled with a Spectrum Weight Function,
Radiat. Prot. Dosim., in press.
C RSH 11048

11J131
E. Kim, A. Endo and Y. Yamaguchi,
Development of SCINFUL-CG Code to Calculate Response Function of Hybrid Neutron Detectors Using Scintillators,
J. Nucl. Sci. Tecnol., in press.
C RSH 11048

11J132
E. Kim, A. Endo, Y. Yamaguchi, M. Yoshizawa, T. Nakamura and D.R.D. Rasolonjatovo,
Hybrid Neutron Detector Consisting of an Organic Liquid Scintillator and a Li-6 Glass Scintillator for Wide Energy Range,
Trans. Atomic Energy Soc. Jpn., in press.
C RSH 11048

11J133
T. Sato, K. Shin, R. Yuasa, S. Ban and H.S. Lee,
Measurement of the Neutron Spectrum by the Irradiation of a 2.04-GeV Electron Beam into Thick Targets,
Nucl. Instrum. Meth., A463, 299-308 (2001).
C RSH 11048

11J134
H.S. Lee, S. Ban, K. Shin, T. Sato, S. Maetaki, C. Chung and H.D. Choi,
Systematics of Differential Photoneutron Yields Produced from Al, Ti, Cu, Sn, W, and Pb Targets by Irradiation of 2.04 GeV Electrons,
J. Nucl. Sci. Tech., submitted.
C RSH 11048

11J135

K. Oda, H. Ichijo, N. Miyawaki, T. Yamauchi and Y. Nakane,
Improvement of Neutron Detection Efficiency with High Sensitive CR-39 Track Detector,
Radiat. Meas., 34 (2001) 171-175.
C RSH 11048 S ACT Machine Study

11J136
K. Oda, Y. Saito, N. Miyawaki, T. Yamauchi, Y. Nakane and Y. Yamaguchi,
Characteristic Response pf Plastic Track Detectors to 40-80 MeV Neutrons,
Radiat. Prot. Dosim., (2002), in press.
C RSH 11048

11J137
T. Sawamura, T. Joji and A. Homma,
Measurement of Neutron Detection Sensitivity of Liquid in Metastable States,
Radiat. Prot. Dosim., submitted.
C RSH 11048

11J138
Yuichi SAITOH,
Acceleration of Cluster Ions to MeV Energy Region,
Ionizing Radiation、Vol. 27 No.3 July. 2001. pp.19-25.
T ACT 12050

11J139
T. Sakai, T. kamiya, M. Oikawa, T. Sato, A. Tanaka and K. Ishii,
JAERI TAKASAKI IN-AIR MICRO-PIXE SYSTEM FOR VARIOUS APPLICATIONS,
Nucl. Instr. Meth. B 190 (2002) 271.

A1.2 Publications in Proceeding

11C01

A. Makihara, S. Kuboyama, S. Matsuda, N. Nemoto, H. Ohtomo, K. Furuse, S. Baba and T. Hirose,

Non-Damaging Beam Blanking SEM Test Method and its Application to Highly Integrated Devices,

The IEEE Nuclear and Space Radiation Effects Conference(NSREC 2001).

C SCS 11002

11C02

A. Makihara, H. Shindou, N. Nemoto, S. Kuboyama, S. Matsuda T. Ohshima, T. Hirao, H. Itoh, S. Buchner, A. B. Campbell,

Analysis of Single-Ion Multiple-Bit Upset in High-Density DRAMs,

The IEEE Nuclear and Space Radiation Effects Conference(NSREC 2000).

C SCS 11002

11C03

N. Nemoto, H. Shindou, S. Kuboyama, S. Matsuda, H. Itoh, S. Okada, I. Nashiyama,

Relationship between Single-Event Upset Immunity and Fablication Processes of Recent Memories,

5th Europian conference radiation and its Effects on Components and system (RADECS99).

C SCS 11002

11C04

N. Nemoto, H. Shindou, S. Kuboyama, S. Matsuda, K. Sugimoto, I. Nashiyama, H. Itoh,

Development of 1M Gate CMOS Gate Array,

Europian Space Components Conference.

C SCS 11002

11C05

M. Imaizumi, T. Takamoto, T. Ohshima, M. Yamaguchi, H. Itoh, S. Matsuda,

Radiation Effects on High-Efficiency InGaP/InGaAs/Ge Triple-Junction Solar Cells Developed for Terrestrial Use,

Proc. of 29th IEEE Photovoltaic Specialists Conference, May 2002 (New Orleans) in press.

C T I SCS 12002/11003

11C06

Ayako Sakamoto, Vo Thi Thuong Lan, Naoya Shikazono, Atsushi Tanaka,

Analysis of a UVB and Gamma-ray Sensitive Mutant in Arabidopsis,

Abstracts of Annual Meeting and Symposia of the 2002, March 2002 (Okayama) p.158.

C BIT 11009

11C07

M. Okamura, N. Yasuno, M. Ohtuka, A. Tanaka, N. Shikazono and Y. Hase,

Mutation generation in carnation plants regenerated from in vitro leaf cultures irradiated with ion beams: Development of mutation varieties "Vital ion series",

Breeding Research, vol 4 supplement (2002).

C BIT 11012

11C08

K. Ueno, S. Nagayoshi, Y. Hase, N. Shikazono and A. Tanaka,
Establishment of line breeding system using tissue culture of chrysanthemum,
Ikushugaku Kenkyu 3 (2001) (Suppl. 2): 62.
C ACT 11013

11C09

S. Nagayoshi, K. Ueno, Y. Hase, N. Shikazono and A. Tanaka,
Mutation Breeding by Irradiation in Chrysanthemum cv. 'Jimba',
Kyushu Agric. Res. 64, (2002). 187.
C ACT 11013

11C10

Y. Yamamoto, T. Tashiro, A. Tanaka, N. Shikazono, Y. Hase,
Basic Study on Mutation Induction with Ion Beam Irradiation in Garlic (Allium sativum L.),
Jpn. J. Crop Sci. 70(extra issue 2) :237-238(2001).
C BIT 11015

11C11

M. Masuda, S. G. Agong, A. Tanaka, N. Shikazono and Y. Hase,
Mutation Spectrum of Tomato, cv. First, Induced by Seed Radiation with Carbon and Helium Ion- beam,
Acta Horticulturae, 2002.
C BIT 11016

11C12

M. Mizobuchi and A. Iwasaki,
The Use of the Ion Beam to the Rice Breeding,
Shikoku J. Crop Sci. 2001 p.50-51.
C BIT 11017

11C13

H. Katai, M. Taneishi, A. Tanaka, N. Shikazono, Y. Hase and H. Otsuka,
Effects of ion beam irradiation on the growth of netted melon (*Cucumis melo* L.),
Breeding Research 2001(1) p 243.
C BIT 11019

11C14

G. Takata, M. Ikeda, K. Nakaya, K. Koizumi, Y. Sasuga, Y. Sakata, H. Takenaga, and S. Tanaka,
A Search for Genes Responsible for Hydrotropism in Roots of Arabidopsis thaliana,
Plant Cell Physiology 43 (supplement) 2002 p232.
C BIT 11024

11C15

Y. Kobayashi, T. Funayama, M. Tanaka, S. Wada, H. Watanabe and K. Yamamoto,
SYSTEM OF CELL IRRADIATION WITH A PRECISE NUMBER OF HEAVY IONS,
Abstracts of the 2nd International Workshop on Space Radiation Research (IWSSRR-2), Nara, March 11-15, 2002, p. 37.
C BIT 11025

11C16

T. Funayama, Y. Kobayashi, S. Wada, M. Tanaka and K. Yamamoto,

THE EFFECT OF SINGLE HEAVY ION HIT ON THE MAMMALIAN CULTURED CELLS,

Abstracts of the 2nd International Workshop on Space Radiation Research (IWSSRR-2), Nara, March 11-15, 2002, p. 93.

C BIT 11025

11C17

S. Wada, Y. Kobayashi, T. Funayama, M. Natsuhori, N. Ito and K. Yamamoto,

DETECTION OF DNA DAMAGE IN THE INDIVIDUAL CELLS INDUCED BY HEAVY ION IRRADIATION WITH COMET ASSAY,

Abstracts of the 2nd International Workshop on Space Radiation Research (IWSSRR-2), Nara, March 11-15, 2002, p. 104-105.

C BIT 11025

11C18

Y. Kobayashi, T. Funayama, S. Wada, M. Taguchi, T. Kamiya, W. Yokota, H. Watanabe,

The effect of single ion irradiation on mammalian cells,

Abs. of The 11th TIARA Research Reviewing Meeting (Takasaki, July 11-12, 2002).

C BIT 11025

11C19

N. Ohtake, T. Kawachi, H. Fujikake, T. Suganuma, T. Ohyama, K.Sueyoshi, A. Osa, M. Koizumi, S. Watanabe, T. Sekine, S.Matuhashi, N. Ishioka, C. Mizuniwa, H. Uchida and A. Tsuji,

Effect of different phosphate application onsoybean nitrate absorption and translocation,

The 38th Annual Meeting on Radioisotopes and Radiation in the Physical Sciences and Industries. 2001 (Tokyo), 168.

C BIT 11030

11C20

Y. Kunimi, S. Seki, and S. Tagawa,

Investigation on Hole Drift Mobility in Poly(n-hexylphenylsilane),

Solid State Commun. 114 (2000) 469-472.

C RCO 11039

11C21

S. Seki, K. Maeda, Y. Kunimi, S. Tagawa, Y. Yoshida, H. Kudoh, M. Sugimoto, Y. Morita, T. Seguchi, T. Iwai, H. Shibata, K. Asai, and K. Ishigure,

Ion track structure in poly(di-n-hexylsilane)

Proceedings of the 8th Japan-China bilateral symposium on radiation chemistry (2000) 287.

C RCO 11039

11C22

S. Seki, Y. Kunimi, Y. Sakurai, S. Tagawa

High-sensitive Negative Resist Materials Based on Polysilane Derivatives,

J. Photopolym. Sci. Technol, 13 (2000) 395.

C RCO 11039

11C23

S. Seki, K. Nishida, Y. Kunimi, Y. Yoshida, S. Tagawa,

Electronic Structure of σ -conjugated System of Polysilanes Studied by Electron Beam Pulse Radiolysis,

Proc. IEEE 13th ICDL, 646-649 (1999).

C RCO 11039

11C24

T. Nakazawa, V. Grishmanovs, D. Yamaki, Y. Katano, T. Aruga, A. Iwamoto,

Study of ion-induced damage in Li_2TiO_3 ceramics,

In ternational Conference on Ion Implantation Technology Proceedings, September 2000 (Alpbach) p.753.

TIS IOM 12006

11C25

Y. Katano, T. Aruga, S. Yammoto, T. Nakazawa, D. Ymaki,

Implantation Mode Dependence of Damage Structure Depth Profiles in Al_2O_3

Irradiated with Triple eam of H, He and Heavy Ions,

In ternational Conference on Ion Implantation Technology Proceedings, September 2000 (Alpbach) p.805.

TIS IOM 12006

11C26

Y. Shimomura and I. Mukouda,

Atomistic Mechanism of Nucleation and Growth of Voids in Cu studied by Computer Simulation,

Mat. Res. Soc. Symp. Proc., 650 (2001) R3.23.1-R3.23.6.

T I S IOM 12008

11C27

N. Sekimura, K. Kobayashi and T. Morioka,

Surface Irradiation Effects by STM Observation,

Proceedings of SCR-2000 (2000).

T S I IOM 12009

11C28

T. Okita, N. Sekimura, L. R. Greenwood, W. G. Wolfer, Y. Isobe and F. A. Garner,

Neutron-induced Microstructural Evolution of Fe-15Cr-16Ni at ~400°C During Neutron Irradiation in the FFTF Fast Neutrons,

Proceedings of the 10th International Symposium on Environmental Degradation of Materials in Nuclear Power Systems 2001, in press.

T S I IOM 12009

11C29

T. Okita, N. Sekimura T. Iwai and F. A. Garner,

Investigation of the Synergistic Influence of Composition, Irradiation Temperature and Atomic Displacement Rate on the Microstructural Evolution of Ion-irradiated Model Austenitic Alloys,

Proceedings of the 10th International Symposium on Environmental Degradation

of Materials in Nuclear Power Systems 2001, in press.
T S I IOM 12009

11C30
T. Okita, N. Sekimura and F. A. Garner,
The Effect of Flux and Nuclear Transmutants on Microstructural Evolution and Swelling in Austenitic Model Alloys Irradiated with Heavy Ions and Fast Neutrons,
Proceedings of PRICM-4 2002, in press.
T S I IOM 12009

11C31
F. A. Garner, M. L. Hamilton, T. Okita, N. Sekimura, D. L. Porter and T. R. Allen,
The unexpectedly strong influence of displacement rate on the neutron-induced void swelling of pure metals, and iron-based FCC and BCC alloys,
Proceedings of PRICM-4 2002, in press.
T S I IOM 12009

11C32
M. Ando, H. Tanigawa, E. Wakai, T. Sawai, S. Jitsukawa, Y. Katoh, A. Kohyama, K. Nakamura, H. Takeuchi,
Investigation of Irradiation-Induced Hardening Changes on Ion-Irradiated Reduced Activation Ferritic/Martensitic Steels,
Proc. of 4th Meeting of Fusion and Energy, JPSF, Osaka, (2002), p260.
T I S IOM 12011

11C33
I. Ioka, M. Futakawa, Y. Nanjyo, K. Kiuchi, Y. Kuroda and T. Anegawa,
Effect of Triple Ion Beam Irradiation on Mechanical Properties of High Chromium Austenitic Stainless Steel,
Material Chemistry '02, March 13-15, 2002(Tsukuba).
T I S MAN 12012

11C34
I. Ioka, K. Kiuchi, Y. Kuroda and T. Anegawa,
Evaluation of New Fe-Cr-Ni Alloy for Ultra High Burnup Fuel Cladding Tube,
International Congress on Advanced Nuclear Power Plants, June 9-13, 2002(Florida).
TIS MAN 12012

11C35
K. Kiuchi, H. Ogawa, I. Ioka, Y. Kuroda and T. Anegawa,
Development of New Cladding Materials Applied for Advanced LWR Aiming at Ultra-high Burn-up and Fast Neutron Spectrum,
International Congress on Advanced Nuclear Power Plants, June 9-13, 2002(Florida).
TIS MAN 12012

11C36
K. Kiuchi, H. Ogawa, I. Ioka, Y. Kuroda, T. Anekawa,
Development of New Cladding Materials Applied for Advanced LWR Aiming at Ultra High Burnup and Fast Neutron Spectrum,
Int.Cong.Advanced Florida, June 9-13(2002).
T I S MAN 12014

11C37
I. Ioka, K. Kiuchi, Y. Kuroda, T. Anekawa,
Evaluation of New Fe-Cr-Ni Alloy for Ultra High Burnup Fuel Cladding Tube,
Int. Cong. Advanced Florida, June 9-13(2002).
T I S MAN 12014

11C38
H. -S. Lee, H. Okada, A. Wakahara, A. Yoshida, T. Ohshima, H. Itoh, S. Kawakita, M. Imaizumi, and S. Matsuda,
Effect of proton irradiation on electrical properties of CuInSe2 thin films,
Technical Digest of the International PVSEC-12 (June 20-22, 2001, Jeju, Korea) pp.91-92.
I SCS 12004

11C39
M. Takeda, S. Ohnuki, T. Suda, S. Watanabe, H. Abe and I. Nishiyama,
Effect of Mass and Energy on Preferential Amorphization in Polycrystalline Si Film During Ion-Irradiation,
Effects of Radiation on Materials 20th Symposium STP1405 836-845 (2001).
TI IOM 12021

11C40
S. Ohnuki, F. Arimoto, S. Watanabe, P. R. Okamoto, N. Q. Lam and H. Abe,
Inter-Diffusion and Amorphization During Ion-Irradiation in Mo/Si Nano-Multi-Layer Materials,
The Forth Pacific Rim International Conference on Advanced Materials and Processing, Vol-1, pp1331-1333, (2001).
TI IOM 12021

11C41
M. Takeda, T. Suda, S. Watanabe, S. Ohnuki, H. Abe,
Preferential Amorphization and Crystallization in polycrystalline Silicon under Ion-Irradiation,
The Forth Pacific Rim International Conference on Advanced Materials and Processing, Vol-2, pp2539-2542, (2001).
TI IOM 12021

11C42
E. Shioya, T. Suda, S. Watanabe, S. Ohnuki, M. Ishino, O. Yoda, H. Abe, F. Phillipp,
Electron-Irradiation-Induced Amorphization in Mo/Si Nano-Multilayer Material,
The Forth Pacific Rim International Conference on Advanced Materials and Processing, Vol-1, pp1351-1353, (2001).
TI IOM 12021

11C43
K. Narumi and H. Naramoto,
SPM Investigation of C_{60} Thin Films Irradiated with Energetic Ions,
Proc, 3rd International Symposium on Atomic Level Characterizations for New Materials and Devices '01, Nara, Japan, November 11-14, 2001.
I IOM MAN 12030

11C44

S. Ishino, T. Hasegawa, Y. Chimi, N. Ishikawa, A. Iwase, T. Tobita, M. Suzuki,
Electrical Resistivity Measurements in Fe-Cu Alloys Irradiated with Energetic Heavy Ions and Electrons,
The (129th) 2001-Fall Meeting of the Japan Institute of Metals, Fukuoka, September 21-24, 2001.
S IOM 12035

11C45

S. Ishino,
Studies of Dose Rate Effects by Means of Ion Irradiation,
EPRI/CRIEPI Workshop on Dose Rate Effects in Reactor Pressure Vessel Materials, Olympic Valley, CA, U.S.A., November 12-14, 2001.
S IOM 12035

11C46

S. Ishino, T. Hasegawa, Y. Chimi, N. Ishikawa, A. Iwase, T. Tobita, M. Suzuki,
In-situ Measurements of Electrical resistivity in Fe-Cu Alloys Using Heavy Ion and Electron accelerators,
Symposium on 'The Mechanism of Irradiation Embrittlement in Pressure Vessel Materials', Tohoku University, Sendai, November 22-24, 2001.
S IOM 12035

11C47

N. Mizuochi, J. Isoya, S. Yamasaki, H. Takizawa, N. Morishita, T. Ohshima and H. Itoh,
ESR study on the single vacancy related defects in 4H-, 6H-SiC,
Proceedings of International Conference on Silicon Carbide and Related Materials 2001(Oct. 28-Nov. 2, 2001, Tsukuba, Japan), Matetr. Sci. Forum 389-393, 497-500 (2002).
T IOM 12037

11C48

E. Shioya, T. Suda, S. Watanabe, S. Ohnuki, M. Ishino, O. Yoda, H. Abe,
Electron-irradiation-induced amorphization in Mo/Si nano multilayer material,
4th Pacific Rim International Conference on Advanced Materials and Processing, 2001.12.11-15, Hawaii.
I IOM 12019

11C49

S. Yamamoto, T. Sumita, A. Miyashita, H. Itoh,
Characterization of TiO_2 films prepared by pulsed laser deposition,
Proc. of the third symposium on advanced photon research, Dec. 2001 (Kyoto).
S IOM 12023

11C50

V. Laverentiev, H. Abe, S. Yamamoto, H. Naramoto, and K. Narumi,
Formation of carbon nanotubes under condition of Co+C_{60} film,
Anniversary of its Discovery, October 3-5, 2001 (Tsukuba, Japan) p.142.
O IOM

11C51
V. Laverentiev, H. Abe, S. Yamamoto, H. Naramoto, and K. Narumi,
Formation of promising Co-C nano-compositions,
3rd International Symposium on Atomic Level Characterizations for New Materials and Devices '01, ALC '01, November 11-14, 2001 (Nara-Ken New Public Hall, Japan), Program & Abstracts. p. 113.
O IOM

11C52
V. Laverentiev, H. Abe, S. Yamamoto, H. Naramoto, and K. Narumi,
Co and C_{60} interaction under conditions of mixture
International Symposium on Nano Carbons, ISNC 2001, November 14-16, 2001 (Nagano, Japan). Program & Abstracts, p. 259.
O IOM

11C53
V. Laverentiev, S. Yamamoto, H. Naramoto nad K. Narumi,
Structural Features of Epitaial Cobalt Films
Abstracts of the Thirteenth International Conference on Crystal Growth, ICCG-13/IGVGE-11, 30 July - 4 August 2001 (Doshisha University, Kyoto, Japan) p. 136.
O IOM

11C54
V. Laverentiev, H. Abe, S. Yamamoto, H. Naramoto, and K. Narumi,
Formation of intriguing carbon-related structures in Co+C60 mixed films,
Abstract of the 21th Fullerene General Symposium, July 25-27, 2001 (Tsukuba, Japan) p.34.
O IOM

11C55
P. Wei, Y. Xu, K. Narumi, H. Naramoto and S. Nagata,
Structural and optical properties of Ge/C Multikayers Deposited on Si and Sapphire Substrates by Magnetron Sputtering,
The 8th Inter.Conf. on Electronic Materials (IUMRS-ICEMS2002, Xi'an, 2002).
I S IOM 12029

11C56
T. Ohshima, A. Uedono, H. Itoh, M. Yoshikawa, K. Kojima, I. Nashiyama,S. Okada and K. Abe,
Relationship between donor activation and defect annealing in 6H-SiC hot-implanted with phosphorus ions,
Materials Science Forum, 338-342 (2000), p.857.
I IOM 12039

11C57
H. Abe, A. Uedono, H. Uchida, A. Komatsu, S. Okada and H. Itoh,
Positron annihilation studies of defects in ion implanted Palladium,
Materials Science Forum, 363-365 (2001), p. 156.

I IOM 12039

11C58

T. Ohshima. A. Uedono, H. Abe, Z. Q. Chen, H. Itoh, and M. Yoshikawa,
Positron annihilation study of vacancy-type defects in silicon carbide co-implanted with aluminum and carbon ions,
21st Internat. Conf. on Defects in Semiconductors (ICDS21): Giessen, German, July 16-20, 2001.
I IOM 12039

11C59

M. Hattori, Y. Nishihara, M. Fujimaki, Y. Ohki, T. Souno, H. Nishikawa, T. Yamaguchi, E. Watanabe, M. Oikawa, T. Kamiya, K. Arakawa,
Evaluation of Three Dimensional Microstructures on Silica Glass Fabricated by Ion Microbeam,
Abstracts of The 10th TIARA Research Review Meeting, p. 106 – 107.
S IOM 12041

11C60

H. Nishikawa, Y. Ohki,
Functionnal Silica-Based Glasses for Photonics,
The Transactions of The Instutute of Electrical
Engineers of Japan,pp.721-724, Vol. 121-A No.8.
S IOM 12041

11C61

N. S. Ishioka, S. Watanabe, S. Matsuhashi, C. Mizuniwa, T. Itoh and T. Sekine,
Excitation Functions of Rhenium Isotopes on the natW(d,xn) Reactions and Production of No-carrier-added 186Re,
Proc. of Nuclear Data for Science and Technology (ND2001),Oct. 7-12, 2001, Tsukuba, Japan.
C, NRI, 11036

11C62

C. J. Ma, M. Kasahara, S. Tohno, R. Holler and T. Kamiya,
Chemical composition of single raindrops fallen in yellow rainfall episode in Japan,
The 2nd Asia Aerosol Conference, July 2001 (Pusan, Korea) p.7-8.
S ACT 12046

11C63

C. J. Ma, M. Kasahara, S. Tohno, T. Kamiya and T. Sakai,
Sampling of individual fog droplets and its chemical analysis,
2nd International Conference on Fog and Fog Collection, July 2001, (Newfoundland, Canada) p.45-48.
S ACT 12046

11C64

M. Kasahara, C.-J. Ma and S. Tohno
Physical and chemical properties of single fog droplets applying fixation technique,
Fog 2001, July 2001 (Newfoundland, Canada) p.69-72.
S ACT 12046

11C65
C. J. Ma, Y. Inoguchi, M. Kasahara, S. Tohno and T. Kamiya,
New approaches for the characterization of single and size-segregated raindrops,
The 18th Symposium on Aerosol Science and Technology, July 2001 (Tokyo, Japan) p.140-141.
S ATC 12046

11C66
M. Ibaraki, M. Baba, T. Miura, T. Aoki, T. Hiroishi, H. Nakashima, S. Meigo, Su. Tanaka,
Measurement of Neutron Non-Elastic Cross Sections of C, Si, Fe, Zr and Pb in 40- 80 MeV Region,
Proc. Int. Conf., on Nuclear Data for Sci. & Technol,, (2001, Thukuba) To be published.
C NRI 11047

11C67
T. Sanami, T. Hiroishi, M. Baba, M. Hagiwara, T. Miura, T. Aoki, T. Kawata, Su. Tanaka, H. Nakashima, S. Meigo,
Double-differential hydrogen and helium production cross section of oxygen and nitrogen for 75 MeV neutrons,
Proc. Int. Conf., on Nuclear Data for Sci. & Technol,, (2001, Thukuba)To be published.
C NRI 11047

11C68
M. Baba, M. Ibaraki, T. Miura, T. Aoki, Y. Hirasawa, H. Nakashima, S. Meigo, Su. Tanaka,
Experiments on Neutron Scattering and Prompt Fission Neutron Spectra,
Proc. Int. Conf., on Nuclear Data for Sci. & Technol,, (2001, Thukuba) To be published.
C NRI 11047

11C69
M. Hagiwara, M. Hosokawa, M. Baba, T. Sanami, M. Takada,
Development of a Bragg curve spectrometer (BCS) for fragment spectroscopy from neutron and proton induced reactions,
Proc. Symposium on Radiation detectors and their uses(2002),KEK-proceedings, to be published.
C NRI 11047

11C70
S. Ban, H.S. Lee, T. Sato, S. Maetaki and K. Shin,
Measurements of Photo-Neutrons from Thick Aluminum Target by 2 GeV Electrons,
Proc. of 9th EGS4 Users' Meeting in Japan, August 2001, Tsukuba, pp.48-55.
C RSH 11048

11C71
T. Sawamura, J. H. Kaneko, M. Abe, M. Tamura, I. Murai, A. Homma, F. Fujita and S. Tsuda,
Effect of lead converter on superheated drop detector response to high energy neutrons,
Proc.10th Symp on Rad. Meas. and Application, 2002, in press.
C RSH 11048

C ATC Machine Study

11C72

Y. Saitoh, Y. Nakajima, K. Narumi, H. Shibata, T. Majima, L. K. Ohno, A. Itoh,
Measurement of secondary charged particle from Cu by MeV cluster Irradiation,
Proceedings of 14Th Workshop on Tandem Accelerator and Technology, JNC TN7200 2001-001,pp.122-125.
T ACT 12050

11C73

S. Okumura, K. Arakawa, M. Fukuda, Y. Nakamura, W. Yokota, T. Ishimoto, S. Kurashima, I. Ishibori, T. Nara, T. Agematsu, H. Tamura, A. Matsumura, M. Sano, T. Tachikawa,
Temperature Control of a Cyclotron Magnet for Stabilization of the JAERI AVF Cyclotron Beam,
Proc. of the 16th International Conference on Cyclotrons and their Applications, 2001 (Michigan, USA) p.330.
C ACT Machine Study

11C74

S. Kurashima, M. Fukuda, Y. Nakamura, T. Nara, T. Agematsu, I. Ishibori, W. Yokota, S. Okumura, K. Arakawa, Y. Kumata, Y. Fukumoto,
Design of the Flat-Top Acceleration System for the JAERI AVF Cyclotron,
Proc. 16th Int. Conf. on Cyclotron and Their Applications, East Lansing, USA, 303 (2001).

11C75

S. Kurashima, N. Miyawaki, M. Fukuda, Y. Nakamura, T. Nara, T. Agematsu, I. Ishibori, W. Yokota, S. Okumura and K. Arakawa,
Design of the Flat-Top Resonator for the JAERI AVF Cyclotron,
Proc. 13th Symp. on Accelerator Science and Technology, Suita, Japan, 232 (2001).
C ACT Machine Study

11C76

Y. Nakamura, T. Nara, T. Agematsu, I. Ishibori, H. Tamura, S. Kurashima, W. Yokota, S. Okumura, M. Fukuda, K. Akaiwa, To. Yoshida, S. Ishiro, A. Matsumura, Y. Arakawa, Tsu. Yoshida, S. Kanou, A. Ihara and K. Takano,
STATUS REPORT ON THE JAERI AVF CYCLOTRON SYSTEM,
Proc. of 13th Sympo. Accel. Sci. Technol., Suita, Osaka, Japan, October (2001) pp.193-195.
C ACT Machine Study

11C77

Y. Nakamura, T. Nara, T. Agematsu, I. Ishibori, H. Tamura, S. Kurashima, W. Yokota, S. Okumura, M. Fukuda and K. Arakawa,
STATUS REPORT ON THE JAERI AVF CYCLOTRON SYSTEM,
Proc. of 16th Int. Conf. Cyclo. Their Applic., East Lansing, Michigan, USA (2001) pp.129-132.

C ACT Machine Study

11C78

K. Mizuhashi, S. Uno, K. Ohkoshi, A.Chiba, Y. Saithoh, Y. Ishii, T. Kamiya, I. Takada, S. Tajima,

Status of TIARA electrostatic accelerators facility,

Proc. 15th Workshop on tandem accelerator and technique(2003).

TIS ACT Machine Study

Appendix 2. Type of Research Collaboration

Section of this Report	Reseach Program Number	Type of Research Collaborations*	Section of this Report	Reseach Program Number	Type of Research Collaborations*
1.1	11001／12002	JAERI			
1.2	11002	Joint.Res	4.1	11005	Proj.Res.Univ
1.3	11003／12002	Joint.Res	4.2	12010	Proj.Res.Univ
1.4	11004／12005	Joint.Res	4.3	12006	Proj.Res.Univ
1.5	12001	JAERI	4.4	12007	Proj.Res.Univ
1.6	12003	JAERI	4.5	12008	Proj.Res.Univ
			4.6	12009	Proj.Res.Univ
2.1	11006	Coop.Res.Univ	4.7	12011	JAERI
2.2	11007	Joint.Res	4.8	12012	JAERI
2.3	11008	Joint.Res	4.9	12013	JAERI
2.4	11009	JAERI	4.10	12014	JAERI
2.5	11010	Joint.Res	4.11	12015	Joint.Res
2.6	11012	Joint.Res	4.12	12016	Joint.Res
2.7	11012	Joint.Res	4.13	12020	Coop.Res.Univ
2.8	11013	Joint.Res	4.14	12004	Coop.Res.Univ
2.9	11014	Joint.Res	4.15	12021	Coop.Res.Univ
2.10	11015	Coop.Res.Univ	4.16	12025	JAERI
2.11	11016	Coop.Res.Univ	4.17	12030	JAERI
2.12	11017	Joint.Res	4.18	12031	JAERI
2.13	11018	Coop.Res.Univ	4.19	12032	Coop.Res.Univ
2.14	11019	Joint.Res	4.20	12033	JAERI
2.15	11020	Coop.Res.Univ	4.21	12034	JAERI
2.16	11021	Coop.Res.Univ	4.22	12035	Coop.Res.Univ
2.17	11022	Joint.Res	4.23	12036	Coop.Res.Univ
2.18	11023	Joint.Res	4.24	12037	Coop.Res.Univ
2.19	11024	Coop.Res.Univ	4.25	12038	Coop.Res.Univ
2.20	11025	JAERI			
2.21	11026	Coop.Res.Univ	5.1	12019	JAERI
2.22	11027	Coop.Res.Univ	5.2	12022	Coop.Res.Univ
2.23	11028	Coop.Res.Univ	5.3	12023	JAERI
2.24	11029	JAERI	5.4	12023	JAERI
2.25	11030	Proj.Res.Univ	5.5	12024	JAERI
2.26	11031	Proj.Res.Univ	5.6	12026	Coop.Res.Univ
2.27	11032	Proj.Res.Univ	5.7	12027	Coop.Res.Univ
2.28	11033	Proj.Res.Univ	5.8	12028	Coop.Res.Univ
2.29	11034	Proj.Res.Univ	5.9	12029	JAERI
2.30	11035	Joint.Res	5.10	off line	JAERI
2.31	12017	Coop.Res.Univ	5.11	off line	JAERI
2.32	12018	JAERI	5.12	off line	JAERI
			5.13	12039	JAERI
3.1	11037	JAERI	5.14	12040	Joint.Res
3.2	11038	Coop.Res.Univ	5.15	12041	Coop.Res.Univ
3.3	11039	Coop.Res.Univ	5.16	12042	JAERI
3.4	11040	JAERI			
3.5	11041	Coop.Res.Univ	6.1	11036	JAERI
3.6	11042	Coop.Res.Univ	6.2	off line	JAERI
3.7	11044	JAERI			

Section of this Report	Reseach Program Number	Type of Research Collaborations*
7.1	11045／12043	JAERI
7.2	12044	Coop.Res.Univ
7.3	12045	Proj.Res.Univ
7.4	12046	Proj.Res.Univ
7.5	12047	Proj.Res.Univ
7.6	12048	Proj.Res.Univ
7.7	12049	JAERI
8.1	11046	Proj.Res.Univ
8.2	11047	Proj.Res.Univ
8.3	11048	Proj.Res.Univ
9.1	12050	JAERI
9.2	12051	Coop.Res.Univ
9.3	Machine Study	JAERI
9.4	Machine Study	JAERI
9.5	Machine Study	JAERI
9.6	Machine Study	JAERI
9.7	Machine Study	JAERI
9.8	Machine Study	JAERI
9.9	Machine Study	JAERI
9.10	Machine Study	JAERI
9.11	Machine Study	JAERI

*Joint Res.: Joint research with private company or governmental institution
Coop. Res. Univ.: Cooperative research with a university or universities#
Proj. Res. Univ.: The JAERI-Universities Joint Research Project#
#For administration of these programs, we appreciate the cooperation of:
Research Center for Nuclear Science and Technology, The University of Tokyo.

Appendix 3. Organization and Personnel of TIARA (FY 2001)

1) Organization for the Research and Development of Advanced Radiation Technology

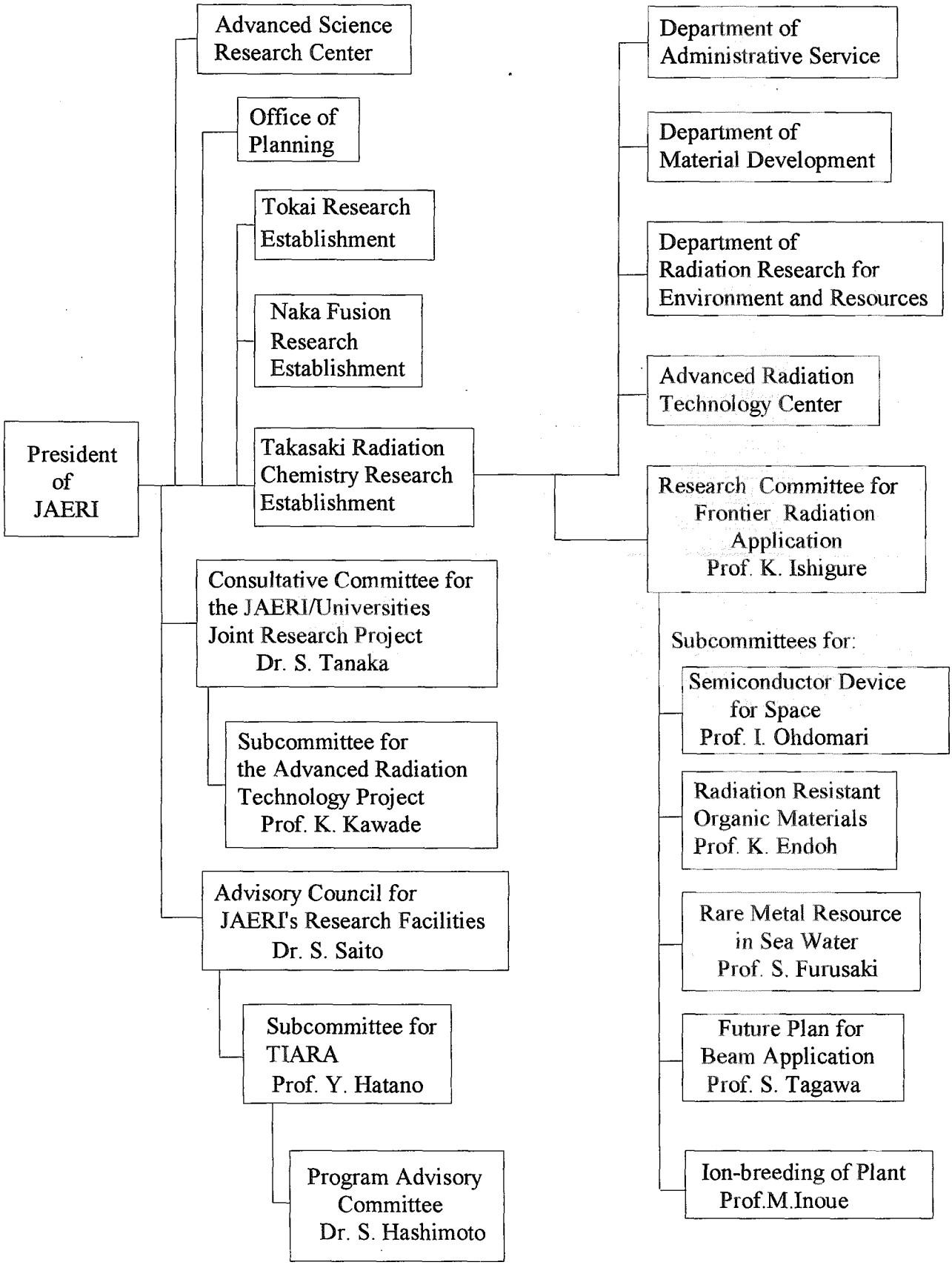

2) Personnel for the Administration, Operation and Control of TIARA

Advanced Radiation Technology Center

Director	M. Saidoh
Deputy Director	Y. Ohara

Administration Division

General Manager	M. Ottsubo
Staff Member	K. Morishita, A. Habuto

Utilization and Coordination Division

General Manager	Su. Tanaka
Staff Member	K. Nishimura, H. Takizawa, M. Hosono

Ion Accelerator Operation Division

General Manager	S. Tajima

Group of Cyclotron Operation

Staff Member	Y. Nakamura, T. Nara, T. Agematsu, I. Ishibori, H. Tamura, S. Kurashima

Guoup of Electrostatic Accelerators Operation

Staff Member	I.Takada, K.Mizuhashi, S. Uno, K. Ohkoshi, Y. Nakajima, A. Chiba

Ion Beam Engineering Division

Head	K. Arakawa
Staff Member	T. Kojima, W. Yokota, H. Tachibana, M. Fukuda, T. Kamiya, S. Okumura, Y. Saito,Y. Ishii, T. Sakai, S. Oikawa, N. Miyawaki

Irradiation Service Division

General Manager	H. Sunaga
Staff Member	T. Kanazawa, Y. Haruyama, T. Ohkubo, N. Haneda, H. Hanaya

Department of Administrative Services

Safety Division

Staff Member	Y. Ohi, H. Miyauchi

(Radiation Monitoring and Control in TIARA)

Utilities and Maintenance Division

Staff Member	S. Kaneko, Y. Takayama

(Radioactive Waste Management and Utility Control in TIARA)

This is a blank page.

国際単位系 (SI) と換算表

表 1　SI基本単位および補助単位

量	名称	記号
長さ	メートル	m
質量	キログラム	kg
時間	秒	s
電流	アンペア	A
熱力学温度	ケルビン	K
物質量	モル	mol
光度	カンデラ	cd
平面角	ラジアン	rad
立体角	ステラジアン	sr

表 2　SIと併用される単位

名称	記号
分，時，日	min，h，d
度，分，秒	°，′，″
リットル	l，L
トン	t
電子ボルト	eV
原子質量単位	u

1 eV = 1.60218 × 10^{-19} J

1 u = 1.66054 × 10^{-27} kg

表 5　SI接頭語

倍数	接頭語	記号
10^{18}	エクサ	E
10^{15}	ペタ	P
10^{12}	テラ	T
10^{9}	ギガ	G
10^{6}	メガ	M
10^{3}	キロ	k
10^{2}	ヘクト	h
10^{1}	デカ	da
10^{-1}	デシ	d
10^{-2}	センチ	c
10^{-3}	ミリ	m
10^{-6}	マイクロ	μ
10^{-9}	ナノ	n
10^{-12}	ピコ	p
10^{-15}	フェムト	f
10^{-18}	アト	a

表 3　固有の名称をもつSI組立単位

量	名称	記号	他のSI単位による表現
周波数	ヘルツ	Hz	s^{-1}
力	ニュートン	N	m·kg/s^2
圧力，応力	パスカル	Pa	N/m^2
エネルギー，仕事，熱量	ジュール	J	N·m
工率，放射束	ワット	W	J/s
電気量，電荷	クーロン	C	A·s
電位，電圧，起電力	ボルト	V	W/A
静電容量	ファラド	F	C/V
電気抵抗	オーム	Ω	V/A
コンダクタンス	ジーメンス	S	A/V
磁束	ウェーバ	Wb	V·s
磁束密度	テスラ	T	Wb/m^2
インダクタンス	ヘンリー	H	Wb/A
セルシウス温度	セルシウス度	℃	
光束	ルーメン	lm	cd·sr
照度	ルクス	lx	lm/m^2
放射能	ベクレル	Bq	s^{-1}
吸収線量	グレイ	Gy	J/kg
線量当量	シーベルト	Sv	J/kg

表 4　SIと共に暫定的に維持される単位

名称	記号
オングストローム	Å
バーン	b
バール	bar
ガル	Gal
キュリー	Ci
レントゲン	R
ラド	rad
レム	rem

1 Å = 0.1 nm = 10^{-10} m

1 b = 100 fm^2 = 10^{-28} m^2

1 bar = 0.1 MPa = 10^5 Pa

1 Gal = 1 cm/s^2 = 10^{-2} m/s^2

1 Ci = 3.7 × 10^{10} Bq

1 R = 2.58 × 10^{-4} C/kg

1 rad = 1 cGy = 10^{-2} Gy

1 rem = 1 cSv = 10^{-2} Sv

(注)

1. 表1－5は「国際単位系」第5版，国際度量衡局 1985年刊行による。ただし，1 eVおよび1 uの値はCODATAの1986年推奨値によった。
2. 表4には海里，ノット，アール，ヘクタールも含まれているが日常の単位なのでここでは省略した。
3. barは，JISでは流体の圧力を表わす場合に限り表2のカテゴリーに分類されている。
4. EC閣僚理事会指令ではbar，barnおよび「血圧の単位」mmHgを表2のカテゴリーに入れている。

換算表

力

N(=10^5 dyn)	kgf	lbf
1	0.101972	0.224809
9.80665	1	2.20462
4.44822	0.453592	1

粘度　1 Pa·s(N·s/m^2) = 10 P(ポアズ)(g/(cm·s))

動粘度　1 m^2/s = 10^4 St(ストークス)(cm^2/s)

圧力

MPa(=10 bar)	kgf/cm^2	atm	mmHg(Torr)	lbf/in^2(psi)
1	10.1972	9.86923	7.50062 × 10^3	145.038
0.0980665	1	0.967841	735.559	14.2233
0.101325	1.03323	1	760	14.6959
1.33322 × 10^{-4}	1.35951 × 10^{-3}	1.31579 × 10^{-3}	1	1.93368 × 10^{-2}
6.89476 × 10^{-3}	7.03070 × 10^{-2}	6.80460 × 10^{-2}	51.7149	1

エネルギー・仕事・熱量

J(=10^7 erg)	kgf·m	kW·h	cal(計量法)	Btu	ft·lbf	eV
1	0.101972	2.77778 × 10^{-7}	0.238889	9.47813 × 10^{-4}	0.737562	6.24150 × 10^{18}
9.80665	1	2.72407 × 10^{-6}	2.34270	9.29487 × 10^{-3}	7.23301	6.12082 × 10^{19}
3.6 × 10^6	3.67098 × 10^5	1	8.59999 × 10^5	3412.13	2.65522 × 10^6	2.24694 × 10^{25}
4.18605	0.426858	1.16279 × 10^{-6}	1	3.96759 × 10^{-3}	3.08747	2.61272 × 10^{19}
1055.06	107.586	2.93072 × 10^{-4}	252.042	1	778.172	6.58515 × 10^{21}
1.35582	0.138255	3.76616 × 10^{-7}	0.323890	1.28506 × 10^{-3}	1	8.46233 × 10^{18}
1.60218 × 10^{-19}	1.63377 × 10^{-20}	4.45050 × 10^{-26}	3.82743 × 10^{-20}	1.51857 × 10^{-22}	1.18171 × 10^{-19}	1

1 cal = 4.18605 J (計量法)
= 4.184 J (熱化学)
= 4.1855 J (15 °C)
= 4.1868 J (国際蒸気表)

仕事率　1 PS (仏馬力)
= 75 kgf·m/s
= 735.499 W

放射能

Bq	Ci
1	2.70270 × 10^{-11}
3.7 × 10^{10}	1

吸収線量

Gy	rad
1	100
0.01	1

照射線量

C/kg	R
1	3876
2.58 × 10^{-4}	1

線量当量

Sv	rem
1	100
0.01	1

(86年12月26日現在)

TIARA Annual Report 2001